

Measuring Actual Evaporation Rates from a Tailings Pond

by

Janeen R. Ogloza

A thesis submitted in partial fulfillment of the requirements for the degree of

Master of Science

in

MINING ENGINEERING

Civil and Environmental Engineering

University of Alberta

© Janeen R. Ogloza, 2017

Abstract

The focus of the research presented here was to directly measure actual evaporation rates from a tailings surface using a micrometeorological technique known as the eddy covariance method. Depending on the results, it would be determined whether current drying models need to be calibrated with these measurements. The eddy covariance method allows for continuous observation of large areas, without disturbing the area of interest, which in this case is the test cell.

The eddy covariance method typically operates over large areas, such as forest, ocean, plains, and the data is typically trimmed by quality. However, large portions of data are rarely removed from the data analysis, as was the case for this research due to the relatively small size of the test cell. This excessive trimming did make the interpretation of the data difficult. Nevertheless, once the footprint analysis was complete it was clear why gaps or sudden changes in the data were seen. To combat this issue, it was concluded that the system should be placed over the center of a larger, more active pond. Actual evaporation rates were found to be low, which suggests current drying models that use reduced potential evaporation rates maybe overestimating how much dewatering is occurring.

Dedications

I would like to dedicate this to my parents for always being there for me, and to my brother for always motivating me.

Acknowledgements

I would like to thank my supervisor Dr. Ward Wilson for all his support, guidance, and positive energy. Thank you Dr. Wilson's research team, especially Dr. Nicholas Beier, Vivian Giang, and Sally Petaske, for helping with the site preparation and getting all the logistics done to get access to site and Bereket Fisseha for helping me on and off site. Thank you Suncor, specifically Keith Everard and Field Services Department for giving my access to the site and doing their best to accommodate my team and me. Dr. Arturo Sánchez-Azofeifa, and Peter Carlson from the Earth and Atmospheric Science department for the access of eddy covariance equipment, and Saulo Castro for teaching me how to operate the system and guiding me through the data processing. I could not have done this without any of you.

Table of Contents

Abstract	ii
Dedications	iii
Acknowledgements	iv
Table of Contents	v
List of Figures	vii
List of Tables	ix
1 Introduction.....	1
1.1 Background Information on the Oil Sands	1
1.2 Background Information on MFT Drying	4
1.3 Background Information on Evaporation Measurement Methods	5
1.4 Objective of Research.....	6
1.5 Thesis Outline.....	6
2 Literature Review.....	7
2.1 Estimating evaporation rates on freshwater tailings using evaporation pans, Bowen Ratio station, and micro-lysimeters.....	7
2.2 Estimating evaporation rates on saline tailings using evaporation pans, Bowen Ratio station, and micro-lysimeters.....	10
2.3 Determining water balance of a waste rock pile using an Eddy Covariance system	12
2.4 Estimating productivity of a soil cover system using an Eddy covariance system	14
2.5 Estimating greenhouse gas emissions from an oil sands tailings pond using an Eddy covariance system.....	17
2.6 Chapter Summary	20
3 Relevant Theory	22
3.1 Surface Energy Balance.....	22
3.2 Hydrology	25
3.3 Eddy Covariance Method	27
3.4 Footprint Theory.....	30
4 Methods.....	33
4.1 Instruments	33
4.2 Site Description	36
4.3 Field Campaign 2014	41

4.4 Field Campaign 2015	42
4.5 Data Processing	43
5 Results and Analysis	50
5.1 Meteorological and Atmospheric Data.....	50
5.2 Footprint Results and Analysis.....	53
5.3 Data quality	58
5.4 Energy and Evaporation Flux Data	58
5.5 Comparing Actual Evaporation Rates to Other Data	64
6 Discussion	68
7 Conclusion	72
Bibliography	75
Appendices.....	78
Appendix A Site Data collect by ECV	78
Appendix B Site Data provided by Suncor.....	86
Appendix C Footprint Analysis	89
C.I MatLab Script.....	89
C.II Results of Footprint Analysis.....	95
Appendix D Sources	97

List of Figures

Figure 4.1 CSAT3 Sonic Anemometer	33
Figure 4.2 EC155 Closed-path Gas Analyser	34
Figure 4.3 ECV System setup in 2014.....	35
Figure 4.4 Aerial view of ECV	37
Figure 4.5 ECV Setup in 2014 (facing south-west)	38
Figure 4.6 ECV Setup in 2014 (face east)	39
Figure 4.7 ECV Setup in 2015 (face north-west)	40
Figure 4.8 ECV Setup in 2015 (looking down)	41
Figure 4.9 Weighting Factor (Δ/γ) in terms of Temperature	47
Figure 4.10 Monthly Average of Solar Radiation (R_a) at different Latitudes in terms of Days ...	48
Figure 4.11 Theoretical Black Body Radiation (σT^4) in terms of Temperature	49
Figure 5.1 Plot comparing temperature data collected by the ECV system to data collected by Suncor weather data in 2014.....	50
Figure 5.2 Plot comparing temperature data collected by the ECV system to data collected by Suncor weather data 2015	51
Figure 5.3 Plot comparing relative humidity data collected by the ECV system to data collected by Suncor weather data (2014)	52
Figure 5.4 Plot comparing relative humidity data collected by the ECV system to data collected by Suncor weather data (2015)	52
Figure 5.5 Footprint contribution map from September 15 th , 2014 (at 4:30PM)	54
Figure 5.6 Footprint contribution map from September 22 nd , 2014 (night)	55
Figure 5.7 Footprint contribution map from May 9 th , 2015 (at 4:30PM)	55
Figure 5.8 Footprint contribution map from May 23 rd , 2015 (at 4:30AM)	56
Figure 5.9 Histogram of overall relevance of ECV measurements according to the footprint analysis (2014)	57
Figure 5.10 Histogram of overall relevance of ECV measurements according to the footprint analysis (2015)	57
Figure 5.11 Quality of data of flux data according to Eddy Pro	58
Figure 5.12 Plot of sensible heat and latent heat flux from Sept. 9 to Sep. 12, 2014	59
Figure 5.13 Plot of sensible heat and latent heat flux from May 10 to May 13, 2015	60
Figure 5.14 Analysis of raw and trimmed evaporation data collect in 2014 (using data quality) ..	60
Figure 5.15 Analysis of raw and trimmed evaporation data collect in 2015 (using data quality) ..	61

Figure 5.16 Analysis of raw and trimmed evaporation data collect in 2014 (using quality and footprint data).....	62
Figure 5.17 Analysis of raw and trimmed evaporation data collect in 2015 (using quality and footprint data).....	63
Figure 5.18 Comparison of evaporation data collected in 2014 and potential evaporation	64
Figure 5.19 Comparison of evaporation data collected in 2015, site data, and potential evaporation	65
Figure 5.20 Plot comparing actual evaporation rate to temperature in 2015	66
Figure 5.21 Plot comparing actual evaporation rate to amount of rainfall in 2015	66
Figure 5.22 Plot comparing actual evaporation rate to amount of relative humidity in 2015	67
Figure 5.23 Plot comparing the changes of the actual evaporation rate to height of lift poured in 2015.....	67

List of Tables

Table 4.1 Instrument location information (EddyPro inputs).....	43
Table 4.2 Instrument information (EddyPro inputs).....	44
Table 5.1 Statistic of daily average temperature data in °C.....	51
Table 5.2 Statistic of daily average relative humidity data in %	52
Table A.1 Atmospheric data collect by the ECV (2014)	78
Table A.2 Atmospheric data collect by the ECV (2015)	79
Table A.3 Evaporation data collected by ECV (2014)	80
Table A.4 Evaporation data collected by ECV (2015)	81
Table A.5 Summary of percent difference between evaporation rates (2014)	82
Table A.6 Summary of percent difference between evaporation rates (2015)	83
Table A.7 Quality of latent heat flux data (2014).....	84
Table A.8 Quality of latent heat flux data (2015).....	85
Table B.1 Atmospheric data collect by Suncor weather station (2014)	86
Table B.2 Atmospheric data collect by Suncor weather station (2015)	87
Table B.3 Rainfall data collected by Suncor weather station (2015)	88
Table B.4 Test cell tailing pouring data.....	88
Table C.1 Number of occurrences where footprint resulted in specified relevance (2014)	95
Table C.2 Percentage of occurrences where footprint resulted in specified relevance (2014).....	95
Table C.3 Number of occurrences where footprint resulted in specified relevance (2015)	96
Table C.4 Percentage of occurrences where footprint resulted in specified relevance (2015).....	96
Table D.1 Weight factor (Δ/γ) and temperature	97
Table D.2 0.75 Ra expressed in equivalent evaporation (mm day^{-1}).....	98
Table D.3 Values of theoretical black body radiation (mm of water)	99
Table D.4 Preliminary estimates of the mineral production of Canada (Natural Resource Canada, 2016)	100
Table D.5 Summary of Alberta Oil Sands plant statistics (Alberta Energy Regulator, 2016) ...	101

1 Introduction

1.1 Background Information on the Oil Sands

All modern mining operations go through six stages: consultation, exploration, evaluation, development, production, and closure. Each stage of the mining project has its own set of obstacles to overcome. During consultation, companies must engage the communities and gain a social licence to mine; without community support, a project cannot go through. Exploration and evaluation are when a company evaluate and estimate what will be found once the project starts. At these stages, the employees require years of experience with the specific commodity and geology of the area, and understand that most of the project will not make it past this point. If the project does make it to the development and production stages, this is when companies need to follow through with their plans and promises, which can be difficult, since no amount of exploration and statistically analysis can fully prepare one for what is found. However, assuming the project can be carried out according to the plan, and then the final stage is closure of the mine.

Mine closure is one of the most complicated stages, not only because engineers need to work with natural systems, which are difficult to predict, but they must also predict how the manmade landforms will behave for the next 100 years. Unfortunately, too many mining projects have approached their mine planning in a chronological fashion, and deal with the issues as they arise, when they should be planning with closure in mind. Only in recent years has the social demands for a more sustainable form of mining started to change the mindset from we-will-deal-with-it-as-it-comes to what-are-all-the-foreseeable-problems-and-how-can-we-avoid-them. In 2013, it was reported by the Government of Alberta that more than 976 million m³ of fluid fine tailings (FFT) has been produced since 1967 (Alberta Energy, 2017) and in general for every barrel

(0.15 m³) of crude oil produced, 0.25 m³ of mature fine tailings (MFT) is created (as cited in Beier & Sego, 2007). The oil sands industry has been researching methods to resolve the MFT problem for years; however, there has yet to be found a single, easy-to-implement solution.

There are several stages in a tailings management operation: the slurry waste is created when bitumen is extracted from the sand, and is then pumped to a large surface tailings ponds, where it is left to dry for several days. When the tailings are placed in the containment pond, they segregate; the large particles, also called coarse tailings (CT), settle on the beach, while the water is released to the surface, and fluid fine tailings (FFT) are created in the central region of the pond. During this stage, most of the water is released and recycled back into the system. The FFT consist of clay and silt particles that remain suspended in the water. The FFT material is left to settle for three to five years to increase the solids content from 8% to 30%-35% (OSRIN., 2010). After the material has settled for several years, the tailings are referred to as mature fine tailings (MFT). The production of MFT creates are operational problems, such as how to remove the remaining water from the MFT to create a material that is trafficable and reclaimable.

Common methods of dewatering for many types of mines that create a tailings slurry are thin lift deposition and atmospheric drying; these methods require large areas to be sterilized, and long periods of sun. In 2016, the oil sand industry produced 66 million m³ (415 million barrels) of crude bitumen and mined 651 million tonnes of oil sands (Alberta Energy Regulator, 2016). The production of oil sands almost equates to the production of all other mining in Canada, 615 million tonnes of metal and non-metal material (Natural Resource Canada, 2016) and assuming all the mines included produce tailings and that the ratio of ore to tailings is the same for all mines, oil sands produce as much tailings annually as all mines in Canada. Note, that while this can be

considered as a gross overestimation, as quarry mines produce no tailings, and in metal mines the tailings to final product is much lower.

While atmospheric drying of tailings is practical and sustainable for other types of mine in Canada it becomes a problem of lack of space for the oil sands, due to large volume of ore that is processed annually. Suncor has found that the optimal lift height at which to pour MFT is 15 cm (18 cm maximum allowable); lifts could be poured in smaller increments, however, this not possible operationally. Equipment can only be moved so quickly and systems are not flexible enough to cycle through several ponds in a day; therefore, the drying process is operationally limited (Keith Everard, personal communication, December 15, 2015). The other factor that complicates tailings management is the fact that for most of the year the ground is frozen, and covered in snow, with temperatures well below zero, which is not as optimal as at other operations in Chile or Australia.

Operations have started investigating adding other system or stage in the tailings management processes such as filtration systems, centrifuge systems, electrolysis, co-disposal methods, plant dewatering, or adding chemicals or biological products: thickeners, flocculants, and bacteria (OSRIN, 2010). However, these additions have been found to be either not effective in large scales or uneconomically feasible. Currently, centrifuge and adding flocculants appear to be the most promising. Shell and Syncrude have tested the use of a centrifuge on a small scale and Syncrude proceeded to the next stage in 2012 and constructed a 2 billion CAD centrifuge plant (Canada's Oil Sands Innovation Alliance, 2012a; Syncrude Canada Ltd., 2016). The plant construction is complete, but it is not currently operating at its full capabilities. Suncor decided to focus on chemical additives, rather than physical forms of separation, and implemented the use of flocculants (Canada's Oil Sands Innovation Alliance, 2012b), but like the large centrifuge plant,

when the technology was applied on a larger scale, the results were not as good as expected. Therefore, thin lifts and atmospheric drying remains the main form of managing MFT, and the question becomes: has this form of tailings management being properly quantified?

1.2 Background Information on MFT Drying

During the drying of MFT, there are three stages of evaporation: initially, the evaporation rate is atmospherically driven, and actual evaporation rate is equal to potential evaporation (Wilson, Fredlund, & Barbour, 1994). As the MFT become unsaturated and can no longer meet the atmospheric demands, the evaporation rate decreases rapidly. At this point, the soil is in stage II of drying, where both atmospheric conditions and soil properties, such as permeability, determine the evaporation rate. As water is removed from the soil, soil suction increases and the permeability of the MFT decreases since the void spaces are no longer connected (Wilson, Fredlund, & Barbour, 1997), and the soil has reached stage III of drying. The evaporation rate effectively approaches zero, since the soil is at its residual water content (Newson & Fahey, 2003).

Currently, companies are using drying models that are based on historical potential evaporation rates measured using evaporation pans that are scaled down using factors determined from empirical data and field observations. This drying model will be referred to as the simple model. Alternatively, Suncor is developing a complicated model that uses a stochastic engine to account for different processes that occur after the MFT is placed. The complicated model does not assume a constant evaporation rate for an entire month, and accounts for other process (other than atmospheric drying) to occur after the MFT is placed. For example, once MFT with flocculant is placed in a drying cell, the first 24hrs of initial dewatering is assumed to be flocculant driven. The flocculated water is forced to the surface and is drained immediately to be recycled. Therefore,

for the first 24 hrs there's little to no evaporation (Keith Everard, personal communication, December 15, 2015). However, neither model has been calibrated with actual evaporation rates.

1.3 Background Information on Evaporation Measurement Methods

Evaporations rates can also be indirectly measured using lysimeters and evaporations pans. Lysimeters are cylindrical containers that take soil samples. The soil sample is weighed then replaced back to its original location, then re-weighed after a certain amount of time. The change in mass corresponds to how much water it lost and is therefore assumed to equal the actual evaporation rate. Evaporation pans are the simplest method for estimating evaporation but also the most inaccurate, since evaporation pans measure potential evaporation rather than actual evaporation. Potential evaporation is the maximum rate of evaporation if the water source is infinite for a given atmospheric demand (Arya, 2001). In other words, it does not consider soil properties, and only determines how much free water would evaporate in an area solely under climatic conditions at the site. Both these methods require constant monitoring: the evaporation pan needs water added to them periodically and the lysimeter weight needs to be measured as often as necessary. The measurements are daily or hourly and therefore not continuous.

The eddy covariance method requires the use of a sonic anemometer to measure wind direction and speed, and a gas analyzer to measure gas concentration and atmospheric variables. The eddy covariance method relies on turbulent flow, which creates eddies that flow through the instrumentation. Changes in temperature, pressures, and gas concentration are measured at rates of 10 to 40 Hz, and then averages and variances of the variables are calculated in 10 or 30-minute intervals. The eddy covariance method and Bowen ratio method take continuous measurements and do not need to be monitored once properly installed, only maintained. The eddy covariance method is generally used for agricultural and natural ecosystems; however, there have been several

studies carried out on mine sites to determine water balance of waste landforms, growth productivity of vegetation covers, and greenhouse gas emission rates from tailings ponds (Brown, 2013; Carey, Barbour, & Hendry, 2005; Carey, 2008).

1.4 Objective of Research

The purpose of the research was to determine how an Eddy covariance system should be installed in a tailings pond setting, and what will be the major benefits and obstacles of the system on site. If the system were to be installed for a long-term analysis of a tailings impound, the data could be used to properly calibrate drying models. Current drying models use potential evaporation reduced by a factor base on material properties, which is based on lab data. Therefore, if these drying models could be calibrated with actual evaporation rates measured in the field, then the models would be more accurate and result in the proper quantification of water removed by atmospheric drying. This would lead to further optimization of tailings management; actual evaporation rate would be obtained without the need to disturb or interrupt operation flow.

1.5 Thesis Outline

The first chapter of this thesis has provided background information on the issues with MFT in the oil sands, and what the current drying (evaporation) models are based on. Chapter 2 presents a literature review and summarizes previous research completed on evaporation of tailings ponds and the use of the eddy covariance systems on mine sites. Chapter 3 provides a brief explanation of relevant theories. Chapter 4 describes the instruments and methods used in the field. The evaporation results from the field are presented in Chapter 5 and discussed in Chapter 6. Finally, Chapter 7 states the conclusions of the research.

2 Literature Review

Fujiyasu et al. (2000) completed a field investigation comparing different methods (evaporation pans, Bowen ratio, and micro-lysimeters) for measuring actual evaporation rates off freshwater tailings surfaces. The study was carried out over a 6-month period on clayey tailings slurry in the southwest of Western Australia. In 2003, Newson and Fahey did a similar study on saline tailings of a gold mine. Carey et al. (2005) measured actual evaporation rates on a dump surface of a uranium mine using the eddy covariance method, and then later, Carey (2008) did a study on the growth productivity and water balance of a reclaimed overburden pile in the oil sands. Most recently, Brown (2013) carried out research on greenhouse gas emissions of oil sands tailings, using the eddy covariance system.

2.1 Estimating evaporation rates on freshwater tailings using evaporation pans, Bowen Ratio station, and micro-lysimeters

The Fujiyasu et al. (2000) conducted a study on the evaporation of freshwater tailings at an Australian mining operation, Yoganup North Mine, which is located 200 km south of Perth. Different mines (e.g., oil sands, alumina, gold, nickel, and iron) all over the world use atmospheric drying as a method for their tailings to undergo sedimentation and consolidation to achieve the required strength and density, the main difference between them being the production output rate. Yoganup North Mine used hydraulic separation to remove the clay from the sands; this produces fine tailings or slimes composed of kaolinite (80%), quartz (10%), and goethite (10%). The slimes (2000% to 3000% water content and 3% to 5% solids content) are pumped to large shallow containment ponds, where sedimentation rapidly occurs and the surface water is recovered. At this stage, the tailings are typically 350% water content and 22% solids content. Once the ponds are

full, they are left to dry for 6 months or more, after which they are remined and mixed back into the sand fraction for the backfilling of the open pit. Fujiyasu et al. (2000) wanted to quantify the evaporation behaviour of clayey tailings slurry, since the evaporation potential is not constant year-round, and depends not only on the atmospheric evaporative demand, but also on the material that is being dewatered. Like the oil sands, being able to predict how long a lift will need to dry to reach the required strength and density is important for tailings management.

It was observed that the tailings surface desiccated, due to the rapid change in volume (similarly to the oil sands tailings). Due to previous field and laboratory tests, it was understood that once the cracks are formed, evaporation occurs at both the horizontal surface and in the vertical surfaces of the crack (as cited in Fujiyasu et al., 2000). It was further suggested that once horizontal surface evaporation stops due to the crust formed on the surface, vertical evaporation from the cracks becomes the main source of evaporation. At the time, the numerical modelling of tailings sedimentation and consolidation was a one-dimensional moisture flow model and therefore could not account for the evaporation produced from the cracks. This suggests that the models may underestimate the evaporation rate off the tailings ponds.

The climate at the Yoganup North Mine experiences cool, wet winters and hot, dry summers with an annual precipitation of 818 mm and an annual Class A pan evaporation of 1,200 to 1,400 mm (as cited in Fujiyasu et al., 2000); the average annual temperature is 16.2°C. The dominant wind direction in the summer and autumn was southeast and southwest; during the spring, it was southwest and northwest, and in the winter, it was mainly southwest. Their study focused on effects of shrinkage cracks on evaporation and measured evaporation rates from the entire intact horizontal surface with the vertical surface of cracks. They limited their crack formation observations to a 5 m by 5 m crack observation zone (COZ), and measured the dimensions of the

cracks (depth, width, and length) every few weeks. Water content and vane shear strength profiles were frequently taken in the area surrounding the COZ and finally, the settlement of the tailings was measured relative to the tops of two steel rods. A Class A evaporation pan (1.22 m in diameter and 0.25 m deep) was set up adjacent to the test site, and potential evaporation rates were compared to the evaporation rates from the tailings surface.

During the 12-month period of their field investigation, they experienced total rainfall of 815 mm and a cumulative evaporation of 1,749 mm, which results in a net evaporation of 934 mm. Readings were taken every morning. The surface evaporation was estimated directly using the micro-lysimeter method and indirectly using a Bowen ratio weather station. The micro-lysimeter method uses a 100-mm diameter and 100 mm long sample tube made of PVC pipe with sealed base to extract a sample that was weighed initially and 24 hours later. A similar process was used for measuring the evaporation in the cracks, except a thin-walled aluminum alloyed sampler (65 mm width by 65 mm depth by 400 mm length) was used, and the samples extracted were separated into three sections to get a profile. The Bowen ratio weather station was composed of a pyranometer and net radiometer (to measure net radiation), humidity and temperature sensors located at 1 m and 2 m above the surface (to measure sensible heat), and temperature and heat flux sensors (to measure soil heat flux).

The conclusion of this study for Yoganup North Mine was that evaporation estimates were carefully performed and monitored constantly, which resulted in a good overall estimate of evaporation, but that the process may not be practical for all sites. The cracks that formed due to shrinkage of the tailings surface resulted in a ratio of initial surface to exposed cracked surface of 1:4 with 80% of the evaporation occurring from the cracks once a crust was formed on the horizontal surface. The Bowen ratio weather station method was preferred to the micro-lysimeters

because it allowed for constant monitoring and accounted for both the evaporation at the surface and in the cracks, while micro-lysimeters required two sets of measurements; in other words, using only the horizontal surface measurements would not have been enough to estimate evaporation of the tailings. Initially, the evaporation of the tailings surface was similar to the pan evaporation. However, once the cracks were formed, the unit evaporation per surface area could be much higher than the pan rate due to the 1:4 ratio. Finally, it was determined that the one-dimensional consolidation and evaporation model could not model evaporation from the cracks. Nevertheless, a simple and crude adjustment method was suggested to more closely model the total evaporation rate.

2.2 Estimating evaporation rates on saline tailings using evaporation pans, Bowen Ratio station, and micro-lysimeters

Newson and Fahey (2003) studied the drying behaviour of saline tailings at a gold mine operation in Western Australia. Similar to freshwater tailings, once saline tailings are deposited and after the initial sedimentation has occurred, the material starts to desiccate and desaturate due to evaporation (Fujiyasu et al., 2000). The dewatering of the material increases its density and shear strength. Having a more complete and accurate understanding of the drying rate of the material is important for tailings management. The tailings are saline because hypersaline ground water is used in processing with a salt concentration (C) of up to 0.2 (mass of salt divided by mass of solution), which can cause the tailings to have a $C=0.26$. Unlike freshwater tailings, once the saline tailings are placed, a surficial salt crust is formed, as the water moves to the surface due to evaporation causing the accumulation of salt precipitates. These salt crusts have been found to reduce the evaporation rate from the tailings surface. Newson's and Fahey's goal was to determine how detrimental the salt crust is to the drying capacity of the tailings.

The upper bound of monthly evaporation was calculated using average daily extraterrestrial radiation (as cited in Newson & Fahey, 2003), which was adjusted for the site location; the total annual energy input was estimated to be 11.6 GJ m^{-2} . Knowing the heat of vaporization of pure water is 2.4 GJ m^{-3} , and considering that dust and water vapour would reduce the radiation in the air by 75%, an annual evaporation rate of 3600 mm was estimated.

Newson et al. (2003) also explain the different stages of drying for freshwater tailings and saline water tailings. In freshwater tailings, there are three distinct stages of drying. During stage I, the evaporation rate depends solely on atmospheric demand (climatic and environmental conditions), and the evaporation rate is equal to potential evaporation (Wilson et al., 1994). Stage II drying begins when the soil can no longer meet the evaporative demands and the soil surface has become unsaturated. In stage II, the evaporation rate decreases rapidly, and both atmospheric and soil properties, such as permeability, govern the evaporation rate. When the rate of evaporation approaches zero, the soil has reached its residual water content and is in stage III. In stage I of saline tailings drying, it was determined in laboratory tests that the salt in the tailings reduces the initial evaporation by a factor of 0.1 to 0.6 (Fahey & Fujiyasu, 1994). Depending on the salt concentration, and once the salinity in the pore water reaches saturation, a salt crust is formed (stage II). The salt crust causes the evaporation to drop drastically, even though the soil is still saturated (unlike the freshwater tailings). The salt crust acts as a barrier between soil and atmosphere. Furthermore, it increases the albedo of the soil, which reduces the tailings' ability to transfer moisture from the soil to the atmosphere and decreases the saturation vapour pressure of the pore fluid. An increase in albedo results also causes more reflection of short-wave radiation, therefore resulting in less energy to be used for evaporation. In stage III, the tailings and salt crust

desaturate and the salt crust disintegrates, at which point the material enters into stage IV. When it has reached its residual moisture content and has an effective evaporation rate of zero.

Newson et al. (2003) used similar equipment as Fujiyasu et al. (2000): micro-lysimeters to directly measure changes in water content of tailings samples and a Bowen ration weather station to do a complete energy balance. From their findings, it was concluded that micro-lysimeters appear to give an accurate measurement of actual evaporation, compared to the results from the Bowen ration weather station, and that using both methods would provide an accurate and inexpensive method to measure actual evaporation over a large field. The results showed that the salt crust drastically lowers the evaporation rate compared to freshwater tailings. The evaporation rate can be reduced by a factor of 0.2 over the drying period, which confirmed the laboratory findings. Finally, the assumed evaporation rate overestimated how much evaporation actually occurs, and needs to be drastically adjusted, which could have downstream effects on tailings disposal strategies.

2.3 Determining water balance of a waste rock pile using an Eddy Covariance system

Carey et al. (2005) completed a water balance analysis on a waste rock pile on a uranium mine located near Key Lake, Saskatchewan, to assess concerns associated with decommissioning of mine waste structures. Geochemical weathering is known to occur in structures containing sulphide material and the oxidation of sulphides can lead to acid rock drainage, also known as ARD. ARD results in the decrease of pH of water and therefore the increase in solubility of heavy metals. The main concern was the net percolation that occurs through the waste rock pile, which was indirectly estimated with direct the measurement of evaporation.

It was noted that there are several ways to measure evaporation, such as evaporation pans, micro-lysimeters, and Bowen ratio weather stations (Fujiyasu et al., 2000; Newson & Fahey, 2003); however, the eddy covariance system is the only method that can directly measure evaporative flux. It was also noted that the numeric models used to estimate evaporation are based on laboratory results, and have not been calibrated with actual evaporation rates (as cited in Carey et al., 2005). Therefore, the goals of the research were to directly measure evaporation using the eddy covariance system and to compare the results to the results from an evaporation model.

The waste rock pile at the uranium mine had a total volume of $2 \times 10^7 \text{ m}^3$ with a height of 28 m. It was composed of broken sandstone, had no plant cover, and was level. The mean volumetric moisture content of the mine waste dump ranged from 2% to 30%. The area has an annual precipitation of 481 mm, where 45% of the rainfall occurs during June, July, and August. The eddy covariance system consisted of a CSAT3 sonic anemometer, an open-path infrared gas analyzer (LI – 7500), and a CM3 pyranometer. The sonic anemometer measures the variables needed to calculate sensible heat, the sonic anemometer and gas analyzer are used to estimate latent heat, and the pyranometer measures the ground flux. The eddy covariance system took measurements at 10 Hz, and fluctuations were calculated in 30-minute intervals. A weather station was also installed to measure air temperature, relative humidity, net radiation, short-wave radiation, all-wave radiation, wind speed, and wind direction. Measurements were taken every 10 seconds and were averaged or cumulated in 30-minute intervals. The CM3 pyranometer was placed at 0.05 m depth.

Carey et al. (2005) used the eddy covariance technique to measure turbulent fluxes continuously, using the turbulent flow theory. The Schuepp et al. (1990) flux footprint analysis

was then carried out and the analysis showed that waste rock pile surface was being measured and not the surrounding area (i.e. 90% of the cumulative flux footprint was within 170 m of the tower).

The results showed that the evaporation regime of the waste rock pile was different from the surrounding forest. The albedo of the surface reduces the energy available for evaporation, and the lack of vegetation meant no evapotranspiration (water would drain rather than evaporate). Due to the lack of vegetation and the mine waste pile being well drained, only 145 mm of evaporation was measured compared to the 247 mm of potential evaporation calculated (using Penman's equation). A total of 236 mm of rainfall occurred during the 81 days of the study, which resulted in 91 mm of water percolating through the rock pile.

It was concluded that acid rock drainage could be a concern due to the large water gain of the waste rock pile, although if a vegetation cover were installed, this would reduce the albedo of the surface and increase the evaporation rate over the mine waste structure. The potential evaporation calculated using Penman's equation was 100 mm greater than what was measured by the eddy covariance system, but the evaporation can be measured to within 10% using simple modified models of the Penman equation. If an error of 10% is considered reasonably accurate, the site could use the modified models for operation and site management.

2.4 Estimating productivity of a soil cover system using an Eddy covariance system

Carey (2008) completed a study to determine the productivity of a reclamation soil cover at Syncrude Canada Ltd. Mildred Lake mine. Mine sites are required to reclaim disturbed areas to a state similar to or better than the state it was before mining occurred. In general, when reclaiming an area, the waste material is capped with soil that was salvaged during pre-stripping in attempt to

reproduce the original soil profiles. The success of the reclamation will depend on “its ability to promote the restoration of natural cycles and foster self-sustaining communities” (Carey, 2008). It was noted that although companies such as Fluxnet Canada, Euroflux, and Ameriflux have done studies on natural ecosystems, such as forests and wetlands, and agricultural systems, but there has been little biometeorological research on soil covers during mine reclamation. Understanding the water and energy balance of the soil cover is the best way to determine how successful the cover is. The focus of this study was to determine how much evapotranspiration occurs and how the energy is distributed during the different growing seasons. The results were then compared to atmospheric values for a boreal forest, and the energy distribution was related to atmospheric and surface conditions.

The study site was a saline-sodic clay shale overburden mine waste dump, also referred to as South Bison Hill. The dump was 2 km² (diameter of 500 m) by 60 m high. The landform was reclaimed in 2001 and 2002, and was capped with 0.2 m of peat-glacial till mixture, overlaid with 0.8 m of reworked glacial till soil. The area was fertilized and seeded in 2002. In 2003 (when the study began), the major plant species was foxtail barley, and in 2004, white spruce and aspen were planted to help with erosion. The other minor plant species included fireweed, sow thistle, and white and yellow sweet clovers. The climate of the area is classified as sub-humid continental; the mean precipitation is 456 mm (342 mm of which is rain), and the majority (67%) of the rainfall occurs between June and August.

Carey (2008) had two tower setups: the eddy covariance tower and supplemental tower (100 m away). The same eddy covariance system was used as the 2005 study: a CSAT3 sonic anemometer and an open-path gas analyzer (LI-7500). A fine-wire thermocouple was also installed, which was located at the centre of the sonic anemometer head. The system was approximately 2.9

m above the surface. The instruments also had a CNR1 net radiometer mounted 3.1 m above the ground, two heat flux plates (0.05 m below the surface) and ground sensors for soil temperature and heat storage, and atmospheric sensors for air temperature and relative humidity. Measurements were taken at 10 Hz and compounded in 30 minutes intervals with data were recorded by a datalogger. At the supplemental tower, there was a power source (four solar powered batteries), more meteorological sensors (temperature and relative humidity probes, and a rain gauge), and ground sensors (for soil moisture, suction, and temperature at varying depths of 0.05, 0.15, 0.25, 0.4, 0.95, 1.15, 1.25, and 1.8 m). Measurements were taken every 4 hours and recorded on a second datalogger. Finally, the leaf area index was estimated every 2 weeks using a LAI-2000 leaf area index meter and photographs.

Eddy covariance is known to underestimated turbulent fluxes; therefore, evaporation fluxes were adjusted checking the energy balance (as cited in Carey, 2008), and it was determined that the evaporation fluxes were underestimated by 17% for all measurement periods. Data were also removed if the friction velocity was below 0.1 m s^{-1} , if the measurements were taken during a rainfall, and/or if the flux data changed expectantly (if the mean of the variable was calculated over 30 minutes and if the variable was more than 1.5 standard deviations from the mean) it was removed. For a brief time period (half-hour), missing data were filled by linear interpolation, and for a longer time period, the turbulent fluxes were estimated using the mean diurnal variation method (as cite by Carey, 2008). Overall, approximately 21% of the data were either missing or rejected. The flux footprint analysis used was by Horst and Weil (1994) and it was determine that the peak flux was measured at a range of 70 to 110 m, and 95% of the cumulative footprint was within 200 m upwind of the tower and therefore relevant.

It was determined that the evapotranspiration rate off South Bison Hill was extremely different from the boreal forest. In 2003, when foxtail barley was dominant, the evaporation was higher than 2004 when the sweet clovers were dominant. This change in evaporation rates was attributed to the change in dominant plant species. In 2005, the evapotranspiration rates had similar values to mature aspen and black spruce forest, although there was poor vegetation growth. It was also determined that in years when there is average to above average rainfall, evapotranspiration equals rainfall, and therefore, the water table stays near the surface of the landform, which could result in deeper percolation and drainage of water and its contaminants. Overall, it was determined that as forest growth continues, the rate of growth will decline and energy balance will change. The site will continue to be monitored to document these changes.

2.5 Estimating greenhouse gas emissions from an oil sands tailings pond using an Eddy covariance system

Brown (2013) evaluated how much methane the oil sands tailings ponds produce using an eddy covariance system. When comparing the global warming potential of carbon dioxide to methane (as cited in Brown, 2013), methane is 25 times more harmful. As the human population continues to grow, so does the demand for fossil fuels, agriculture, and livestock, which increase in demand for mining, landfills, and waste treatment. In 2005, the global atmospheric concentration of methane was measured at 1,774 ppb, which is unprecedented (as cited in Brown, 2013). Methane is typically oxidized in the troposphere (the lower layer of Earth's atmosphere); recently, the oxidation rate of methane is less than the production rate of methane by humans and natural ecosystems, leading to the buildup of methane in the atmosphere.

In 2000 and 2007, a study was done by Siddique, which evaluated the emissions of methane from a tailings pond surface. Measuring these emissions normally requires the removal of the

tailings samples from the natural environment, which potentially affecting the methane flux measurements (as cited by Brown, 2013). Brown's research focused on testing the feasibility of using micrometeorological instruments on the tailings surface compared to the traditional flux chambers used in 2000 and 2007. The eddy covariance system and the inverse dispersion analysis of methane were used in the study.

The eddy covariance system consisted of a CSAT3 sonic anemometer, two open-path gas analyzers (LI-7700 and LI-7500A), atmospheric probes (temperature and relative humidity), and a datalogger. The software WindTrax and two infrared laser gas detectors were used for the inverse dispersion method. The WindTrax program also required the input of site and atmospheric data: surface roughness length, friction velocity, the Obukhov length, and the mean horizontal wind direction. For post-processing of the eddy covariance data, a program written in R was used to refine or correct the flux data. Several corrections were performed: a coordinate rotation was applied, using the double rotation method, a frequency response correction, the Webb-Pearman-Leuning (WPL) density correction, a temperature correction for the temperature measurement of the sonic anemometer, and finally, LI-7700 specific corrections related to the temperature and water vapour density (Li-COR Inc., 2010).

Measurements were taken at two different locations: a preliminary site (a biosolids holding cell) and an oil sands tailings pond. The preliminary test area was 115 m by 340 m (area of $3.8 \times 10^4 \text{ m}^2$), and the sonic anemometer was placed 1.68 m above the test site surface to limit the area measured by the system. The system was operational from April 26 to May 5, 2012, of which 57% of the data were lost due to power loss or non-ideal conditions. For the second site, the tailings pond was approximately $4.2 \times 10^4 \text{ m}^2$ and was elliptical in shape (major and minor axis of 1.5 km and 3 km, respectively). The tower was 7 m away from the edge of the pond, and the sonic

anemometer was installed 8.5 m above the tailings surface. Solar panels were also installed to power the system. Measurements were taken from July 11 to 16, 2012. For both sites, readings were taken at 10 Hz, and compiled in 30-minute intervals, and the two infrared laser gas analyzers were installed on the edges of the sites.

Two types of footprint analysis were carried out with the data: Schmid (2004) 50% footprint analysis, and Hsieh et al. (2000) 90% footprint analysis. The footprint analysis depends on similar atmospheric variables, including atmospheric stability (the Obukhov length), measurement height, and surface roughness length. Using the 50% footprint analysis at site one, the source area extends on average a distance of 15 m (maximum 59 m) from the sensor. For site two, the source area extends on average a distance of 61 m (maximum 280 m) from the tower; therefore, the 50% contour model was mostly within the tailings boundaries. The 90% footprint analysis determines that source area extends 253 m from the sensor for site one and 880 m from the tower for site two.

The results from the program written in R were compared to results that were obtained from EddyPro. In EddyPro, most of the default values were left unchanged, and without the frequency response correction, the differences between carbon dioxide and methane fluxes were 0.68% and 0.70%, respectively. However, when the frequency correction was included, the differences between calculated fluxes were 1.69% and 9.71%, respectively. The average methane emission rate over the tailings pond area was calculated to be 0.61 kg hr^{-1} or $3.48 \times 10^{-6} \text{ kg m}^{-2} \text{ day}^{-1}$, and 30% of the emissions were measured to be negative, which was not expected. The negative rates were determined not to be due to errors with the gas analyzer or the sonic anemometer, since the measurements were consistent with the methane concentrations measured by the lasers using the inverse dispersion analysis. No further comment was made on the findings.

It was concluded that the use of an eddy covariance system could be beneficial, as it provides flow rates of undisturbed areas, and that the footprint can be limited to be within the area of interest. The use of lasers for the inverse dispersion analysis, on the other hand, does not provide as much confidence in the estimation of gas emissions, since the system is only accurate in ideal conditions.

2.6 Chapter Summary

The research carried out by Fujiyasu et al. (2000), and Newson and Fahey (2003) show that drying models based on potential evaporation require calibration with estimates of actual evaporation rates. It was determined that the one-dimensional evaporation models could not properly account for cracks forming on the tailings surface, and in the 2003 it was determined that the soils ability to release water to the atmosphere is drastically decreased by the salinity of the soil. This shows that different components of soil can influence the soil's ability to exfiltrate water. In the oil sands for example, tailings can have residual oil, which could impact the tailings ability to dry, for example, since oil is hydrophobia and may increase movement of water. Overall, it shows that all soil properties need to be accounted for and considered. Unfortunately, models have not yet quantified all the known and unknown soil properties and input them into current drying models.

During site testing, it was found that the micro-lysimeters measurements were comparable to measurements using the Bowen ratio instrument (energy balance method), whereas evaporation pan measurements were too low or too high, which was expected as the evaporation pan does not consider any soil properties (cracks or salinity). However, the main disadvantage of micro-lysimeters is the constant monitoring (periodic weight measurements), which requires the disturbance of the tailings surface. Also, once a sample taken from the tailings surface, it is cut off

from the effect of the surrounding soil, and evaporation along the cracks needs to be measured separately.

In 2005 and 2008, Carey showed how the ECV system could be used to determine the water balance of a rock waste pile and measure productivity of a soil cover, and in 2013, Brown directly measured greenhouse gases for oil sands tailings. Although, the ECV system is meant to measure large open spaces, but it can be used for more limited areas with correct placement, proper selection of instruments, and using a footprint analysis to trim the data. Note that for all three studies, a different four footprint analysis method was used, which is due to type of equipment used, and variable available. Water movement through man-made materials is difficult to assess as each mine site creates its own version of the material. Reclamation of these man-made materials is becoming a crucial part of any mining operation. In order to reclaim this massive tailing pond structure or a waste dump, operations need to understand how water moves through the system, and how these materials behave in a natural environment; in order to achieve this an accurate drying model is required. Current drying models use potential evaporation, which may be sufficient for daily operation, but if they are overestimation evaporation rates, then this can create scheduling conflicts in the future.

The main advantage of using an ECV system is that it can be used for long term monitoring, or be moved to different sites when needed. It is limited to periods of warm weather when measuring water vapour, however during periods of cold the water movement is mostly subsurface, and any surface water is going from liquid to solid. ECV can also be used to analyse the greenhouse gases emitted on site; data could be used to show compliance with regulations, and for self-monitoring. The ECV system can be left to operate for months, after the initial installation, and the data can be remotely accessed and downloaded.

3 Relevant Theory

In terms of evaporation, a portion of the sun's radiation, reaches the surface this energy is used to heat the water (this is sensible heat). As the water continues to heat up the energy is used to change the phase of water (change from liquid to gas), which is referred to as latent heat. Instruments can measure the change in the flux of water in the atmosphere, which is equivalent to latent heat flux during the summer. Change in water content in the atmosphere is also equivalent to the evaporation rate over the surface. There is also a portion of the sun's radiation (energy) that remains within the soil or surface.

3.1 Surface Energy Balance

Direct measurement of water content in tailing impoundments can be difficult. The only way to do this is either by taking representative samples of the tailings surface or through measurements of changes of energy. By measuring energy, large areas can be studied without disturbing the surface or putting personal in harms-way. One of the main issues with tailings pond is that they are not safe to walk on due to low bearing capacity as a result of the lack of water being removed from the surface. Currently, the most economic way to remove water from oil sands tailings is through atmospheric drying. Energy balance is the follows the basic principle of energy conservation:

$$Q_s = Q_{rs} + Q_l + Q_e + Q_c \pm Q_g \pm Q_v \quad (Eq. 3.1)$$

Short-wave radiation (Q_s) enters the earth's atmosphere and is broken down into six different energies: reflected short-wave radiation (Q_{rs}), long-wave radiation (Q_l), latent heat (Q_e), sensible heat (Q_c), stored heat (Q_g), and heat transferred between materials (Q_v). The three radiation terms can be combined to be net radiation (R_n):

$$R_n = Q_s - Q_{rs} - Q_l \quad (Eq. 3.2)$$

And can be measured using a net radiometer.

As mentioned sensible heat is the amount of energy required to change the temperature of a substance without changing its phase. Latent heat is the energy absorbed or released by a substance when it goes through a phase change. In terms of evaporation, sensible heat is the energy used to heat up water and latent is the energy used for water to change forms (e.g. ice, liquid, vapour). When positive, then water is either melting or evaporating, when its negative, then water is freezing or condensing. During the summer, the two main phase changes are evaporation and condensation. Stored heat (also referred to as ground heat flux) is the heat transferred into the soil or in the case of large open waterbodies it is the energy that remains in the underlying waterbody.

Ground heat flux depends on mass density, specific heat, and temperature of the soil at some level (z). When ground heat flux is positive (the energy input exceeds the energy output) this is referred to as flux convergence, which means that the surface is warming. If ground heat flux is negative (energy output exceeds energy input) it is known as flux divergence, which implies the surface is cooling. If energy incoming is equal the energy outgoing (ground heat flux equals zero), since mass density and specific heat are constants and cannot equal zero, then the rate of change in energy storage must be equal to zero when temperature remains constant over time. For the eddy covariance method is assumed that the ground heat flux is not convergence or divergence, implying that over a period time (for example a 30-minute interval), temperature is constant.

Latent heat flux (also referred to as latent heat of evaporation) is the term of interest. There are two main methods for measuring the latent heat flux and sensible heat flux: the Bowen ratio method and the eddy covariance method. The Bowen ratio method measures net radiation, sensible

heat flux, and ground heat flux, and then solves for latent heat, whereas the eddy covariance method measures latent heat and sensible heat directly (Arya, 2001).

Once latent heat flux is measured then evaporation is equal to:

$$E = \frac{Q_e}{\lambda} \quad (Eq. 3.3)$$

Where E is evaporation (mm day^{-1})
 λ is specific evaporation heat (J kg^{-1})

Specific evaporation heat changes with temperature:

$$\lambda = (3147.5 - 2.13T_a) \cdot 10^3 \quad (Eq. 3.4)$$

Where T_a is ambient temperature (K)

Latent heat flux is determined using the Penman Method Ascension.

3.2 Hydrology

Using the Penman Method for open water surface as described by Shaw (2005), potential evaporation is:

$$E_o = \frac{\frac{\Delta}{\gamma} H + E_a}{\frac{\Delta}{\gamma} + 1} \quad (Eq. 3.5)$$

Where E_o is evaporation from open water
 Δ/γ is an empirical parameter depending on temperature (weighting factor)
 H is the heat available
 E_a is evaporation at saturation

Note that there are several variations of the following formulas, therefore the formulas relevant for open water evaporation is explained, as it is the most appropriate. The evaporation rate from open water is equivalent to the potential evaporation rate.

Heat available is equal to:

$$H = (1 - r)R_{in} - R_{out} \quad (Eq. 3.6)$$

Where R_{in} is incoming radiation (mm day^{-1})
 R_o is outgoing radiation (mm day^{-1})
 r is albedo

Heat available is also referred to net radiation. As previously mentioned, there are three types of radiation: short-wave radiation, reflected short-wave radiation, and long-wave radiation. The albedo of the surface is proportional to reflected short-wave radiation. In our case albedo of the tailings pond was assumed to be 0.05, which is the albedo of water and is reasonably accurate for saturated tailings.

Incoming radiation is equal to:

$$R_{in} = R_a(0.155 + 0.69n/N) \quad (Eq. 3.7)$$

where R_a is the solar radiation fixed by latitude and time of year (mm day^{-1})
 n/N is possible amount of sunshine

The approximate latitude of the test pond is 56.92° , and the amount of possible sunshine was estimated using the time for sunrise and sunset. If the data was taken between sunrise and sunset then n/N is equal to 1 (n/N was zero during the night), and if the 30-minute interval occurred during sunrise or sunset, N is equal to 30 minutes and n is equal to the amount of time after sunrise or before sunset.

The outgoing radiation is equal to:

$$R_{out} = \sigma T_o^4(0.56 - 0.09\sqrt{e_d})(0.10 + 0.90n/N) \quad (Eq. 3.8)$$

where σT_o^4 is theoretical black body radiation (mm day^{-1})
 e_d is actual vapor pressure (mm of Hg)
 n/N is possible amount of sunshine

The theoretical black body radiation is proportional to the ambient temperature (as seen in section 4.5) and the actual vapour pressure was measured using the ECV system. Blackbody radiation is the energy re-radiated by an object after it absorbed the energy, also referred to as thermal radiation.

Finally, the evaporation at saturation is equal to:

$$E_a = 0.35 \left(0.5 + \frac{u_2}{100} \right) (e_a - e_d) \quad (Eq. 3.9)$$

where u_2 is the mean wind speed at 2 m above the surface (miles/day)
 e_a is saturated vapour pressure (mm of Hg)
 e_d is actual vapour pressure (mm of Hg)

If measurements are not taken 2 m above the surface, then the u_2 is interpolated based on the actual height of the equipment. The saturated vapour pressure is calculated based on the ambient temperature and pressure.

3.3 Eddy Covariance Method

The eddy covariance method is used to calculate fluctuations in turbulent air. It can be used to measure atmospheric data, such as gas concentrations. It typically used to measure greenhouses gas and water, but can be calibrated and program to measure any gas.

The eddy covariance method relies on 9 major assumptions and turbulent flux theory (Burba, 2013):

1. Flux is fully turbulent
2. Measurements are assumed to represent an upwind area
3. Measurements are assumed to be inside the boundary layer of interest and inside the constant flux layer
4. Fetch and footprint are assumed to be adequate, and therefore flux is only measured in the area of interest
5. Terrain is horizontal and uniform
6. Density fluctuations are negligible
7. Flow divergence and convergence are negligible ($\Delta Q_g = 0$), due to small changes in temperature when data is compiled
8. The instruments can detect very small changes with a high frequency
9. The measurements are not distorted by the installation structure or the instruments

The air movement that is measured is turbulent. This implies mixing of the air, and therefore an exchange with surface and air. Without turbulent flow, water cannot leave the soil surface and enter the atmosphere. It should be noted that eddies are small when measurements are taken closer to the surface, therefore the height of the equipment is important and will dictate how far from the instrument measurement are taken. Smaller eddies rotate faster and therefore move or

transport gas at a higher frequency, so in order to properly assess the movement of gases, the higher the reading frequency should be used.

Once the data is collected, the data is compounded into 10 or 30 minute intervals, after which only measurements that are upwind (assumption 2) and within the area of interest are considered in the analysis (assumption 3). During the data processing, the major direction and distance of measurements are outputted. If the angle of measurement shows that the data is coming from behind the ECV system, it is removed the interpretation. Depending on the type of footprint analysis chosen, the output reading can estimate and define distance at which the majority of the readings were taken, and areas (width and depth of the footprint). Compound readings can be removed from the analysis if footprints reach too far outside of the tailings pond test cell (area of interest).

The environment is horizontal and uniform (assumption 4), as the type and composition of tailings material that is outputted is relatively consistent. The flux is not convergent or divergent; in other words, that temperature gradually increases or decreases during the day, implying there are small, negligible changes in temperature during the compound intervals (assumption 5 and 6). Density fluctuations are negligible, as the EVC is measuring a relatively limited small area (a single cell within a tailings pond), and therefore limited to measuring smaller eddies, and measure (assumption 6 and 7). The final two assumptions are met by using highly sensitive and accurate instruments and through correct equipment selection and placement. Depending on the environment and type of variables being analysed, the gas analyzer is selected accordingly.

Once the equipment is installed, different air measurements are taken. Once the data is collected and processed, the vertical flux is calculated. Below is the vertical flux (uncorrected) (Li-

COR Inc., 2015). Note that the mixing ratio and vertical wind speed are measured directly, and the dry air molar volume is calculated in EddyPro:

$$F_{H_2O} = \frac{1}{v_d} \overline{w' r'_{H_2O}} \quad (Eq. 3.10)$$

where

F_{H_2O}	is water flux ($\text{mmol m}^{-2} \text{s}^{-1}$)
v_d	is dry air molar volume ($\text{m}^3 \text{mol}^{-1}$)
w'	is mean standard deviation of vertical wind speed [m s^{-1}]
r_{H_2O}	is mean standard deviation of mixing ratio of water [mmol mol^{-1}]

The sonic anemometer measures the vertical wind speed and the gas analyser measured the air molar volume, and the mixing ratio of water. This raw data is then inputted in Eddy Pro, which calculates the average and standard deviation of these variables and calculates the flux of water. The EddyPro software also carry out corrections for: Webb-Pearman-Leuning (WPL) correction, axis rotation for tilt correction (double-rotation method), detrending and time lag corrections.

The WPL correction, also referred to as the compensation for density fluctuation, accounts for bias or error due to temperature. The axis rotation for tilt correction accounts for any vertical misalignment of the anemometer; the double-rotation method was chosen as it is recommended for homogenous and flat sites. For all remaining settings, the default selections were used.

3.4 Footprint Theory

There are several different types of footprint modeling methods, such as Kormann and Meixner (2001) and Hsieh et al. (2000), but the Kljun et al. (2015a) method as is measures the size and shape of the footprint. It is based on the LPDM-B model, which is valid for a wide range of boundary layer stratifications and receptor heights (as our setup is unique this was chosen). Although any other footprint analysis could have been used, the choice was limited by the type of data available; other footprint models, required more complicated inputs. Also knowing the extents of the footprint was especially important for our site as the test cell (area of interest) was limited.

The footprint of the data collected varies greatly depending on height of instrument and roughness of the surface. At higher heights, the ECV system is able to collect and analyse data over larger area, which is favorable for most cases. The smoother the surface, the larger the air eddies can be and travel before they are disturbed. Therefore, if the area of interest is relatively small, homogenous, and smooth, the equipment needs to be as close to the surface as possible to ensure that data is not collected too far from the instrument.

The environmental variables that are required for the footprint analysis are height of equipment, boundary layer, and roughness length. The height of equipment describes the instrument location, and is the distance between the sonic anemometer instruments and the surface of interest. The roughness length describes the surface that is being studied, and how turbulent the eddies will be. In nature, roughness length ranges from 0.001 cm (ice) to 5 cm (thick grass). For large open water surface the roughness length ranges from 0.01 cm to 0.06 cm. It was assumed that a tailings surface would be on the higher end of the range, due to crack formation.

The footprint analysis also requires calculated values, which are obtained after the data is initially processed in Eddy Pro: wind direction, variance of lateral velocity, friction velocity, and

Obukhov length. Wind direction is measured using the ECV system and the variance of lateral velocity is calculated during the data compositing in Eddy Pro, and refers to the vertical wind speed. Friction velocity (also referred to as shear velocity), shear force of the wind eddy exerted on a surface expressed in velocity units:

$$u_* = \sqrt{\tau_o / \rho} \quad (\text{Eq. 3.11})$$

where u_* friction velocity [m s^{-1}]
 τ_o shear stress at the surface [N]
 ρ is air density [kg m^{-3}]

Friction velocity can also be calculated using wind speed measurements:

$$u_* = \left(\overline{u'^2} + \overline{v'^2} + \overline{w'^2} \right)^{\frac{1}{4}} \quad (\text{Eq. 3.12})$$

where u' is the mean standard deviation wind component along the anemometer x-axis
 v' is the mean standard deviation wind component along the anemometer y-axis
 w' is the mean standard deviation wind component along the anemometer z-axis

The Obukhov length is defines the stability conditions of the atmosphere, and is equal to:

$$L = \frac{T_p \cdot u_*^3}{\kappa \cdot g \cdot \left(\frac{H_o}{\rho_a \cdot c_p} \right)} \quad (\text{Eq. 3.13})$$

where T_p is temperature ($\text{mmol m}^{-2} \text{s}^{-1}$)
 u_* is friction velocity (m s^{-1})
 κ is von Kármán's constant, which is equal to 0.41
 g is gravitational acceleration, which is $9.81 \text{ [m s}^{-2}]$
 H_o is sensible heat flux [W m^{-2}]
 ρ_a is moist air mass density [kg m^{-3}]
 c_p is moist air heat capacity ($\text{J kg}^{-1} \text{K}^{-1}$)

If the Obukhov length is positive then the atmospheric conditions are stable, if negative then they are unstable, and if infinitely large than the conditions are neutral. In physical terms, the

Obukhov length is the height at which turbulence is generated more by buoyancy than by wind shear. For there to be turbulent flow we need unstable conditions.

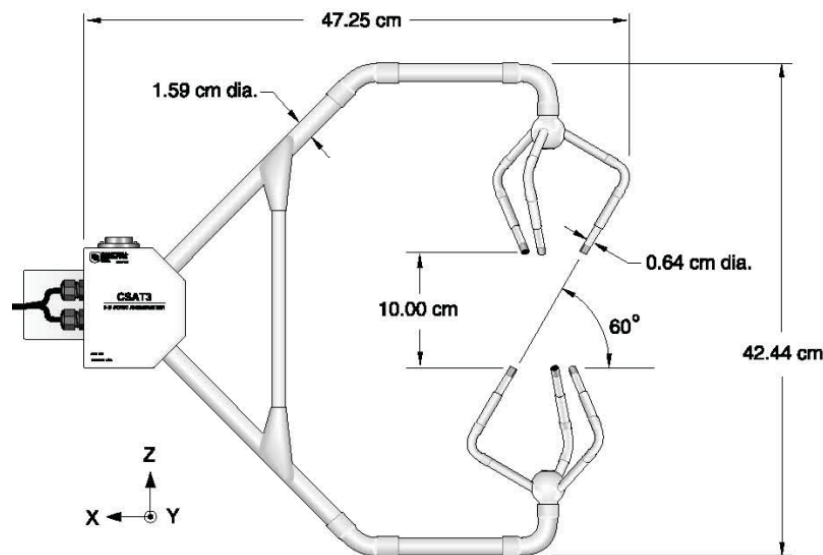
Using the information above the footprint of the flux is calculated for each 30-minute composite using a script published by Kljun et al. (2015b). The Kljun et al. (2015a) method allows for several contribution areas to be calculated at once. In general, most footprint models only consider a specific contribution area. Each contribution area shows where certain percentage of data was collected from, which aids in the data processing. Data is considered to be more precise if the majority (more than 75%) of the data to be from the test cell.

4 Methods

4.1 Instruments

The eddy covariance system used was a CPEC200 closed-path eddy-covariance system provided by Campbell Scientific Inc.; it is composed of two main components: the CSAT3 three-dimensional sonic anemometer and the EC155 CO₂ and H₂O closed-path gas analyzer. The closed-path gas analyzer requires the use of an EC100 electronics module and CPEC200 pump module. Data collected from the eddy covariance was stored in a CR3000 micrologger, and wirelessly transmitted with a IPn3Gb cellular modem and a C2444 9dBd yagi antenna. The entire system was powered by two solar panels (125 W) and four 12V batteries.

Figure 4.1 CSAT3 Sonic Anemometer



Source: *Instruction Manual: CSAT3 3D Sonic Anemometer* (Campbell Scientific Inc., 2015a)

The CSAT3 sonic anemometer (as seen in Figure 4.1) measures wind speed along three non-orthogonal sonic axes, which are then transformed into the orthogonal wind components (u_x , u_y , and u_z) with reference to the anemometer head. Therefore, when setting up the sonic

anemometer it is important that the equipment (the tripod and instruments) be level. It also measures the speed of sound and virtual temperature. It can be programmed to measure at a frequency of 1 to 60 Hz. For our study, the rate was set at 10 Hz. The equipment operates best in temperatures range of -30 to 50°C, at wind speeds less than 30 m s⁻¹ and azimuth angles between $\pm 170^\circ$. Therefore, readings from directly behind the equipment have a high inaccuracy, due to the equipment disturbing the air flow. The instrument was connects to the EC100 electronics module, which connects to the datalogger (Campbell Scientific Inc., 2015a).

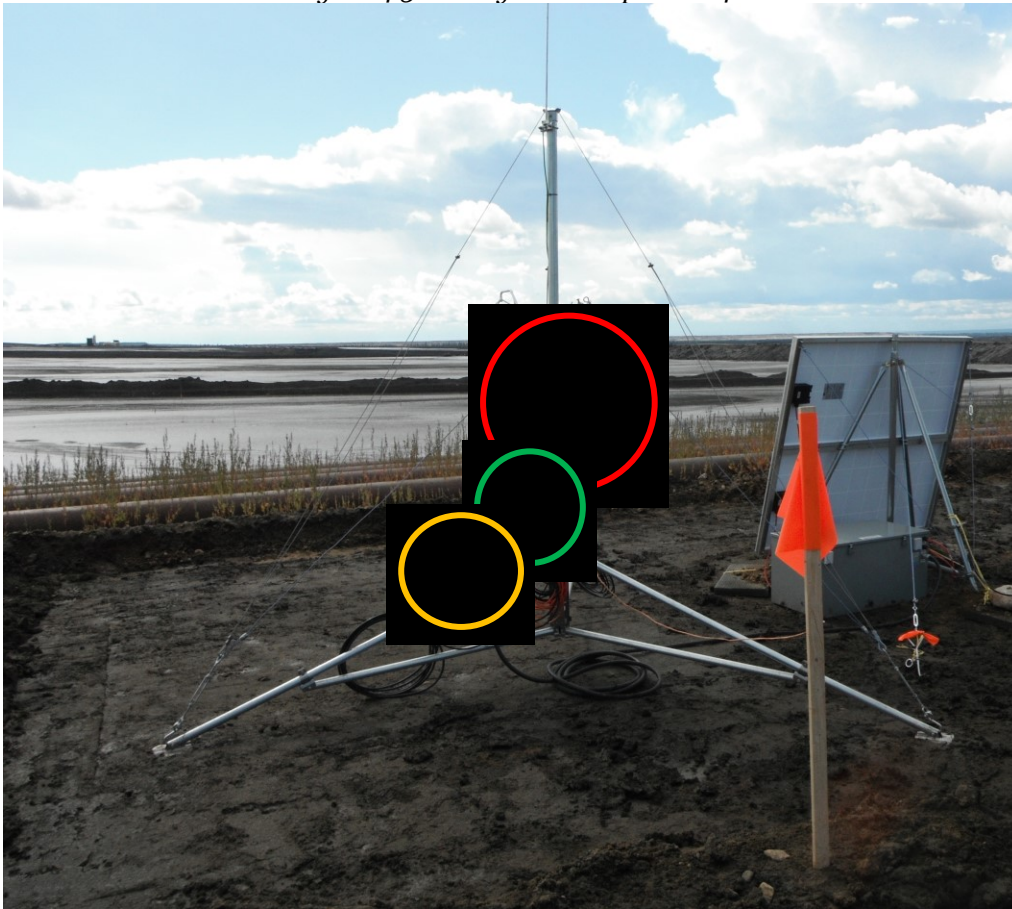
Figure 4.2 EC155 Closed-path Gas Analyser



Source: Instruction Manual: EC155 CO2 and H2O Closed-Path Gas Analyzer (Campbell Scientific Inc., 2015b)

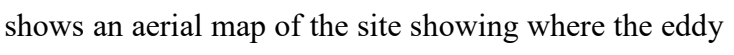
The EC155 closed-path gas analyzer (as seen in Figure 4.2) takes in situ air samples and measures molar mixing ratios of carbon dioxide and water vapour by mid-infrared absorption. It also measured the samples cell temperature and barometric pressure. The EC155 can be programmed to take measurements at a rate of 100 Hz, but it was programmed to take reading at 10 Hz. A 10-micron filter was placed on the sample head, which was later changed to 40-microns due to the high amount of dust in the area. The equipment's ideal operation environment is between -30 to 50°C. It connects to the CPEC200 pump module and the datalogger through the EC100 electronics module. The pump module was operated with a differential pressure of ± 7 kPa in order to maintain accuracy (Campbell Scientific Inc., 2015b). Figure 4.3 shows a typical ground installation on site in 2014.

Figure 4.3 ECV System setup in 2014



Photograph taken at site during the first installation (2014) facing south-west. The datalogger (circled in red), the electronics module (circled in green), and the pump module (circled in yellow) were all mounted on the tripod below the ECV instruments. Beside the tripod are the solar panels and the battery bank.

4.2 Site Description

During the summer of 2014 and 2015, the eddy covariance system was placed at Suncor's test cell. This cell is heavily instrumented and closely monitored. The entire pond system was approximately 270 m by 530 m, but there was a berm placed between the test cell and the remainder of the pond, which limited our area of interest to 270 m by 80 m (21,600 m²) and is extremely small for this type of method.  shows an aerial map of the site showing where the eddy covariance system was erected.

In 2014, the system was erected on the north-side of the test cell, although it was found not to be ideal. During the fall (September to November), the prevailing wind direction for northern Alberta is from north to south and for the east corner of Alberta is from south to north (Government of Alberta, 2010). The eddy covariance system should have ideally been installed downstream and perpendicular to the major wind directions. However, the presence of the scaffolding on the east side of the test cell caused a large zone of disturbance. In addition, there was very limited space on the east side of the test cell and access to the test cell was limited. Figure 4.5 shows how the system was installed. The system installed on the dyke was approximately 9 m away from the edge of the pond and 4 m above the pond surface, which made the dyke a leading edge that could disturb the air flow and lead to poor readings.

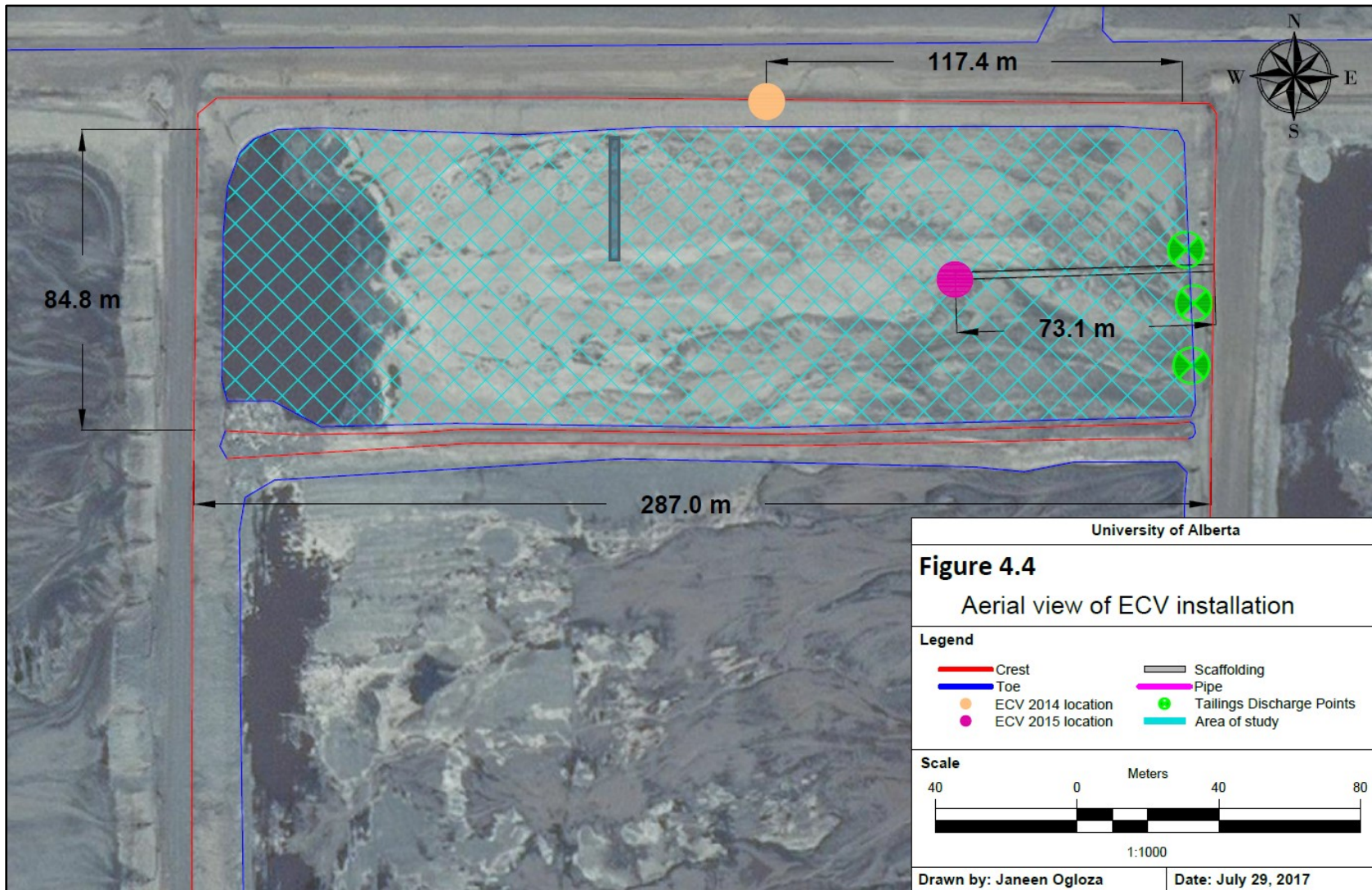


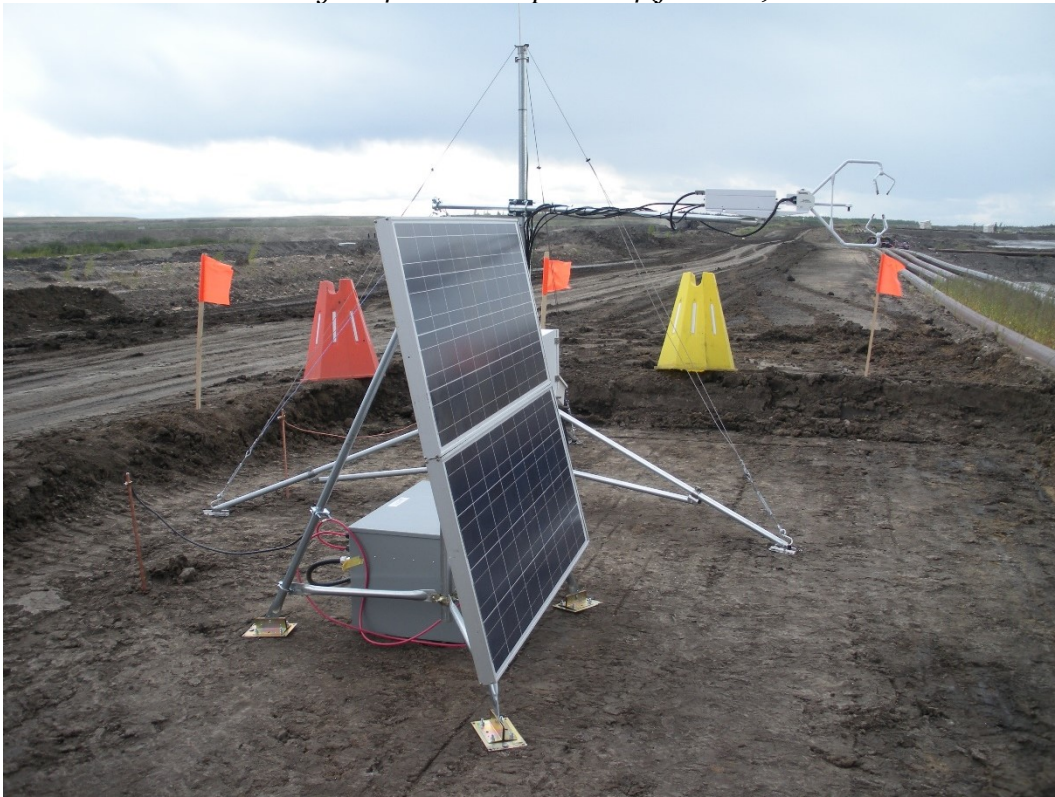
Figure 4.5 ECV Setup in 2014 (facing south-west)



Photograph taken at site during the first installation (2014) facing south-west. Due to safety and maintenance reasons, the equipment had to be 2 m away from the pipelines. Overall, the equipment was 9 m away from the crest of the tailing pond cell.

Pylons and flags were initially used to protect the site personnel and the equipment as seen in Figure 4.6. Later, they were replaced with a larger berm. Although the location did not have heavy traffic, it was used for maintenance and operations and was not isolated. This location was not ideal since personnel and vehicle traffics could affect the water flux measurements, due to the sensitivity of the equipment.

Figure 4.6 ECV Setup in 2014 (face east)



Photograph taken at site during the first installation (2014) facing east. To ensure equipment visibility and personnel safety, pylons and flagging was placed around the equipment. Eventually, a larger berm was also placed around the equipment.

The northward, eastward, and vertical separation describes the distance between the center of the sonic anemometer and gas analyser head. The northward separation is the distance parallel to the gas analyser and the eastward separation is the perpendicular. The northward separation was approximately 17.3 cm, the eastward and vertical separation were zero, since the gas analyzer head and the center of the sonic anemometer were aligned.

In 2015, the system was installed at the end of scaffolding that extended into the drying cell, which was much more ideal. This location limited the amount of readings that would be disturbed by traffic and was much more isolated from other activities. Originally, it was assumed that there was a prevailing wind coming from the south, but this was not supported by the 2014

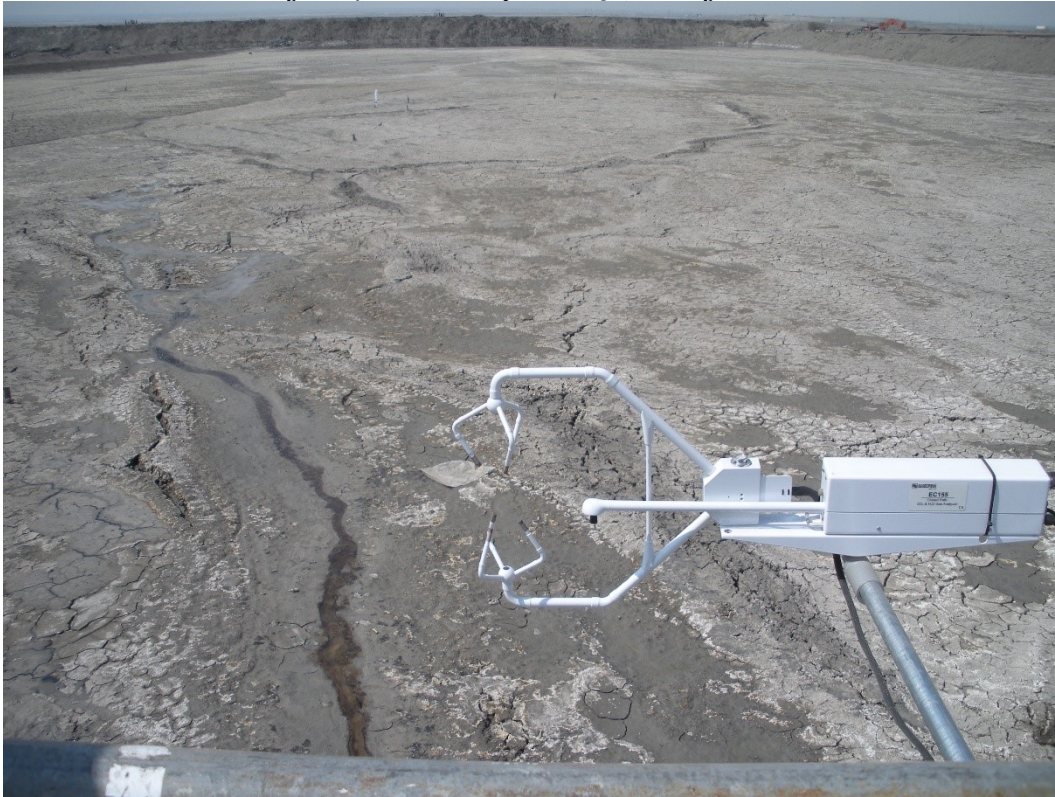
data, so the ECV system was installed in the center the test pond so measurements could be gathered from all directions. This configuration is referred to as an omni-wind direction setup. Figure 4.7 and Figure 4.8 shows how the instruments were installed directly on the scaffolding. The system was 80 m away from the east edge and 40 m away from the north edge and approximately 1.5 m above the tailings surface. The second setup was isolated and other than the scaffolding on the east side there, the amount of disturbed area was limited compared to setup in 2014.

Figure 4.7 ECV Setup in 2015 (face north-west)



Photograph taken at site during the second installation (2014) facing north-west. Equipment was installed at the end of the scaffolding within the test cell.

Figure 4.8 ECV Setup in 2015 (looking down)



Photograph taken at site during the second installation (2015) looking down into the tailing test cell. The ECV instruments were on a cross-bar and placed 0.8 m away from the scaffolding edge.

4.3 Field Campaign 2014

During the data collection period in 2014, the equipment was erected on August 30, 2014 and left to run until October 10; however, only measurements from September 4 to September 28 were used for data analysis. Due to a limited memory, once the amount of data collected reached approximately 2 GB, the program was setup to overwrite earlier measurements. The data collection stopped on September 28 at 02:45:17.1, and it was found to be due to issues with the pump module. When decommissioning the system, a large pellet of dirty was found inside the tubing that was connected to the pump module. The pellet was most likely formed because the tubing was not properly secured to the inlet or outlet. The pellet would cause the equipment to overheat, therefore in order to protect itself it would stop operating at 00:00.5 for approximately 10 minutes every

morning, until it was too much for the system, at which point it shut down. The problem was corrected for the 2015 field campaign.

The datalogger ran on a program written in CRBASIC (provided by Campbell Scientific, altered slightly to give desired outputs), which took direct measurements and processed data. The datalogger stored readings at a rate of 10 Hz, and calculated averages, standard deviations, and covariances of readings in 30-minute intervals.

As mentioned earlier, the site where the eddy covariance system was installed was not ideal, due to lack of isolation, being too far away from the surface of interest, and the leading edge created by the tailings pond impoundment. After the system was erected, a 0.5 m berm was built around the station to for the protection of both the site personnel and the equipment. However, the berm and the light-vehicle traffic also caused wind disturbance and therefore affect the readings.

4.4 Field Campaign 2015

The station was installed again on May 7, 2015. Other than being installed on the scaffolding, the only difference between the 2014 setup and the 2015 setup was the installation of an antenna that allowed for remote access to the equipment. Since the readings were remotely monitored every day, it was noticed that the differential pressure in the pump module was increasing. The pump module works best at a differential pressure of 0 to ± 3 kPa. On the May 19, it was noticed that the differential pressure was increasing (typically it remains at a constant of ± 2 kPa). The equipment can operate accurately until a differential pressure of ± 7 kPa, after which error can occur or the pump module could shut down.

A maintenance visit had been scheduled for May 25, where the filter on the gas analyzer head was upgraded from a 20-micron filter to a 40-micron filter. However, by the time the filter

was replaced, the differential pressure was above ± 7 kPa but the equipment was still operating normally, and the filter replacement was completed before any readings were lost. On May 29, the system went down for power related issues. The system was corrected and reset on June 5, but the sonic anemometer stopped working at June 13 at 23:02:03.5 hours, and there were no further wind readings until it was decommissioned on June 18. Due to the lack of wind readings, no footprint analysis could be completed and therefore the data collected after the June 13 was not considered in the analysis.

The second site where the station was erected (directly over the tailings pond surface) was more ideal. The only issue that carried over from the 2014 setup was that the tailings pond surface was limited to the test cell. Having such a limited area of interest is not typical for ECV systems, and therefore the data analysis was unique.

4.5 Data Processing

The data was processed in EddyPro version 6.1.0, which was created and supported by LI-COR Biosciences. The program required the information about the station location as summarized in Table 4.1:

Table 4.1 Instrument location information (EddyPro inputs)

	2014	2015
Altitude	378 m	376 m
Latitude	56°55'16.860" N	56°55'15.179" N
Longitude	111°17'58.600" N	111°17'56.332" N

And a description of the equipment (as summarized in Table 4.2), which was determined from the equipment manuals:

Table 4.2 Instrument information (EddyPro inputs)

Anemometer Info		Gas Analyser Info	
Manufacturer	Campbell Scientific	Manufacturer	Other
Model	CSAT-3	Model	Generic Closed Path
Instrument ID	a	Instrument ID	b
Height	4.0 m (2014)	Tube length	15.6 cm
	1.5 m (2015)	Tube inner diameter	2.7 mm
North off-set	180 °	Nominal tube flow rate	7.0 l/m
		Northward separation	15 cm
		Eastward separation	0
		Vertical separation	0
		Longitudinal path length	42.7 cm
		Transverse path length	7.4 cm
		Time response	0.01 s

Finally, the format of the raw files was described. For the processing options, statistical analysis, spectral analysis and corrections were left as the programs default.

Once the raw data was computed in EddyPro, the Kljun et al. (2015a) footprint analysis method was used. The functions to create and measure the footprints for each compile readings were provided (Kljun et al., 2015b) and the script created by the author to analyze the EddyPro outputs. It required to following inputs: friction velocity, Obukhov length, wind direction and variance of lateral velocity. The equipment and environmental variables include:

- Height of instrument (4 m in 2014, and 1.5 m in 2015)
- Roughness length = 0.006 cm (Brutsaert,1982)
- Height of boundary layer = 1700 m (Portelli, 1977)

Footprint contribution maps were created for 30%, 50%, 70%, 80% and 90%. Once the footprint was created for the each 30-minute interval, the footprint shape was analysed to determine how much of each footprint contribution curve fell within the area of interest (the test cell). Ideally, the 30% and 50% contribution footprints would lay completely within the area of interest, and at the very minimum more than half of the 70% contribution footprint would lay within the area of interest. The reading was considered more relevant depending on the shape of footprint area. Relevance, overall relevance, and percent data coverage were calculated. Relevance for the 30% contribution footprint that is equal to:

$$Relevance_{30\%} = \left(\frac{\text{Area of the 30\% footprint within the test cell}}{\text{Area of the 30\% footprint}} \cdot 30\% \right) 100\% \quad (Eq. 4.1)$$

Relevance for contributions footprints greater than 30%:

$$Relevance_{>30\%} = \left(\frac{AI_{higher\ footprint} - AI_{lower\ footprint}}{A_{higher\ footprint} - A_{lower\ footprint}} \cdot (FP_{higher} - FP_{lower}) \right) 100\% \quad (Eq. 4.2)$$

where AI is area of the footprint within the test cell (m²)
 A is area of the footprint (m²)
 FP is the footprint percent

For example, for the 50% and 90% contribution footprint, relevance is:

$$Relevance_{50\%} = \left(\frac{AI_{50\%} - AI_{30\%}}{A_{50\%} - A_{30\%}} \cdot (50\% - 30\%) \right) 100\% \quad (Eq. 4.3)$$

$$Relevance_{90\%} = \left(\frac{AI_{90\%} - AI_{80\%}}{A_{90\%} - A_{80\%}} \cdot (90\% - 80\%) \right) 100\% \quad (Eq. 4.4)$$

Overall data relevance (where N is the percent contribution footprint):

$$Overall\ Relevance = \sum_{N\%} Relevance \quad (Eq. 4.5)$$

Percent data coverage:

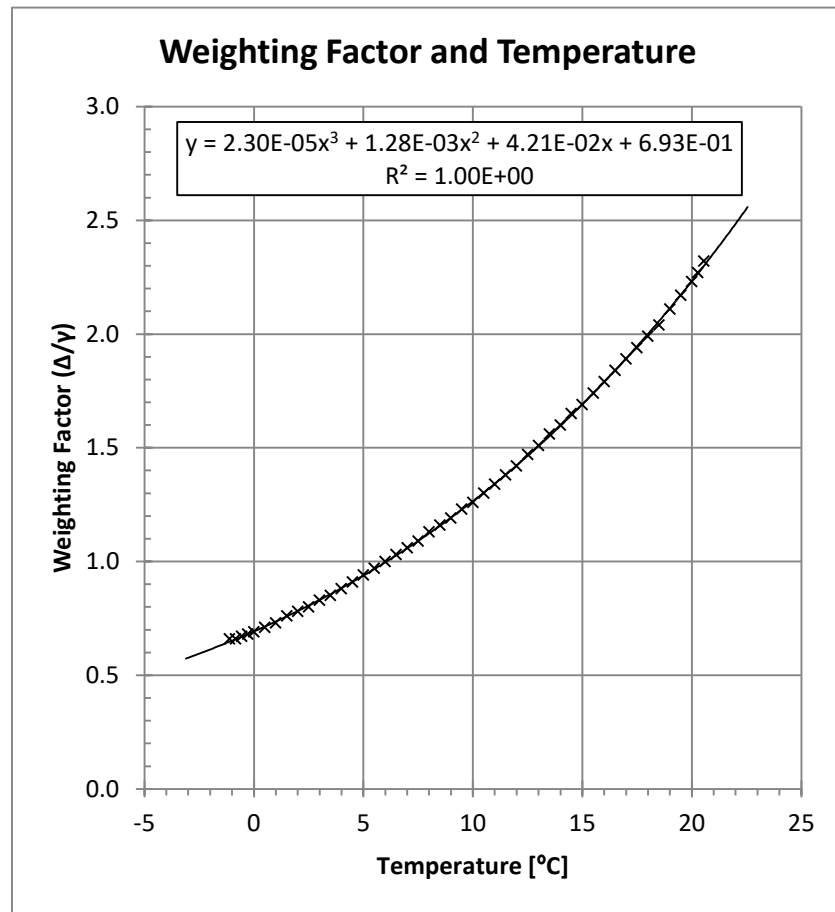
$$Coverage = \frac{\text{Area of the Footprint within the test cell}}{\text{Area of the test cell}} \cdot 100\% \quad (Eq. 4.6)$$

These three values were calculated for each 30-minute composite in order to compare changes in precision between 2014 and 2015, and to evaluate whether or not a composite would be considered in the data analysis. Overall relevance also estimates the percentage of data measured within the test cell. Ideally, the overall relevance would be greater than 65%.

Data quality was also considered when trimming the data. EddyPro has different quality flagging systems available, the one selected was the Mauder and Foken (2004) system. The Mauder and Foken (2004) system performs a steady state and developed turbulence tests provides the flag “0” for high quality fluxes, “1” for intermediate quality fluxes, and “2” for poor-quality fluxes (as cited in Li-COR Inc., 2015). The other systems available provide a finer flux flagging for more depth analysis; however, since the flagging was only used to remove poor quality fluxes, a more in-depth analysis would not be more helpful.

Once data was trimmed, then the potential evaporation rate was estimated. The data provided by Ministry of Agriculture, Fisheries and Food (MAFF, 1967) as cited in Shaw (2005) was used to calculate weighting factor (Δ/γ), incoming solar radiation, and theoretical blackbody radiation. The following plot shown in Figure 4.9 was created.

Figure 4.9 Weighting Factor (Δ/γ) in terms of Temperature



In Figure 4.9, a trend line was added to the data; the equation and R^2 are shown on the plot (data is found in Appendix D). This formula was used to estimate the weighting factor using the mean ambient temperature calculated by EddyPro.

Figure 4.10 Monthly Average of Solar Radiation (R_a) at different Latitudes in terms of Days

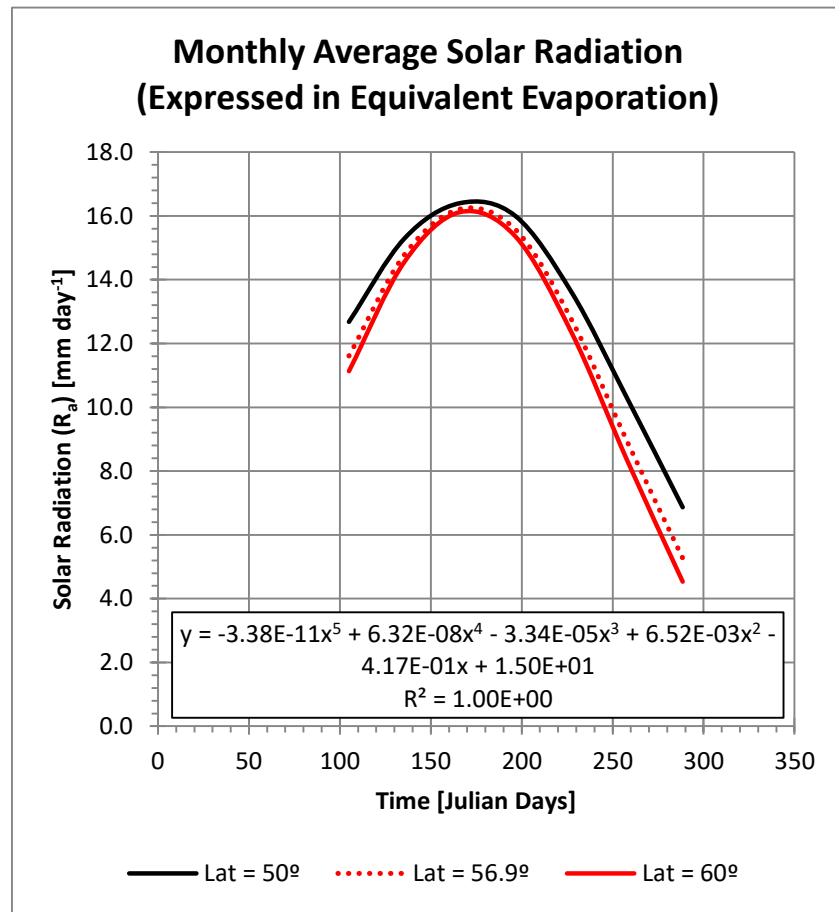


Figure 4.10 shows the monthly average solar radiation reported by MAFF (1967), as cited in Shaw (2005), so it was assumed that the average value reported for the month occurred mid-month, and then values were interpolated in between the average values for each day. The equation plotted shows the formula and R^2 value of the trendline. Values for solar radiation between latitude 50° and 60° were provided (as seen in Appendix D), which were used to estimate the solar radiation at latitude 56.92° .

Figure 4.11 Theoretical Black Body Radiation (σT^4) in terms of Temperature

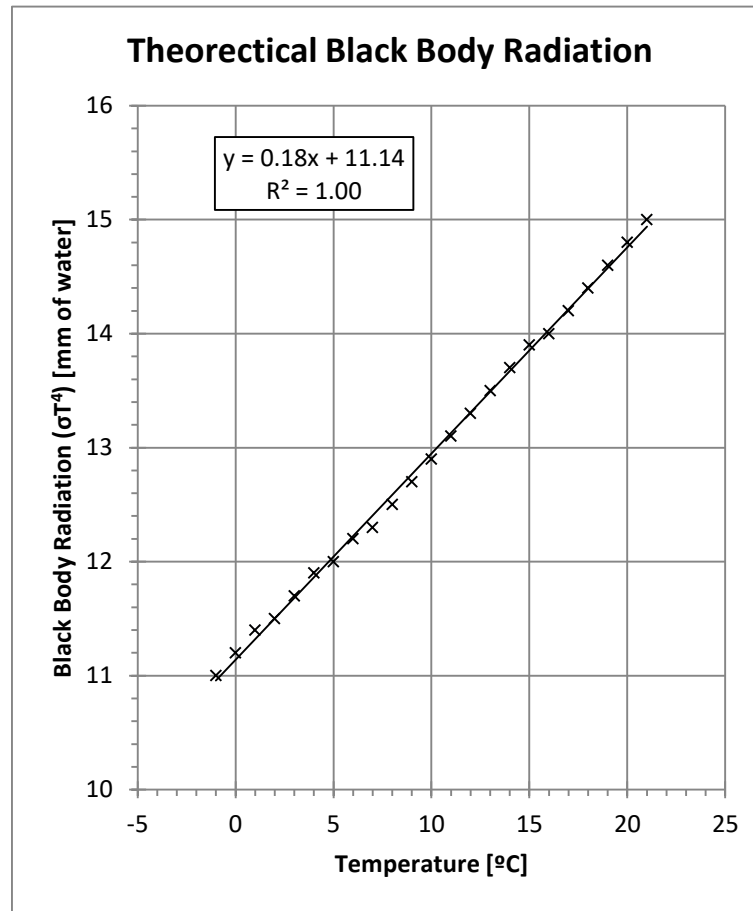


Figure 4.11 shows black body radiation (also referred to as thermal radiation) was plotted in terms of temperature (as cited in Shaw, 2005).

Finally, n/N was equal to one during the day and zero during the night, and if the measurement occurred between sunrise or sunset then it was calculated as the ratio of minutes of available sunlight, over the 30-minute compound interval (Government of Canada, 2016). The potential evaporation rate was then compared to the actual measured evaporation rate.

5 Results and Analysis

5.1 Meteorological and Atmospheric Data

The eddy covariance system took direct measurements of temperature, pressure, and gas mixing ratio. In 2014, measurements were taken from September 4 to September 28, 2014 and in 2015 measurements were taken continuously from May 7 to May 29 and June 6 to June 13, although only May measurements are analysed and plotted.

Temperature data from the ECV system were compared to data collected by the Suncor weather station as seen in Figure 5.1 and Figure 5.2.

Figure 5.1 Plot comparing temperature data collected by the ECV system to data collected by Suncor weather data in 2014

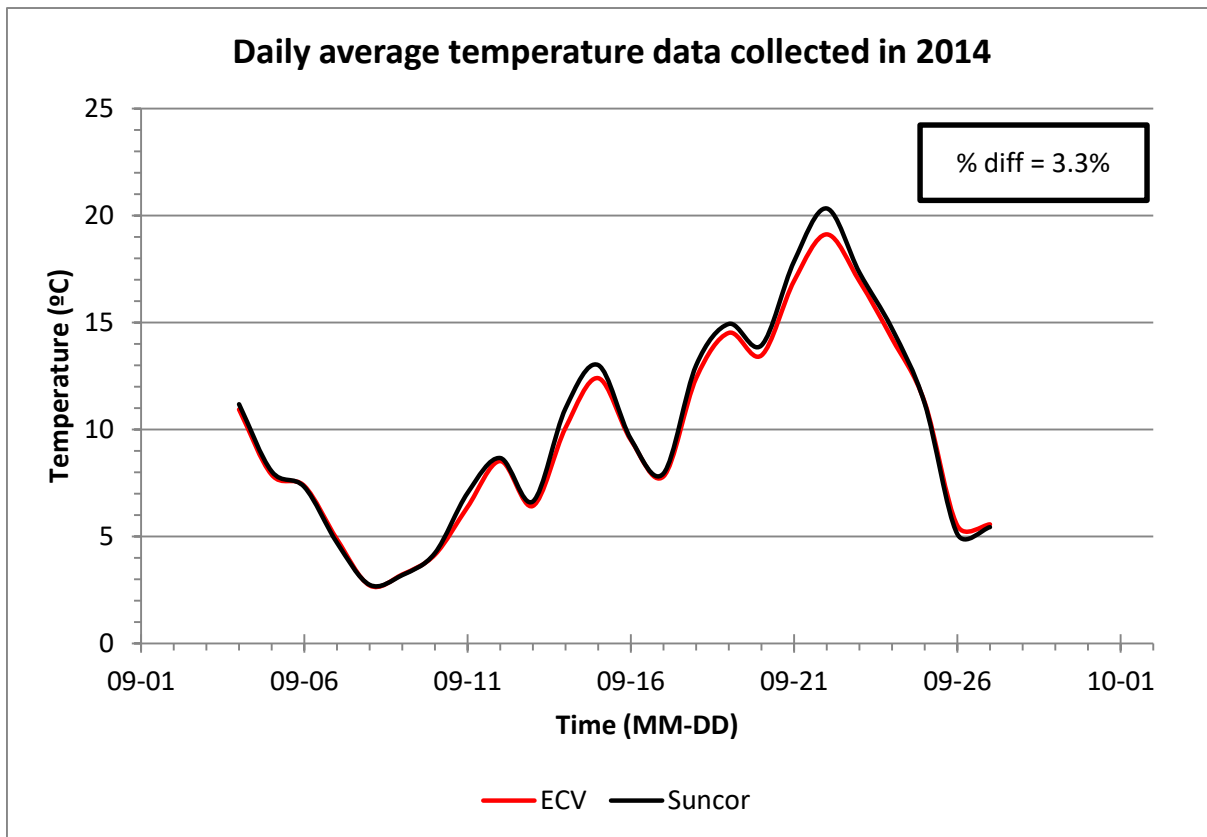
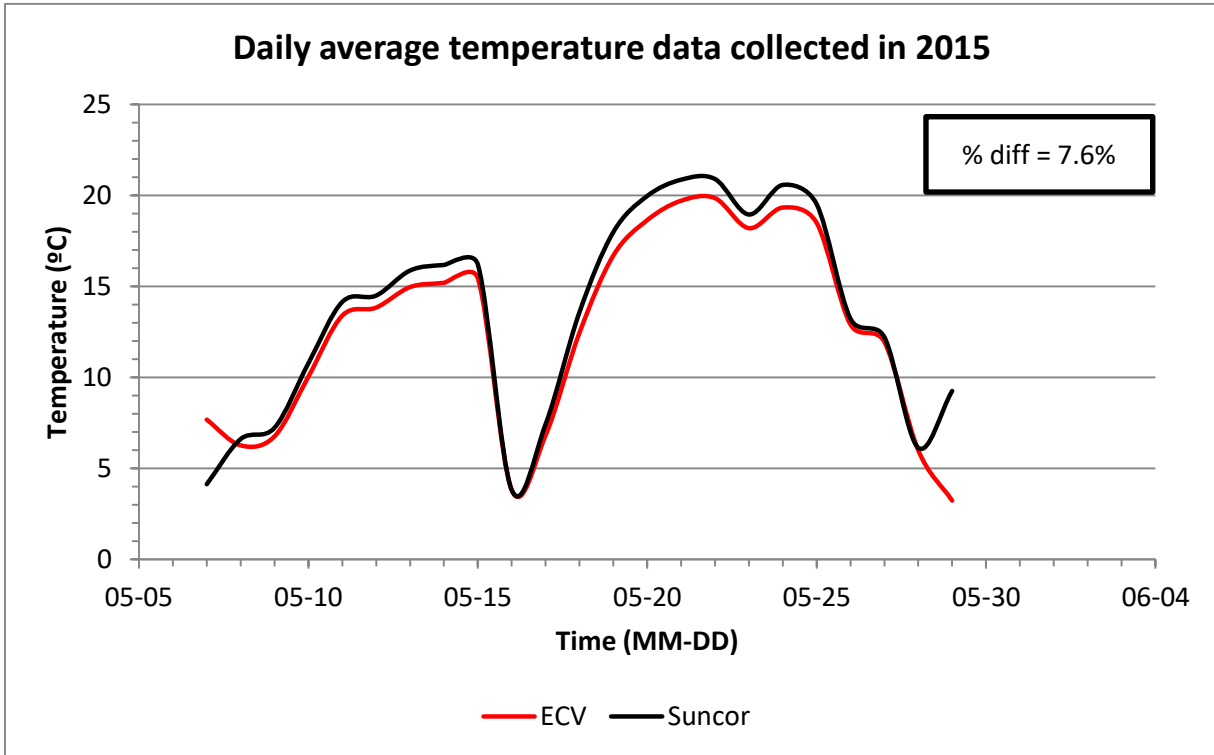


Figure 5.2 Plot comparing temperature data collected by the ECV system to data collected by Suncor weather data 2015



The variance between these sources shows that there are slight differences between areas, due to cloud cover, wind, presence or lack of vegetation. The minimum, maximum, and average temperatures are summarized in Table 5.1.

Table 5.1 Statistic of daily average temperature data in °C

Year	Minimum	Maximum	Average
2014	2.7	19.1	9.6
2015	3.8	19.9	13.1

Overall, the temperature was not ideal for high evaporation rate.

Relative humidity was calculated in Eddy Pro, using measured atmospheric water content, and temperature, and was compared to the relative humidity measured by Suncor. Figure 5.3 and Figure 5.4 show the differences and similarities between the sources.

Figure 5.3 Plot comparing relative humidity data collected by the ECV system to data collected by Suncor weather data (2014)

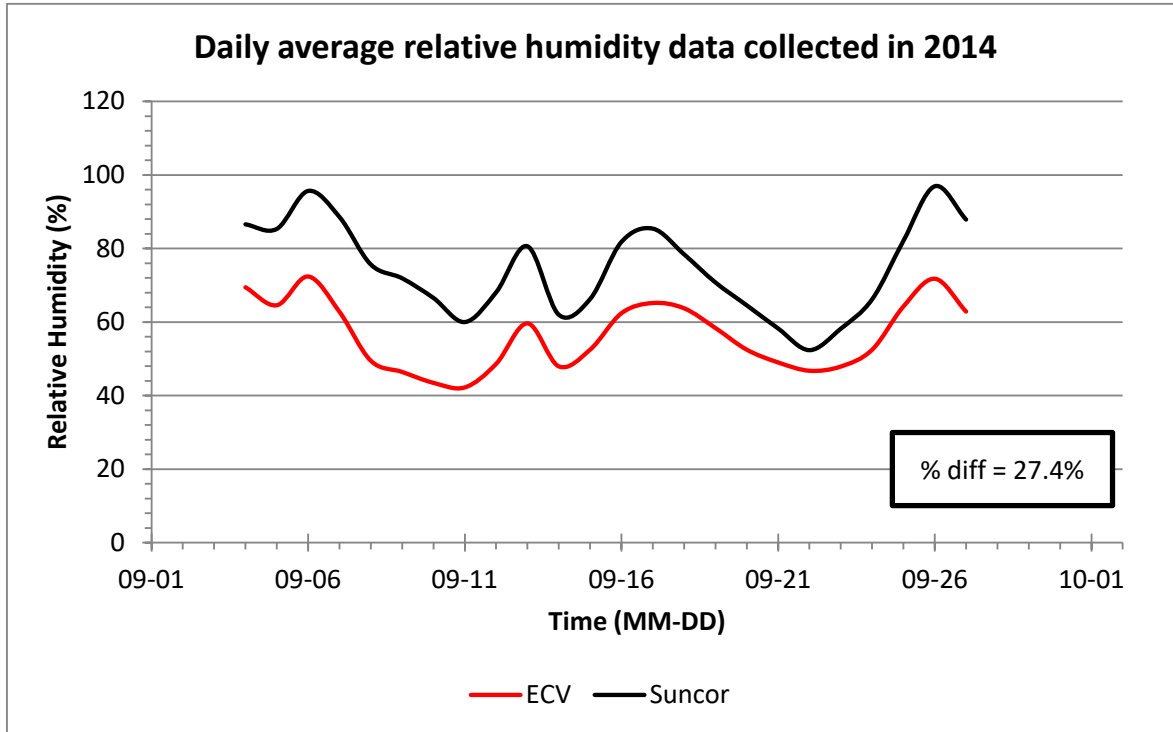


Figure 5.4 Plot comparing relative humidity data collected by the ECV system to data collected by Suncor weather data (2015)

Similar to the temperature readings, the difference between the readings is most likely due to the different location where the measurements were taken. The minimum, maximum, and average values are summarized in Table 5.2.

Table 5.2 Statistic of daily average relative humidity data in %

Year	Minimum	Maximum	Average
2014	42.2	72.4	56.0
2015	23.3	58.4	34.6

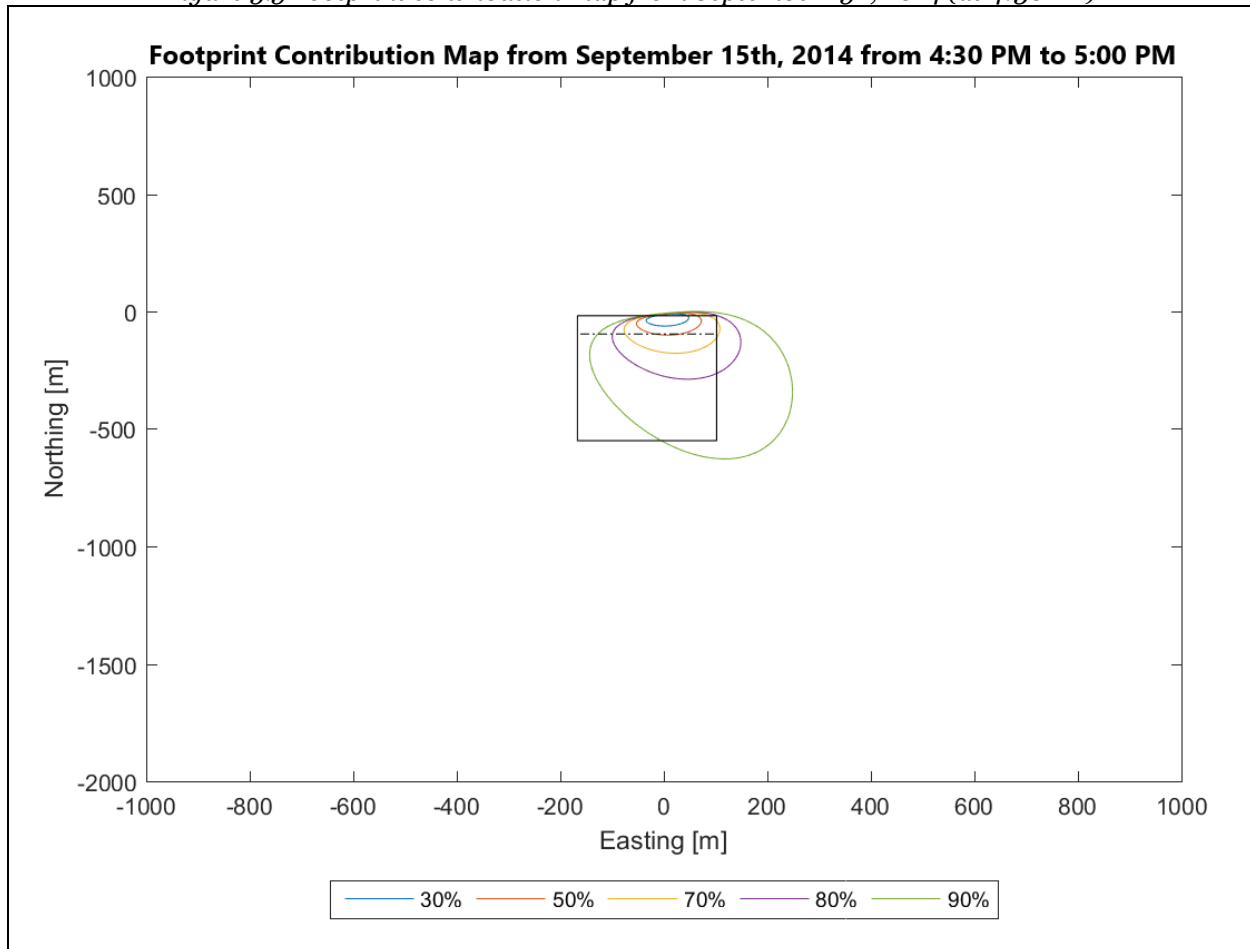
Higher percentages of relative humidity suggest that less evaporation is occurring, or that the area in general has high humidity. For ideal evaporation condition, low relative humidity values are

preferred, as this means the atmosphere has more capacity for excess water from the surface, creating an ideal environment for water to move from the tailings surface to the atmosphere.

5.2 Footprint Results and Analysis

The footprint area was calculated for each 30-minute interval. Footprint contribution areas of 30%, 50%, 70%, 80% and 90% were plotted and analysed. In order, for a reading to be considered valid the 30% and 50% footprint contributions had to lie within the area of interest (the test cell), and more than half of the 70% contour had to lie within the area of interest. This was to ensure evaporation measurements were not from the surrounding tailings cells or area in general. In 2014, data was also automatically removed as the wind direction was from behind the equipment. In 2015, data collected east of the equipment was omitted due to the presence of the scaffolding, as it would interfere with the wind current. Figure 5.5 shows the contribution areas for readings taken between 4:30PM and 5:00PM on September 15th, 2014.

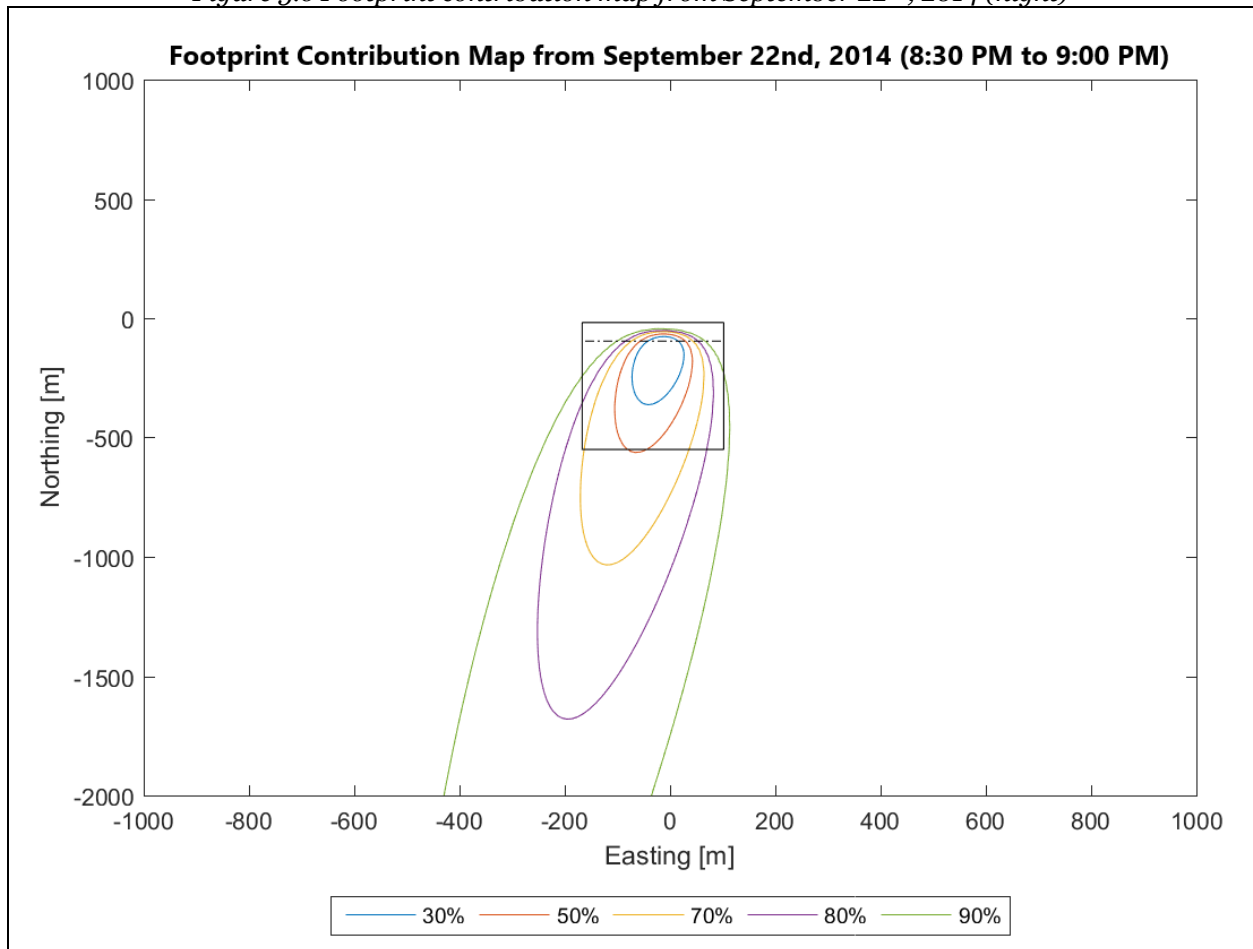
Figure 5.5 Footprint contribution map from September 15th, 2014 (at 4:30PM)



In Figure 5.5, the entire tailings pond section is outlined in a continuous line and the test cell is shown with the dashed line. The 30% and 50% contribution area lie within the area of interest (the test cell); however, the 70% contribution reaches far outside of the test cell, resulting in the reading being not relevant. It was estimated that 52% of the readings were within the area of interest.

In 2014, due to the tailings pond being a very smooth surface, the equipment being 4.5 m above from the tailings pond surface and 12 m away from the tailings pond edge, the ECV system measured far beyond the extents of the test cell and the tailings pond; it measured more than 2 km from the south edge of the test cell, as seen in Figure 5.6.

Figure 5.6 Footprint contribution map from September 22nd, 2014 (night)

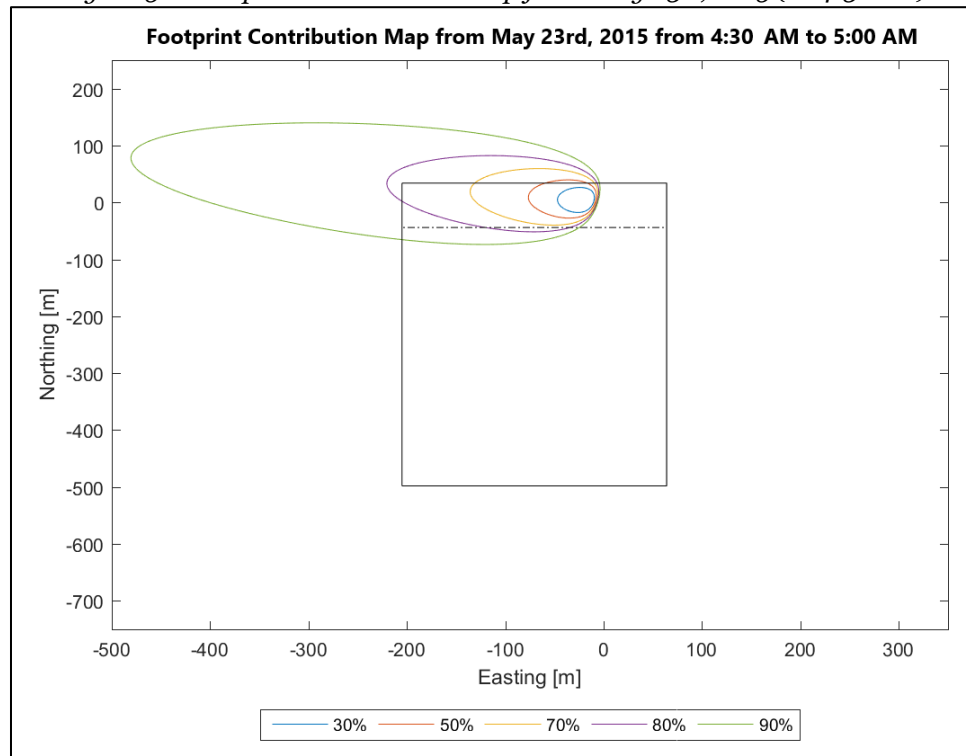


It was estimate that in the above reading only 2.2% of the readings were within the test cell. Unfortunately, this was common for the footprint analysis results, as only 13.7% of the footprint analysis had an overall relevance higher than 60%.

The footprints became smaller, and more relevant in 2015; 83.8% of the footprint analysis had an overall relevance higher than 60%. As seen in Figure 5.7, the 30% and 50% contribution footprints were more consistently within the area of interest, as was the high contribution footprints. There were still instances where measurements were taken far beyond the test cell, as seen in Figure 5.8, however overall measurements were taken closer to the ECV system.

Figure 5.7 Footprint contribution map from May 9th, 2015 (at 4:30PM)

Figure 5.8 Footprint contribution map from May 23rd, 2015 (at 4:30AM)



The overall relevance or percentage of data that was measured within the area of interest for Figure 5.7 and Figure 5.8 is 86% and 67% (respectively). The overall relevance of footprint analysis increased from 22.7% to 62.9%, and the standard deviation decreased from 22.3% to 10.5%. Figure 5.9 and Figure 5.10 illustrates the increase in overall relevance of the footprint analysis:

Figure 5.9 Histogram of overall relevance of ECV measurements according to the footprint analysis (2014)

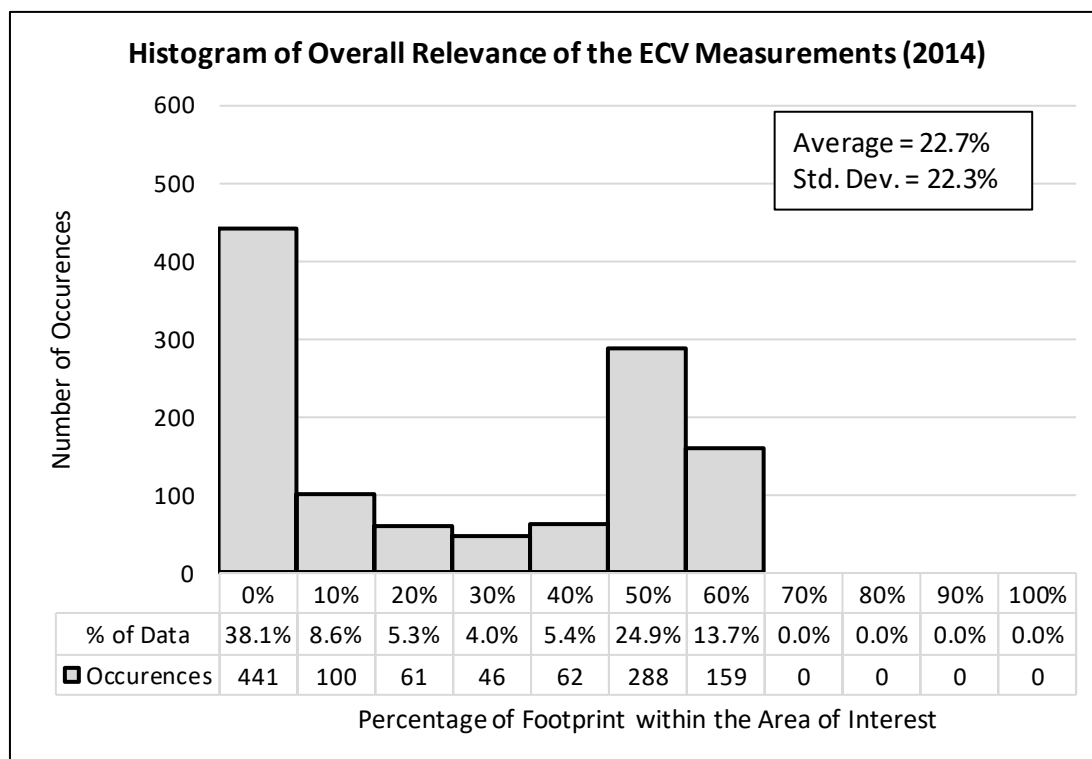
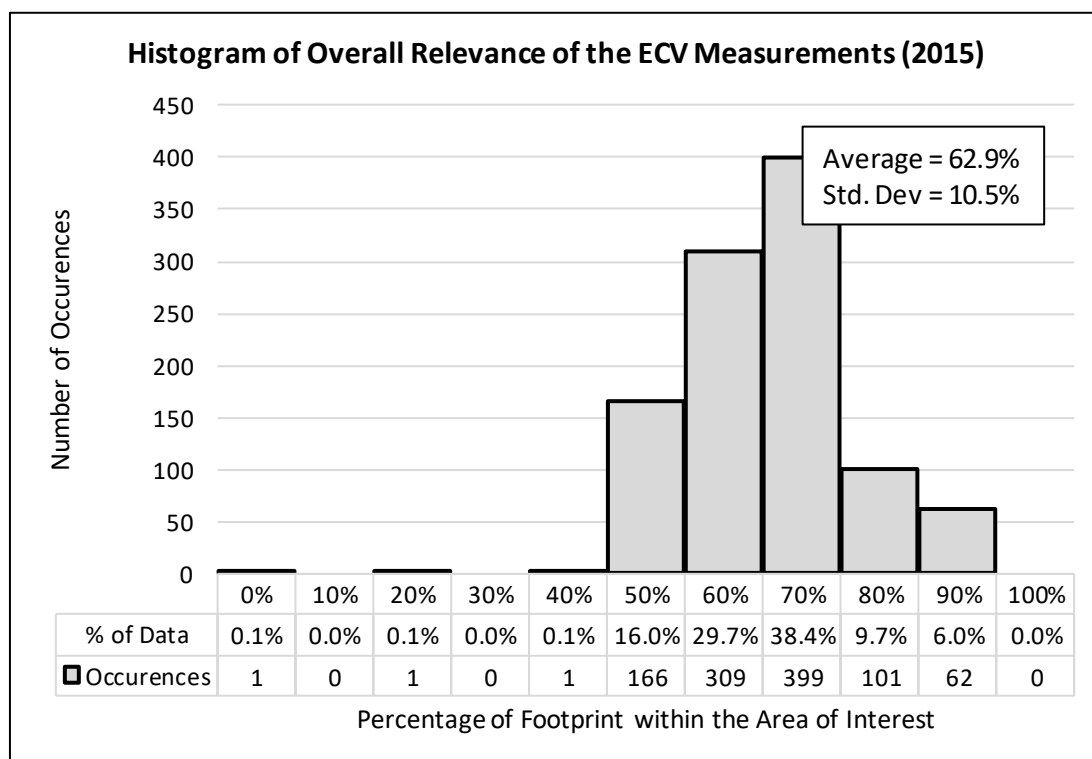


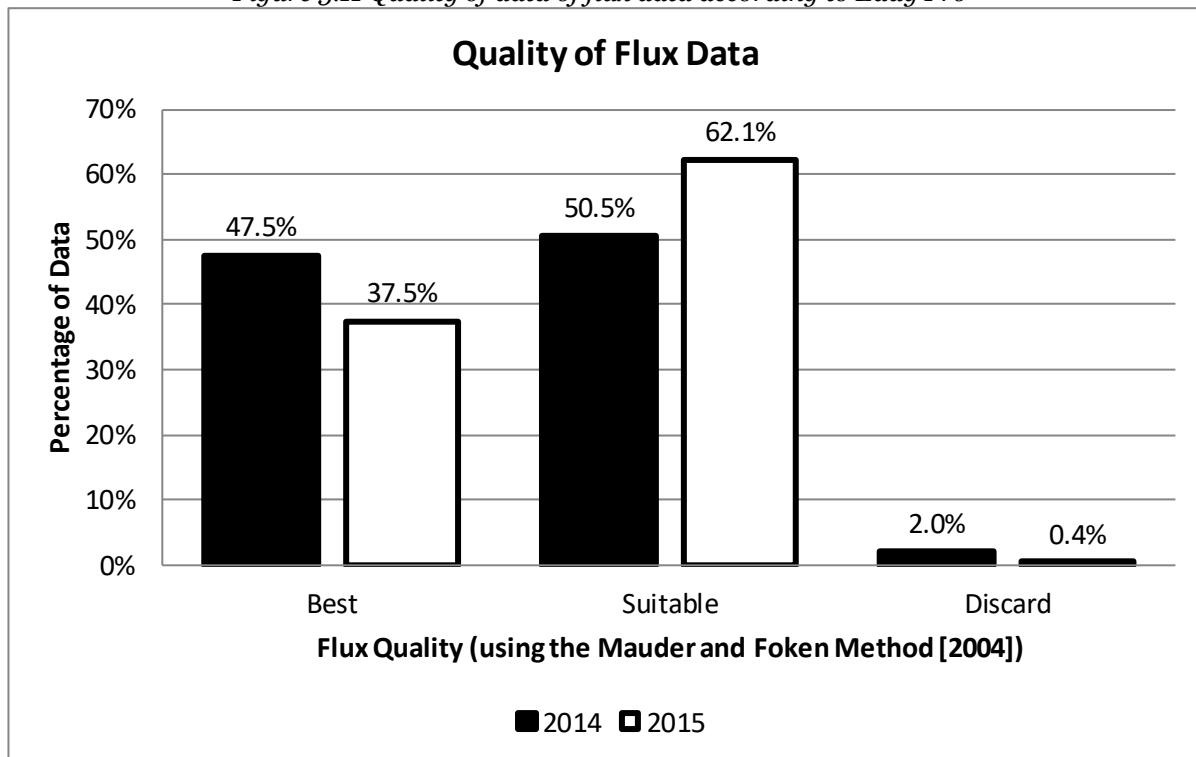
Figure 5.10 Histogram of overall relevance of ECV measurements according to the footprint analysis (2015)



5.3 Data quality

During the analysis of the data, the data quality was also used to trim the data from the analysis. Depending on the strength of the data, EddyPro assigns a quality to each composited reading. The data is labelled high (best), intermediate (suitable), or low (discard), as seen in Figure 5.11. In 2014 there were 1151 composite readings and 1040 in 2015:

Figure 5.11 Quality of data of flux data according to Eddy Pro



Overall, the data quality decreases between 2014 and 2015, however this accounts for all the readings including the readings that were not used due to low relevance.

5.4 Energy and Evaporation Flux Data

A sample of the energy flux were measure by the EVC, were calculated in Eddy Pro are shown in Figure 5.12 and Figure 5.13. Figure 5.12 shows data collected from September 9 to September 12, 2014 and Figure 5.13 shows data collected from May 10 to May 13, 2015. As

expected, during daylight hours, latent heat flux and sensible heat flux increase and then decrease as the day progresses. Sensible heat flux depends on temperature, whereas latent heat depends on temperature, atmospheric water content, and other meteorological variables, therefore there is more fluctuation in the data. Negative energy flux means that energy is being absorbed from the atmosphere to the soil, and positive energy flux means that energy is being released into the atmosphere. It should be noted that data in Figure 5.12 and Figure 5.13 were not filtered or restricted to the area of interest; therefore, measurements outside of the area of interest are included.

Figure 5.12 Plot of sensible heat and latent heat flux from Sept. 9 to Sep. 12, 2014

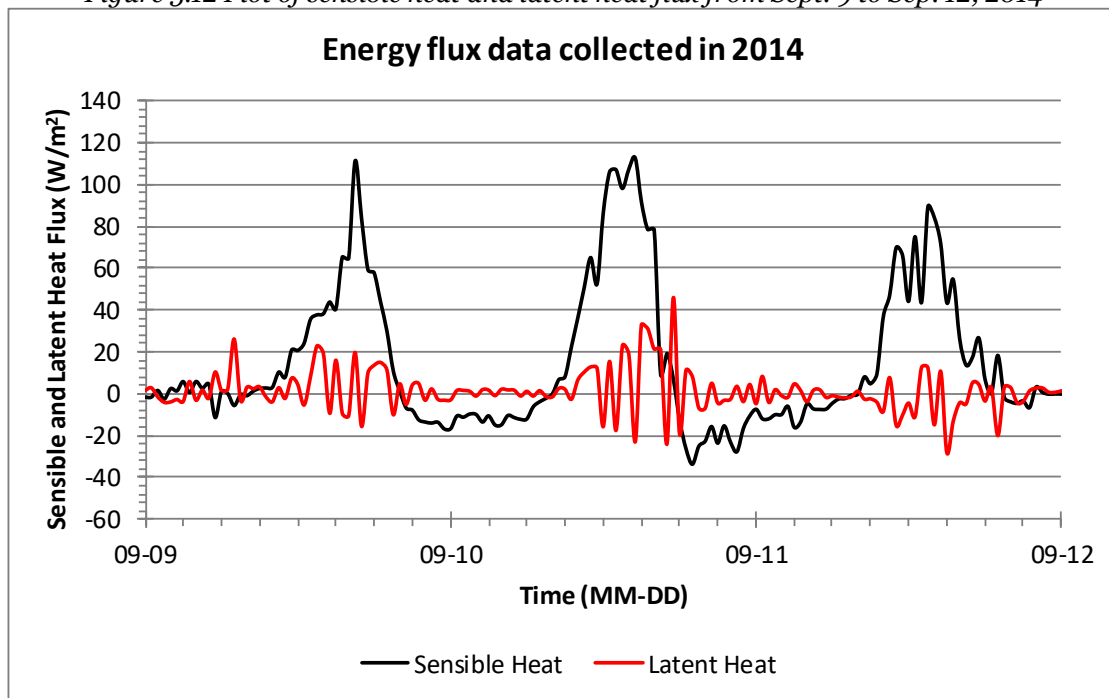


Figure 5.13 Plot of sensible heat and latent heat flux from May 10 to May 13, 2015

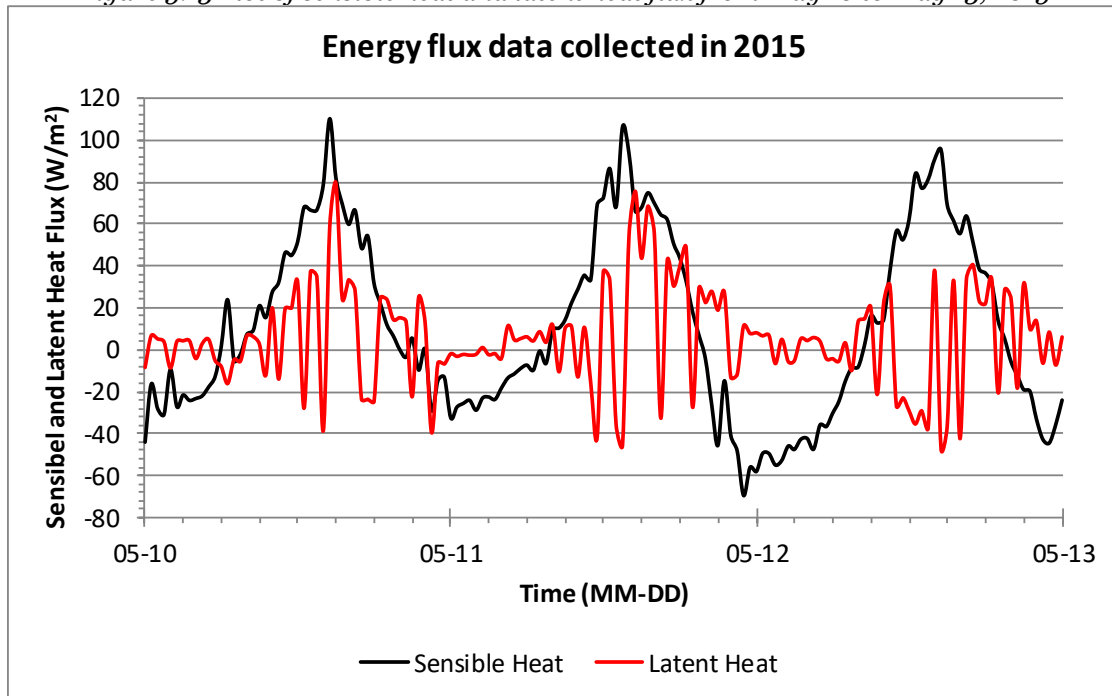


Figure 5.14 and Figure 5.15 compares the untrimmed evaporation rates to the evaporation rates where the poor-quality data was removed.

Figure 5.14 Analysis of raw and trimmed evaporation data collect in 2014 (using data quality)

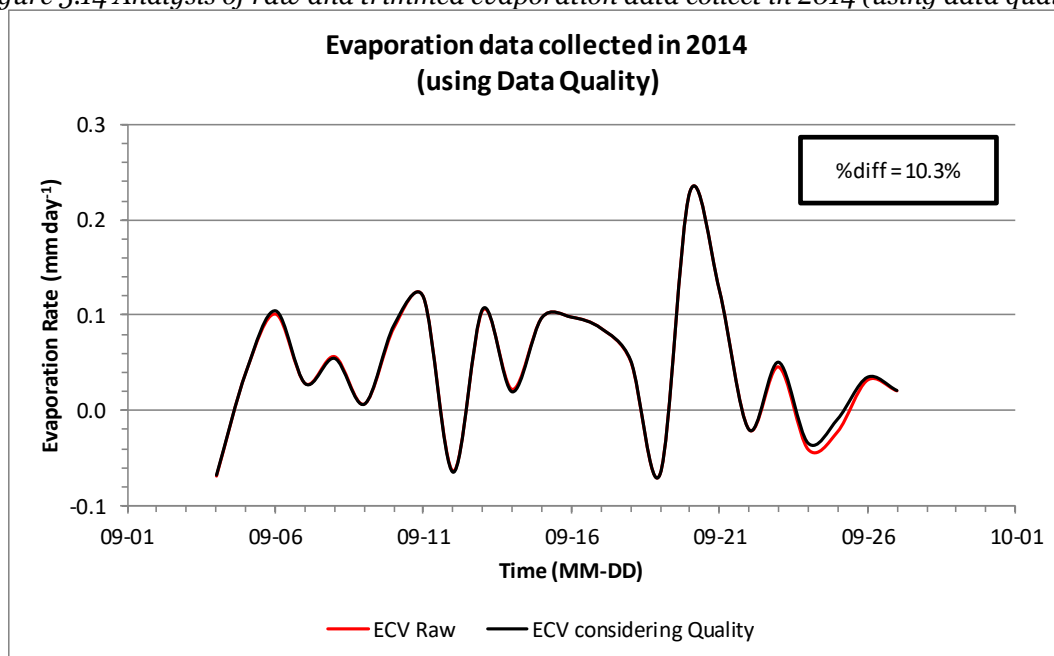


Figure 5.15 Analysis of raw and trimmed evaporation data collect in 2015 (using data quality)

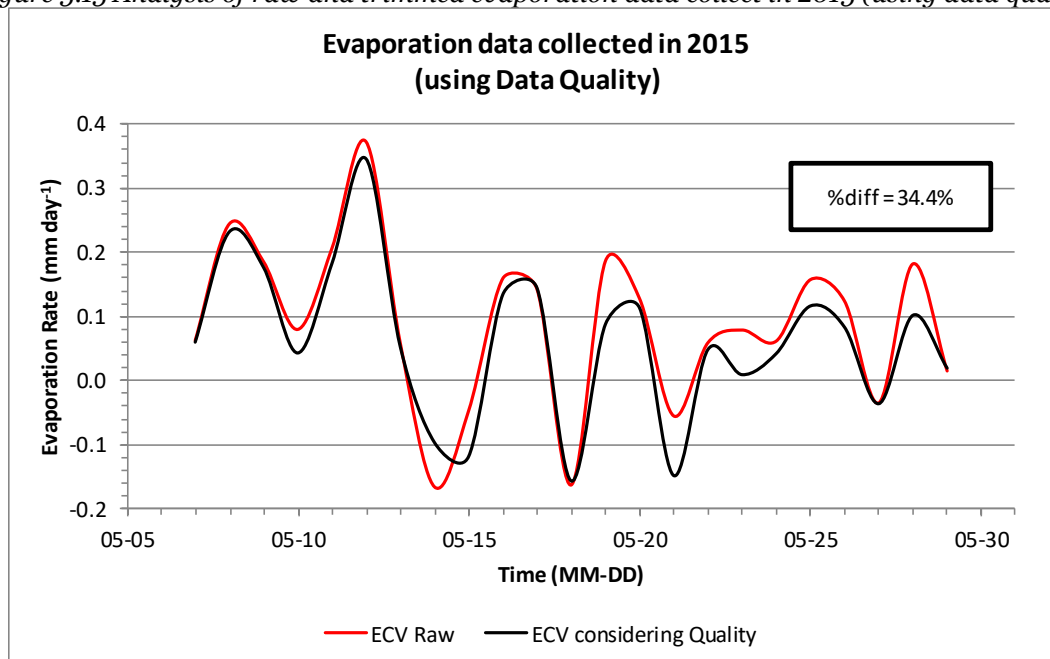


Figure 5.16 and Figure 5.17 compares the untrimmed evaporation data with the evaporation rates after poor quality data and measurements taken outside of the area of interest are removed. As expected the difference between the data increases when the footprint analysis is considered.

Figure 5.16 Analysis of raw and trimmed evaporation data collect in 2014 (using quality and footprint data)

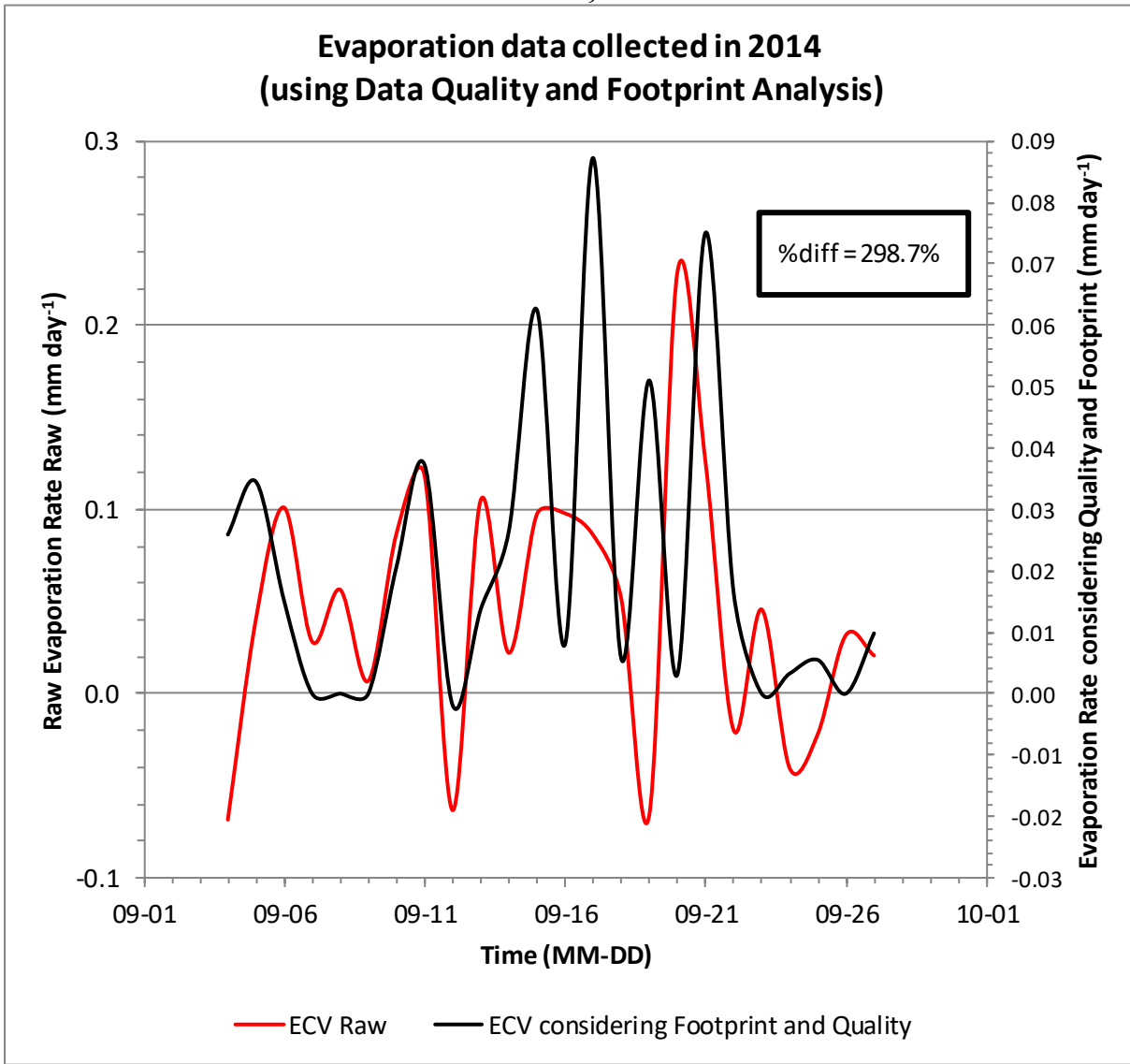
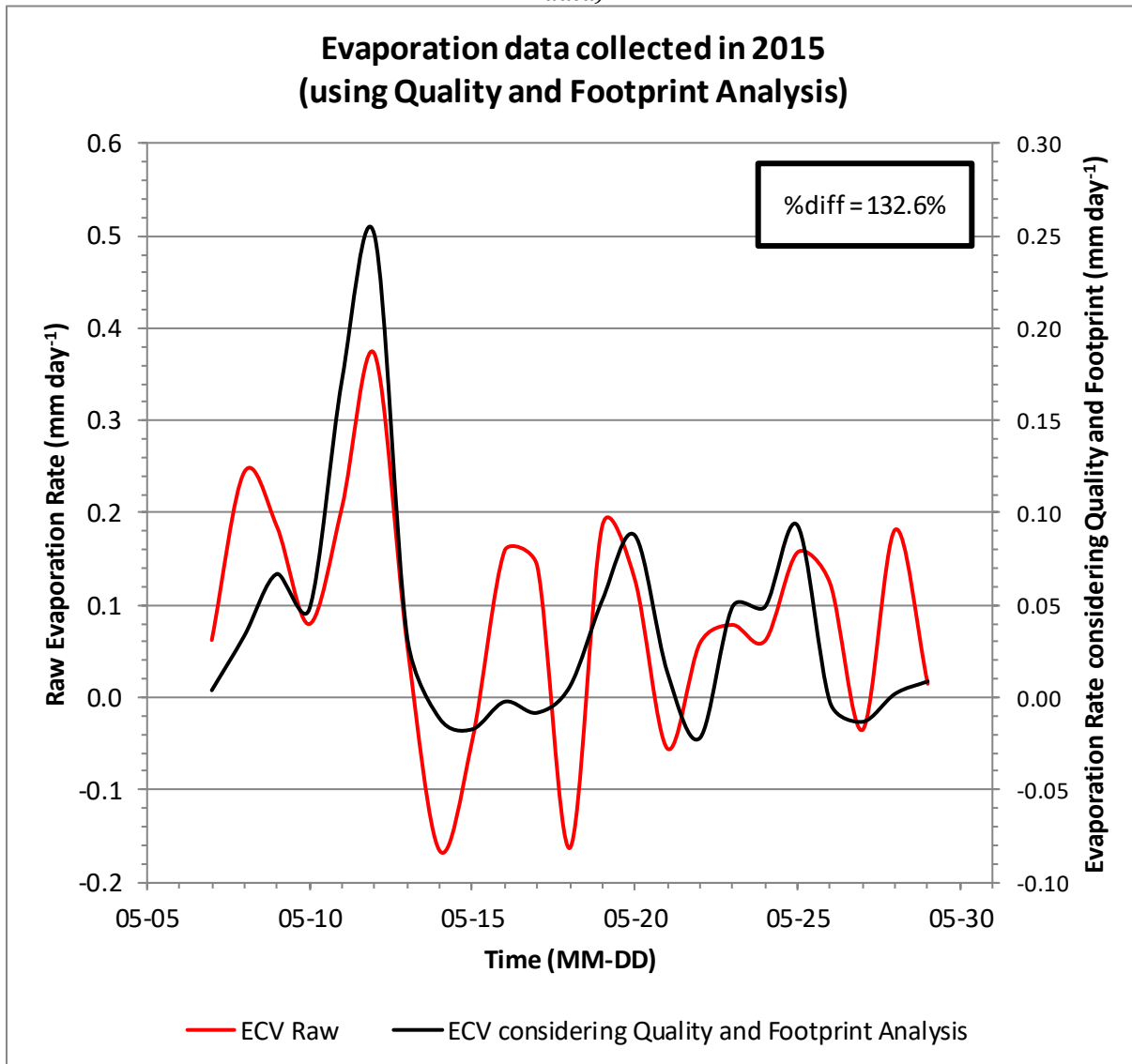


Figure 5.17 Analysis of raw and trimmed evaporation data collect in 2015 (using quality and footprint data)



Overall, the difference between raw and trimmed evaporation decreased from 2014 to 2015, which is expected as the instrument placement was more ideal.

5.5 Comparing Actual Evaporation Rates to Other Data

Latent heat flux measured by the ECV was assumed to equal actual evaporation, because during the summer the only positive type of phase of water that is evaporation. The maximum possible potential evaporation was estimated assuming all net radiation (provided by Suncor) was converted to latent heat and that it was sunny and clear 53% of the day in 2014 and 70% in 2015. The percentages were chosen according to amount of daylight on average in September and May, respectively. In 2014, the average potential evaporation was 2.26 mm/day and the average actual evaporation measured by the ECV was 0.039 mm/day as seen in Figure 5.18, which is 58 times smaller than potential evaporation. In 2015, the average potential evaporation was 4.96 mm/day and the average actual measured evaporation is 0.066 mm/day as seen in Figure 5.19, which is 74 times smaller than the potential value. In 2015, Suncor also provided their atmospheric data, which estimated an evaporation rate of 5.37 mm/day.

Figure 5.18 Comparison of evaporation data collected in 2014 and potential evaporation

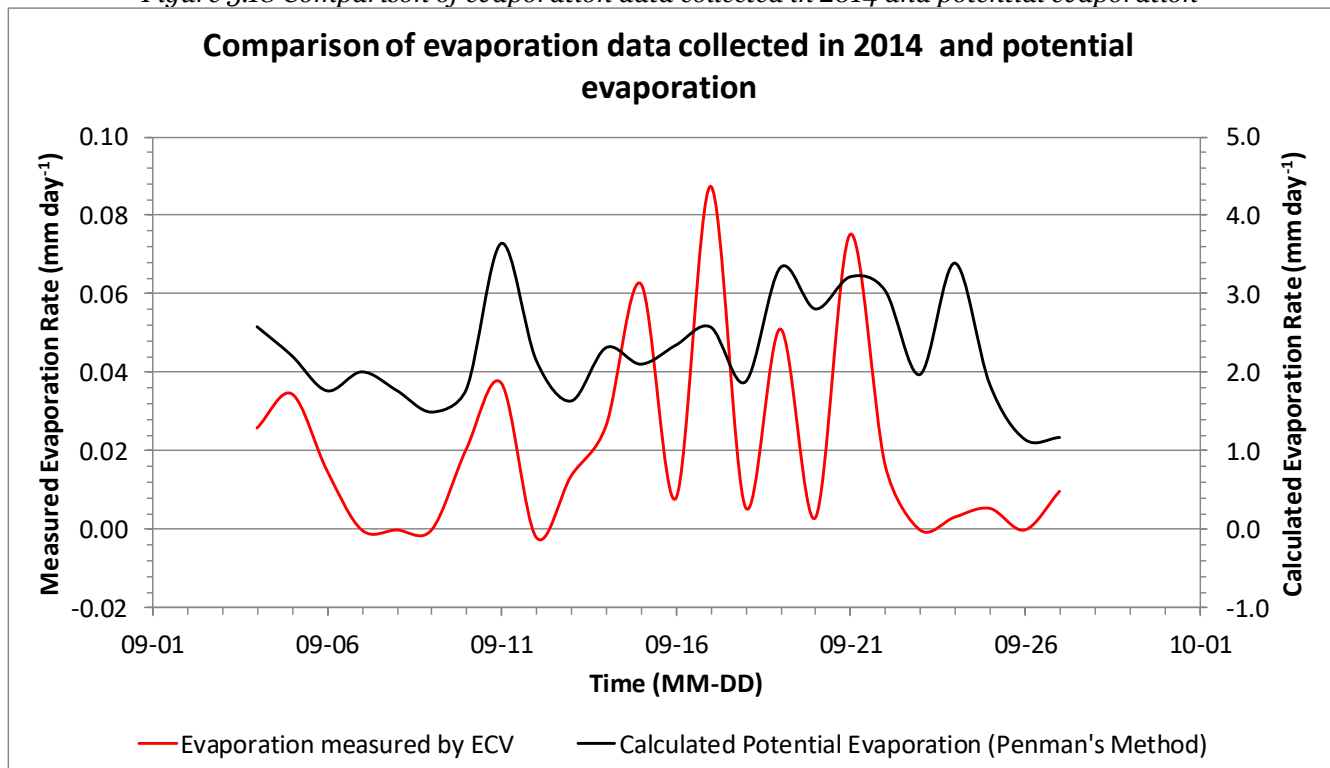
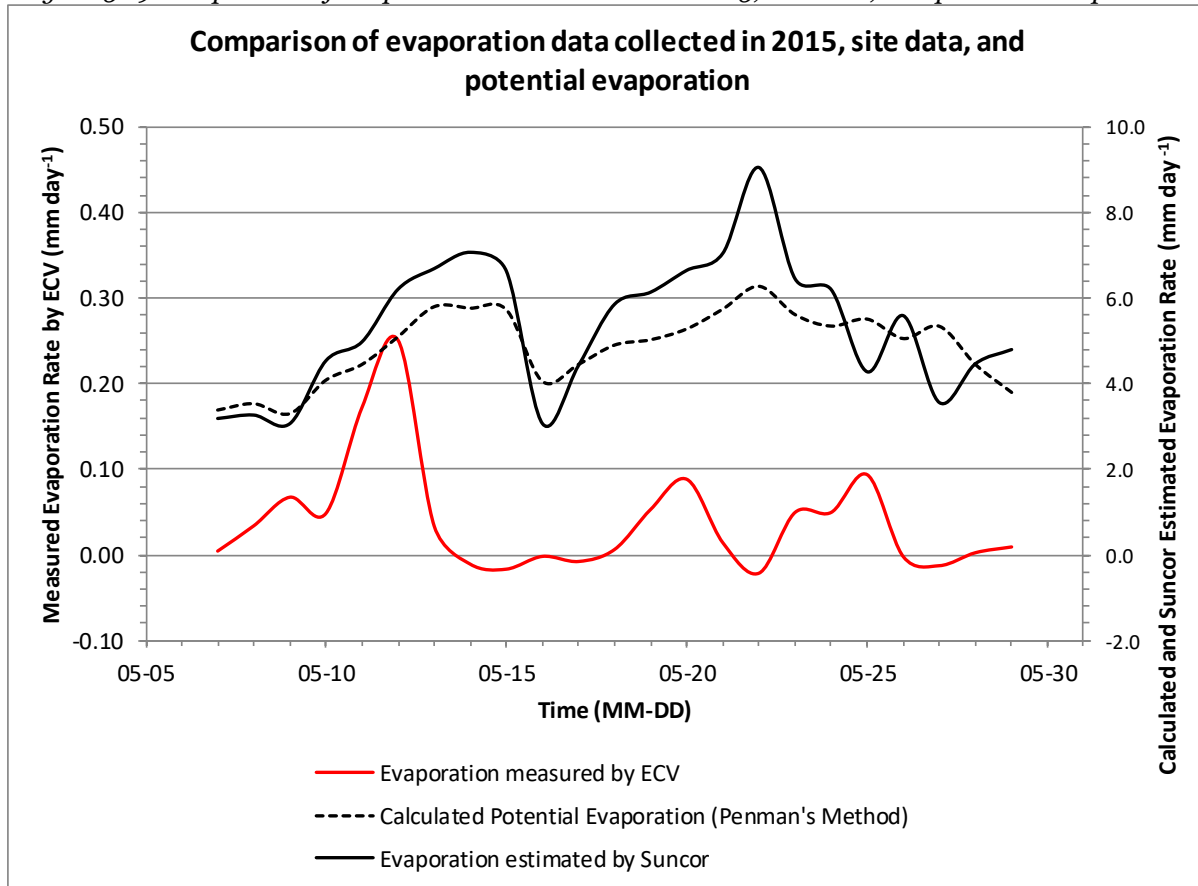


Figure 5.19 Comparison of evaporation data collected in 2015, site data, and potential evaporation



Actual evaporation rates were compared to changes in temperature, precipitation, relative humidity when a lift was poured in order to evaluate if there were any trends or correlation between the variables as seen in Figure 5.20 to Figure 5.23.

Figure 5.20 Plot comparing actual evaporation rate to temperature in 2015

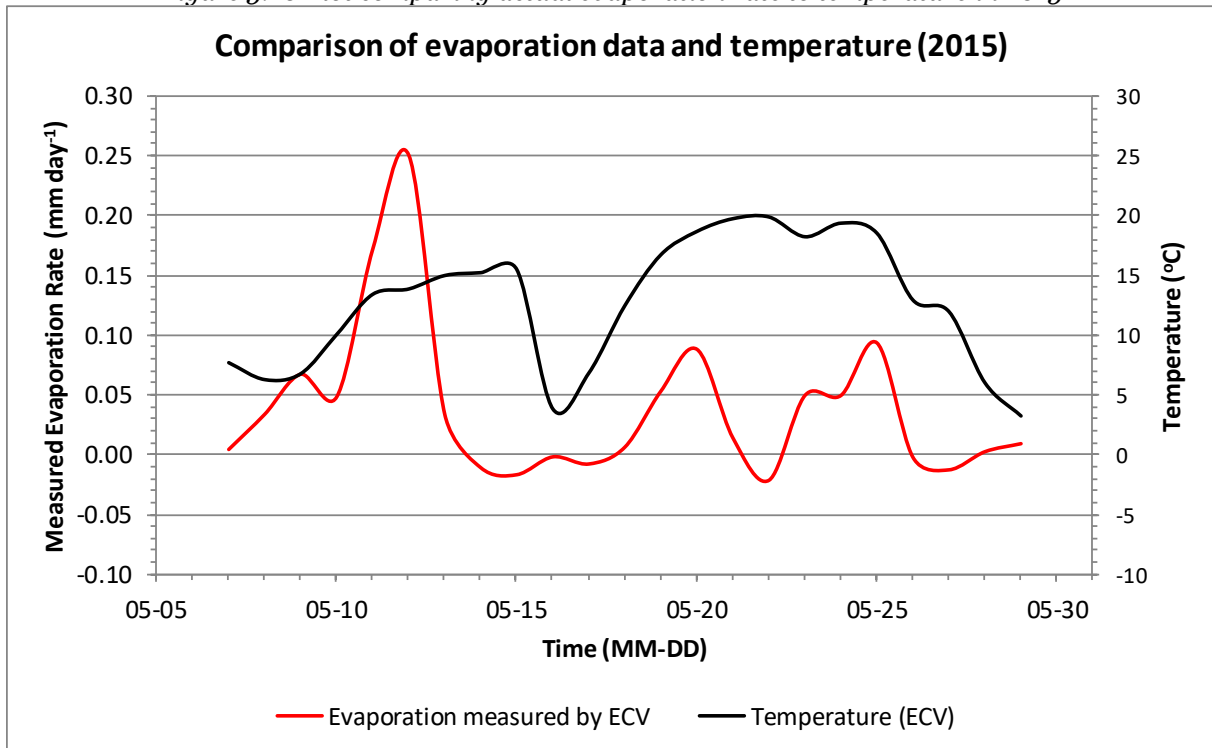


Figure 5.21 Plot comparing actual evaporation rate to amount of rainfall in 2015

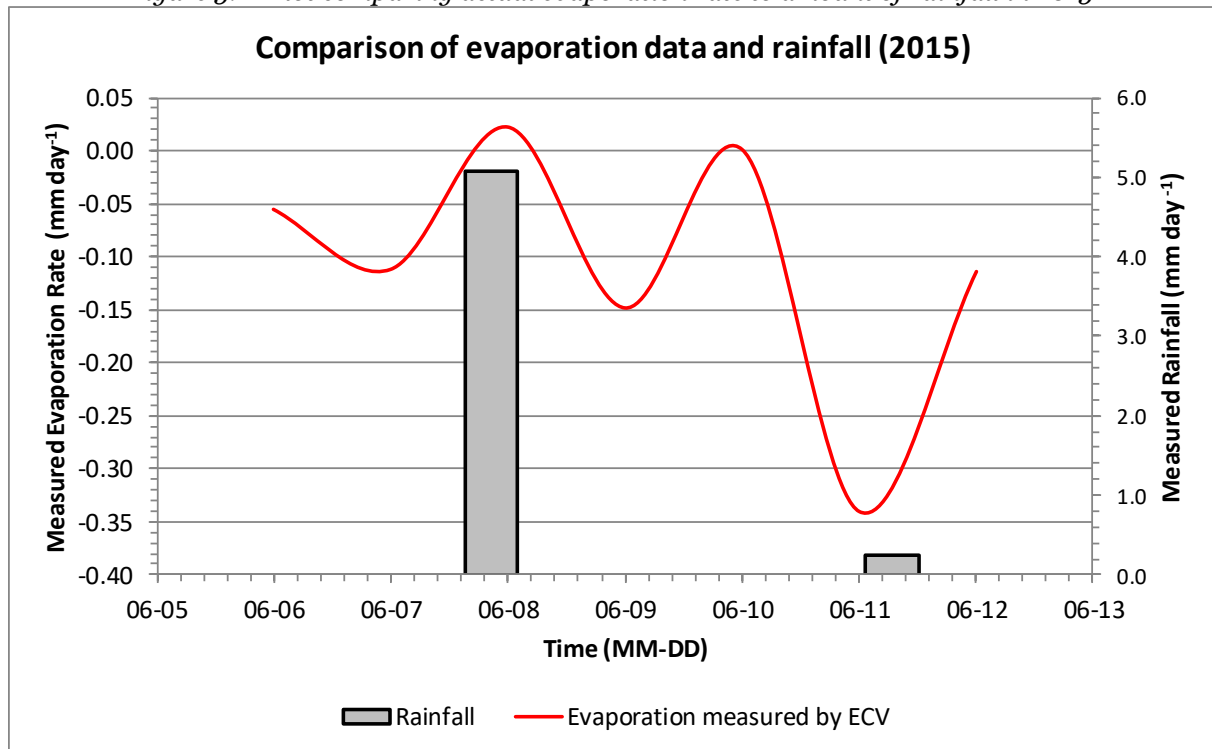


Figure 5.22 Plot comparing actual evaporation rate to amount of relative humidity in 2015

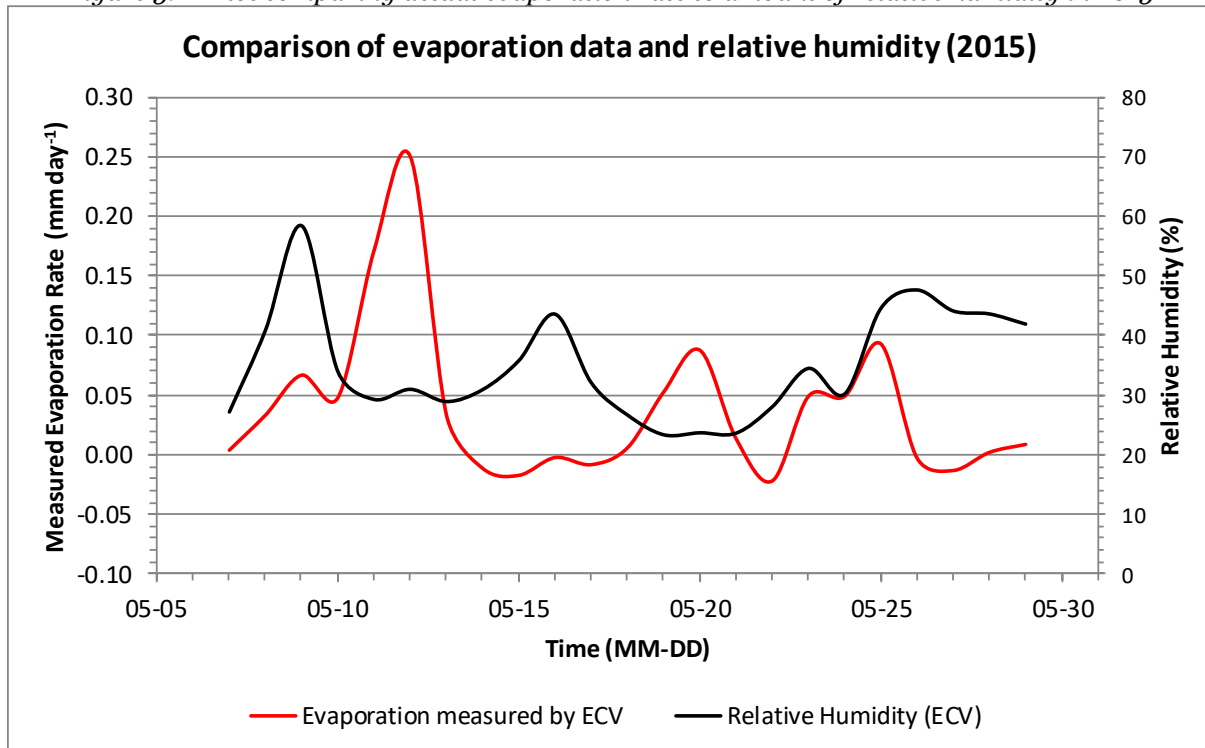
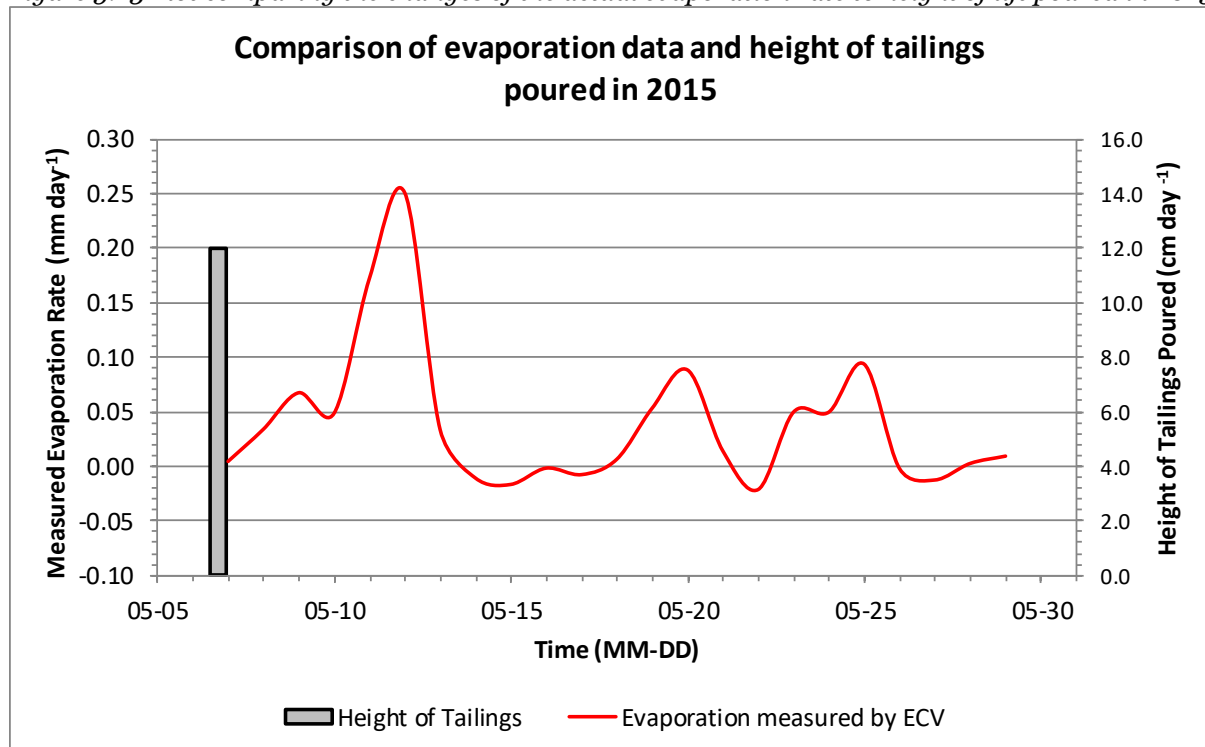


Figure 5.23 Plot comparing the changes of the actual evaporation rate to height of lift poured in 2015



6 Discussion

In terms of the temperature and relative humidity readings, the similarity between the ECV readings and the site readings were expected, since the general temperature and atmospheric conditions of an area does not vary drastically over an area where there is minimal variance in topography and environment. As seen in Figure 5.3, in 2014, there is a percent difference of 27.9% between the relative humidity data collected by the ECV and Suncor weather station, which could be a result of equipment location, or error in one of the instruments. Assuming there was no error with either system, it should be noted that the Suncor weather station was placed adjacent to another tailings impoundment, which could explain the higher humidity reading. It is standard practice to rotate between different tailings impoundment, therefore, the impoundment could have been in use in September of 2014, and not in use in May of 2015.

When comparing the footprint analysis from 2014 and 2015 (as seen in Figure 5.9 and Figure 5.10), it is noted that the overall relevance of the footprint increases drastically (from 22.7% to 62.9%), which was due to the instrument placement. Since the tailing's surface is very smooth, the equipment height relative to the surface is highly influential on the results. This resulted in the measurement obtained in 2014 to be of general area, rather than the test pond specifically. Note that the footprint analysis required that an overall relevance cut-off limit be defined. In typical ECV studies, the 70% footprint is considered the cut-off (industry standard), and in those cases the concern is whether or not the footprint covers enough area to be considered representative. In this case, the footprint needs to be small enough to cover only the test cell. In 2014, the cut-off limit had to decreased from 70% to 50% so that an analysis could be carried out. This reduction in cut-off is the reason why the actual evaporation rate (trimmed using quality data results and footprint analysis results), fluctuates so erratically (as seen in Figure 5.16), since some of the

general area evaporation readings were considered in the analysis rather than only the readings directly from the test cell.

The decrease in data quality, as seen in Figure 5.11, is most likely due to the equipment being closer to the surface. When the equipment is placed further from the surface of interest, eddies can be larger and more defined, whereas if the equipment is taking readings closer to the surface, then the wind flow is less defined and more turbulent, which would decrease high-quality data to intermediate-quality. However, there was a decrease in poor-quality data.

The energy flux results were as expected (Figure 5.12 and Figure 5.13). Sensible heat was low or negative during the night and peaked about mid-day, and latent heat also peaked during the warmest time of the day. Latent heat fluctuates relatively consistently and the amplitude increases and decreases as temperature and humidity increase and decrease throughout the day. The constant fluctuation of latent heat is due to water entering and leaving the surface, as it attempts to find equilibrium.

Once latent heat was converted into evaporation, the untrimmed evaporation rates were compared to the trimmed actual measured evaporation rates (AME). The difference increased between the raw AME and AME trimmed using only quality data, however, this is not unusually. Depending on the reading, if quality was low for a large evaporation measurement, this would cause a noticeable change in the trimmed AME reading for that day. Once the footprint analysis was also considered, a drastic change in the evaporation measurements were noted. The percent difference decreased from 2014 to 2015, which was most likely a result of the decrease in data trimmed as the footprint analysis from 2015 showed an increase in overall relevance of measurements. Since, the footprint analysis showing that the data collected was not limited to the test cell, the untrimmed 2014 data and the overall ECV measurements were of the general area

(and therefore trimming the data using the footprint data is inaccurate). Where as in 2015, the average overall relevance of the footprint analysis was found to be 62.9% (closer to the 70% standard), and therefore the trimmed 2015 AME were more precise and relevant to the test cell. Also note that when a reading was removed, it was essential set to zero, which could also contribute to the drastic change, since more that 37.1% of the data is set to zero.

The trimmed AME (quality and footprint) was compared to potential evaporation, evaporation measurements collected by Suncor and collected atmospheric data. The potential evaporation rates were 56 and 74 times larger than the trimmed AME data in 2014 and 2015 (respectively). This was expected as the potential evaporation does not account for soil properties. It can also be noted that the evaporation data collected by Suncor in 2015, was similar to the calculated potential evaporation (both have a similar shape). This is due to the Suncor data being based on the data on the weather data (which was used in the calculation of potential evaporation); the evaporation rate reported by Suncor was calculated rather than measured.

When comparing relative humidity and trimmed AME, they appeared to be inversely related, and temperature and trimmed AME appear to be correlated, which was expected. When the relative humidity is low, the atmospheric demand for water is high, which results in evaporation increases or vice versa (as seen on May 12th, 2015 on Figure 5.22). When temperature is high, there is adequate energy to cause water to change from liquid to gas. Figure 5.20, we see AME and temperature follow a similar trend (especially from May 13th to May 20th, 2015), the peak on the 12th could be due to the drop in relative humidity. During rain events, an increase in evaporation was noted (as seen on Figure 5.21 on June 8th, 2015). However, rain events can both increase and decrease the amount of evaporation depending on when and how long it rained for. If it rained for an extended period of time the area would cool and evaporation would decrease. However, if the

rain event is short, it does not decrease the ambient temperature, as seen on Figure 5.21 on June 15th, 2015.

In terms of when a lift was poured, evaporation rates over the test pond were expected to increase; however, on the day when a lift was poured (May 8th), relative humidity was high and temperature was low, therefore the atmospheric demand for water was low and it may have been too cold to heat the water in the test pond. Data was never collected for more than one pouring event, and therefore no trends could be identified beyond this one event.

In general, there are many variables to consider when analysing trends in evaporation rates, unfortunately no trends can be clearly identified since the station was only operating properly for a short period of time and no direct measurements were taken of the ground heat flux or tailings composition. Change in solids content, and chemical composition of the tailings could also effect the AME but could not be qualified by the ECV system and could not be compared to the AME reading.

Overall, in terms of the ECV method, the assumption that is by far the hardest to ensure in this type of study area is that the ECV installation and instruments do not distort the measurements. The ECV system will always influence and impact air flow near the equipment. This is typically not a concern since the ECV system is designed to monitored large expansive areas, and therefore eddies are large and measurements are taken a minimum of a couple meters away from the ECV system. In this environment, however, since the ECV is much closer to the surface eddies are smaller and therefore measurements directly in front of the system are taken more frequently. Although this was the goal, as it would limit readings taken from the neighbouring tailings pond cell (which was less than 100 m away), it also means that the percentage of area influence by the

ECV compared to the study area increase, since the area influence does not change, but the study area is dramatically reduced.

7 Conclusion and Recommendations

An eddy covariance system was installed at the Suncor test cell during the summer of 2014 and 2015, during which direct evaporation measurements were taken. Gas mixing ratios and atmospheric measurements were used to calculate actual evaporation flux using EddyPro. Although potential evaporation rates from tailings surfaces have been estimated using lysimeters and evaporation pans, neither of these methods allow for undisturbed, direct, and continuous measurements of actual evaporation rates. Drying models currently used by oil sands companies are based on potential evaporation rates that have been reduced by a factor that was determined in a laboratory (Keith Everard, personal communication, December 15, 2015). Due to soil properties, the rate of actual evaporation is only equal to potential evaporation initially when the surface is wet, but as the soil becomes unsaturated its properties begin to influence the evaporation, which brings to question whether drying models used on site are accurate enough, or can the process be further optimized?

In 2014, an average actual evaporation rate of $0.039 \text{ mm day}^{-1}$ was measured to be 58 times lower than the average potential evaporation rate (2.26 mm day^{-1}); and in 2015, the actual evaporation rate was measured to be $0.066 \text{ mm day}^{-1}$, with a potential evaporation rate of 4.96 mm day^{-1} , which is 74 times higher. The footprint analysis results showed the effects of measuring data on a smooth surface. The test pond was relatively small ($21,600 \text{ m}^2$) for eddy covariance, therefore when the equipment was 4-m above the tailings surface in 2014, measurements were taken up to

a distance of 1 km away from the flux station, which rendered a large portion of the data irrelevant. In 2015, the flux station was installed on the scaffolding in the middle of the test pond and the instrument was placed 1.5 m above the tailings surface. This resulted in readings being more limited to the test pond, therefore increasing the amount of useable data. When analysing the evaporation rate (latent heat flux), there were moments when it was negative, which means that moisture was leaving the atmosphere. In other words, water was condensing and being re-absorbed by the tailings. However, net evaporation was positive, which was expected.

When comparing the atmospheric results to the actual evaporation rates, temperature was found to be positively correlated and that relative humidity was negatively correlated, which was expected. Temperature is indicative of net solar radiation, when radiation increases there is more energy available to heat the water and cause it to change from liquid to vapour (and vice versa). Relative humidity is also coupled to atmospheric water demand. High relative humidity causes a decrease in atmospheric demand, while low relative humidity increases atmospheric demand for water; therefore, if the atmosphere is saturated with water vapours evaporation will not occur.

No clear trends were found when comparing changes in evaporation to height of lift poured and precipitation, as there was only one pour recorded during each summer when the flux station was taking reading with very few rain events, thus it could be that the trends are not clear because of the lack of data.

In 2015, the overall relevance of the data increased from 22.7% to 62.9%, showing that the ECV system can be successfully used over a tailings pond surface to measure evaporation rates, if the equipment is properly installed. To ensure the best results are obtained, the ECV should be placed at the center of a larger and more active pond with the equipment should be no more than 2m above the tailings surface. This will ensure that the measurements are from the tailings and not

from the general surrounding area. Being over a consistently active pond would allow for any trends with the lifts and evaporation rate to be seen. In addition, the ECV should be placed for the entire summer period, which would allow for the instrument to see correlation with rainfall events. It would also be beneficial to place an ECV system over diverse types of tailings ponds. Furthermore, the ECV system should be accompanied by a Bowen ratio system to obtain a full energy balance. If after another summer of data, it is found that the evaporation rate remains lower, it can be concluded that evaporation is not the main form of dewatering.

Bibliography

- Alberta Energy Regulator. (2016). ST 39 - ST39 Alberta Mineable Oil Sands Plant Statistics. Retrieved from <http://www.aer.ca/data-and-publications/statistical-reports/st39>
- Alberta Energy. (2017). Facts and Statistics. Retrieved from <http://www.energy.alberta.ca/OilSands/791.asp>.
- Arya, S. P. (2001). Introduction to Micrometeorology. (H. T. Dmowska, Renata; Holton, James R.; Rossby, Ed.) (2nd ed.). San Diego, CA, USA: Academic Press.
- Beier, N., & Sego, D. (2007). The Oil Sands Tailings Research Facility. Canadian Geotechnical Society Conference - OttawaGeo2007. Retrieved from <http://members.cgs.ca/documents/conference2007/GEO2007/V2/082.pdf>
- Brown, C. (2013). Quantifying Greenhouse Gas Emissions from an Oil Sands Tailings Pond using Micrometeorological Flux Measurements Techniques. University of Alberta.
- Brutsaert, W. (1982). Evaporation into the Atmosphere: Theory, History, and Applications. Dordrecht, Holland: D. Reidel Publishing Company.
- Burba, G. (2013). Eddy Covariance Method for Scientific, Industrial, Agricultural and Regulatory Applications. (R. Nelson, D. G. Fratini, & B. Miler, Eds.). Lincoln, NE, USA: LI-COR Biosciences. <http://doi.org/10.1016/j.infsof.2008.09.005>
- Campbell Scientific Inc. (2015a). Instruction Manual: CSAT3 Three-Dimensional Sonic Anemometer. Edmonton, AB, Canada. Retrieved from <https://www.campbellsci.ca/csats3>
- Campbell Scientific Inc. (2015b). Instruction Manual: EC155 CO2 and H2O Closed-Path Gas Analyzer. Edmonton, AB, Canada. Retrieved from <https://www.campbellsci.ca/ec155>
- Canada's Oil Sands Innovation Alliance. (2012a). Tailings Centrifuge. Retrieved March 2, 2016, from <http://www.cosia.ca/initiatives/tailings/tailings-centrifuge>
- Canada's Oil Sands Innovation Alliance. (2012b). Tailings Reduction Technology. Retrieved March 2, 2016, from <http://www.cosia.ca/initiatives/tailings/tailings-reduction-technology>
- Carey, S. K. (2008). Growing season energy and water exchange from an oil sands overburden reclamation soil cover, Fort McMurray, Alberta, Canada. Hydrological Processes, 22, 2847 – 2857. <http://doi.org/10.1002/hyp.7026>
- Carey, S. K., Barbour, S. L., & Hendry, M. J. (2005). Evaporation from a waste-rock surface, Key Lake, Saskatchewan. Canadian Geotechnical Journal, 42, 1189–1199. <http://doi.org/10.1139/t05-033>
- Fujiyasu, Y., Fahey, M., & Newson, T. (2000). Field Investigation of Evaporation from

- Freshwater Tailings. *Journal of Geotechnical and Geoenvironmental Engineering*, 126(6), 556–567. [http://doi.org/10.1061/\(ASCE\)1090-0241\(2000\)126:6\(556\)](http://doi.org/10.1061/(ASCE)1090-0241(2000)126:6(556))
- Government of Canada. (2010). Canadian Climate Normals – 1981 -2010 Climate Normals & Averages. Retrieved from http://climate.weather.gc.ca/climate_normals/
- Government of Canada. (2016). Sunrise/sunset calculator. Retrieved from <https://www.nrc-cnrc.gc.ca/eng/services/sunrise/index.html>
- Horst, T. W., & Weil, J. C. (1994). How Far is Far Enough? The Fetch Requirements for Micrometeorological Measurement of Surface Fluxes. *Journal of Atmospheric and Oceanic Technology*, 11(4), 1018–1025. [http://doi.org/10.1175/1520-0426\(1994\)011<1018:HFIFET>2.0.CO;2](http://doi.org/10.1175/1520-0426(1994)011<1018:HFIFET>2.0.CO;2)
- Hsieh, C. I., Katul, G., & Chi, T. W. (2000). An approximate analytical model for footprint estimation of scalar fluxes in thermally stratified atmospheric flows. *Advances in Water Resources*, 23(7), 765–772. [http://doi.org/10.1016/S0309-1708\(99\)00042-1](http://doi.org/10.1016/S0309-1708(99)00042-1)
- Kljun, N., Calanca, P., Rotach, M. W., & Schmid, H. P. (2015a). A simple two-dimensional parameterisation for Flux Footprint Prediction (FFP). *Geoscientific Model Development*, 8(11), 3695–3713. <http://doi.org/10.5194/gmd-8-3695-2015>
- Kljun, N., Calanca, P., Rotach, M. W., & Schmid, H. P. (2015b). The simple two-dimensional parameterisation for Flux Footprint Predictions (MatLab Program). Retrieved from http://footprint.kljun.net/download_2.php
- Li-COR Inc. (2015). EddyPro 5 - Eddy Covariance Software (9th ed.). Lincoln, NE, USA: Li-COR Inc. and EddyPro. Retrieved from <https://licor.app.box.com/s/1ium2zmwm6hl36yz9bu4>
- Natural Resource Canada. (2016). Canada's Mineral Production, Preliminary Estimates 2016. Retrieved from <http://sead.nrcan.gc.ca/PDF/Prelim2016-1-en.pdf>
- Newson, T. A., & Fahey, M. (2003). Measurement of evaporation from saline tailings storages. *Engineering Geology*, 70(3-4), 217–233. [http://doi.org/10.1016/S0013-7952\(03\)00091-7](http://doi.org/10.1016/S0013-7952(03)00091-7)
- OSRIN, 2010. OSRIN Annual Report: 2009/10. Oil Sands Research and Information Network, School of Energy and the Environment, University of Alberta, Edmonton, Alberta. OSRIN Report No. SR-3. 26 pp. Retrieved from <https://era.library.ualberta.ca/files/jq085k595#.WaY08siGOHt>
- Portelli, R. V. (1977). Mixing Heights, Wind Speeds and Ventilation Coefficients for Canada. Hull, QB, Canada: Minister of Supply and Services Canada.
- Schuepp, P. H., Leclerc, M. Y., MacPherson, J. I., & Desjardins, R. L. (1990). Footprint prediction of scalar fluxes from analytical solutions of the diffusion equation. *Boundary-Layer Meteorology*, 50(1-4), 355–373. <http://doi.org/10.1007/BF00120530>

- Shawn, E. M. (2005). *Hydrology in Practice* (3rd ed.). London, UK: Taylor & Francis e-Library.
- Syncrude Canada Ltd. (2016). Centrifuged Tails. Retrieved March 2, 2016, from <http://www.syncrude.ca/environment/tailings-management/tailings-reclamation/centrifuged-tails/>
- Wilson, G. W., Fredlund, D. G., & Barbour, S. L. (1994). Coupled Soil-Atmosphere Modelling for Soil Evaporation. *Canadian Geotechnical Journal*, 31(2), 151–161. <http://doi.org/10.1139/t94-021>
- Wilson, G. W., Fredlund, D. G., & Barbour, S. L. (1997). The effect of soil suction on evaporative fluxes from soil surfaces: Discussion. *Canadian Geotechnical Journal*, 34(1), 145 – 155. <http://doi.org/10.1139/t96-078>

Appendices

Appendix A Site Data collect by ECV

Table A.1 Atmospheric data collect by the ECV (2014)

Date	Julian Day	Number of Readings	Temperature (°C)	Relative Humidity (%)	Mean Differential Pressure (kPa)
2014-09-04	247	47	10.9	69.4	-2.7
2014-09-05	248	48	7.9	64.6	-2.7
2014-09-06	249	48	7.4	72.4	-2.7
2014-09-07	250	48	4.9	62.8	-2.7
2014-09-08	251	48	2.7	49.5	-2.7
2014-09-09	252	48	3.2	46.4	-2.7
2014-09-10	253	48	4.2	43.5	-2.8
2014-09-11	254	48	6.4	42.2	-2.8
2014-09-12	255	48	8.5	48.6	-2.9
2014-09-13	256	48	6.4	59.6	-2.9
2014-09-14	257	48	10.1	47.9	-2.8
2014-09-15	258	48	12.4	52.5	-2.8
2014-09-16	259	48	9.5	62.4	-2.9
2014-09-17	260	48	7.8	65.2	-2.9
2014-09-18	261	48	12.4	63.7	-2.9
2014-09-19	262	48	14.5	58.4	-2.9
2014-09-20	263	48	13.5	52.5	-3.0
2014-09-21	264	48	16.9	49.0	-2.9
2014-09-22	265	48	19.1	46.8	-3.0
2014-09-23	266	48	16.9	47.9	-3.1
2014-09-24	267	48	14.3	52.4	-3.2
2014-09-25	268	48	11.3	64.2	-3.2
2014-09-26	269	48	5.5	71.8	-3.5
2014-09-27	270	48	5.6	62.8	-3.0
AVERAGE			9.7	56.5	-2.9
MINIMUM			2.7	42.2	-3.5
MAXIMUM			19.1	72.4	-2.7

Table A.2 Atmospheric data collect by the ECV (2015)

Date	Julian Day	Number of Readings	Temperature	Relative Humidity	Mean Differential Pressure
			(°C)	(%)	(kPa)
2015-05-07	127	14	7.7	27.1	-3.1
2015-05-08	128	48	6.3	40.9	-3.2
2015-05-09	129	48	6.8	58.4	-3.2
2015-05-10	130	48	10.0	33.9	-3.2
2015-05-11	131	48	13.4	29.2	-3.2
2015-05-12	132	48	13.8	30.9	-3.3
2015-05-13	133	48	15.0	28.9	-3.5
2015-05-14	134	48	15.2	30.9	-3.5
2015-05-15	135	48	15.5	35.8	-3.5
2015-05-16	136	48	3.8	43.6	-3.5
2015-05-17	137	48	6.8	32.0	-3.5
2015-05-18	138	48	12.5	26.6	-3.7
2015-05-19	139	48	16.7	23.3	-3.8
2015-05-20	140	48	18.6	23.6	-4.2
2015-05-21	141	48	19.7	23.5	-4.6
2015-05-22	142	48	19.9	28.0	-5.2
2015-05-23	143	48	18.2	34.4	-5.3
2015-05-24	144	48	19.3	30.1	-6.5
2015-05-25	145	46	18.5	44.5	-5.2
2015-05-26	146	48	12.9	47.6	-2.7
2015-05-27	147	48	11.9	44.1	-2.8
2015-05-28	148	48	6.0	43.6	-2.9
2015-05-29	149	20	3.2	41.9	-2.9
AVERAGE			13.1	34.6	-3.8
MINIMUM			3.8	23.3	-6.5
MAXIMUM			19.9	58.4	-2.7

Raw refers to the results from EddyPro. Quality (Q) refers to evaporation rate when poor quality data (quality equal to 2) is omitted, and footprint (FP) refers to evaporation rate where the data with an overall relevance lower than 50% were omitted. Potential evaporation (PE) was calculated using Penman's equation, as described by Shaw (2005).

Table A.3 Evaporation data collected by ECV (2014)

Date	Julian Day	No. of Readings	Actual Evaporation	Actual Evaporation	Actual Evaporation	Potential Evaporation
		FP	Raw	Q	Q & FP	Penman's
			(mm day ⁻¹)	(mm day ⁻¹)	(mm day ⁻¹)	(mm day ⁻¹)
2014-09-04	247	8	-0.068	-0.067	0.026	2.582
2014-09-05	248	9	0.040	0.041	0.035	2.212
2014-09-06	249	2	0.101	0.104	0.015	1.769
2014-09-07	250	0	0.028	0.028	0.000	2.010
2014-09-08	251	0	0.056	0.055	0.000	1.774
2014-09-09	252	0	0.007	0.007	0.000	1.499
2014-09-10	253	5	0.087	0.089	0.021	1.791
2014-09-11	254	3	0.118	0.118	0.037	3.638
2014-09-12	255	1	-0.063	-0.064	-0.002	2.156
2014-09-13	256	10	0.105	0.106	0.014	1.639
2014-09-14	257	7	0.022	0.020	0.026	2.316
2014-09-15	258	10	0.097	0.097	0.063	2.107
2014-09-16	259	7	0.098	0.098	0.008	2.347
2014-09-17	260	25	0.086	0.086	0.087	2.578
2014-09-18	261	1	0.052	0.053	0.006	1.883
2014-09-19	262	15	-0.066	-0.066	0.051	3.333
2014-09-20	263	1	0.229	0.229	0.003	2.807
2014-09-21	264	13	0.126	0.126	0.075	3.215
2014-09-22	265	15	-0.020	-0.020	0.017	3.041
2014-09-23	266	0	0.046	0.051	0.000	1.976
2014-09-24	267	5	-0.041	-0.034	0.003	3.389
2014-09-25	268	7	-0.022	-0.009	0.005	1.852
2014-09-26	269	0	0.032	0.035	0.000	1.155
AVERAGE		6.6	0.045	0.046	0.039	2.260
MINIMUM		0	-0.068	-0.067	-0.002	1.155
MAXIMUM		25	0.229	0.229	0.087	3.638

Table A.4 Evaporation data collected by ECV (2015)

Date	Julian Day	No. of Readings	Actual Evaporation	Actual Evaporation	Actual Evaporation	Potential Evaporation	Evaporation
		FP	Raw (mm day ⁻¹)	Q (mm day ⁻¹)	Q & FP (mm day ⁻¹)	Penman's (mm day ⁻¹)	Suncor (mm day ⁻¹)
2015-05-07	127	4	0.062	0.061	0.004	3.371	3.18
2015-05-08	128	26	0.244	0.233	0.033	3.520	3.26
2015-05-09	129	31	0.185	0.178	0.067	3.286	3.06
2015-05-10	130	35	0.080	0.044	0.048	4.075	4.53
2015-05-11	131	32	0.206	0.184	0.172	4.444	4.97
2015-05-12	132	38	0.372	0.347	0.251	5.096	6.20
2015-05-13	133	16	0.059	0.054	0.033	5.800	6.68
2015-05-14	134	1	-0.165	-0.095	-0.012	5.766	7.06
2015-05-15	135	14	-0.047	-0.117	-0.017	5.728	6.62
2015-05-16	136	3	0.159	0.135	-0.002	4.044	3.06
2015-05-17	137	25	0.142	0.146	-0.008	4.445	4.42
2015-05-18	138	16	-0.162	-0.155	0.006	4.899	5.85
2015-05-19	139	8	0.186	0.089	0.053	5.024	6.13
2015-05-20	140	19	0.128	0.114	0.088	5.279	6.64
2015-05-21	141	12	-0.055	-0.147	0.013	5.745	7.04
2015-05-22	142	8	0.059	0.049	-0.022	6.279	9.04
2015-05-23	143	28	0.079	0.010	0.049	5.614	6.44
2015-05-24	144	23	0.062	0.043	0.049	5.345	6.19
2015-05-25	145	20	0.157	0.117	0.093	5.508	4.27
2015-05-26	146	3	0.124	0.084	-0.003	5.051	5.58
2015-05-27	147	26	-0.035	-0.035	-0.013	5.339	3.55
2015-05-28	148	3	0.182	0.103	0.002	4.440	4.46
2015-05-29	149	17	0.015	0.020	0.009	3.786	4.79
AVERAGE			0.093	0.065	0.066	4.914	5.37
MINIMUM			-0.165	-0.155	-0.022	3.286	3.06
MAXIMUM			0.372	0.347	0.251	6.279	9.04

Percent difference between evaporation rates was calculate:

- EddyPro raw evaporation data and EddyPro evaporation data trimmed using quality data
- EddyPro raw evaporation data and EddyPro evaporation data trimmed using quality data and footprint analysis
- Potential evaporation and EddyPro evaporation data trimmed using quality and footprint analysis

Percent difference was calculated as:

$$\% \text{ difference} = \left(\left| \frac{\text{Variable}_1 - \text{Variable}_2}{\text{Variable}_1 + \text{Variable}_2} \right| \cdot 2 \right) \cdot 100\% \quad (\text{Eq. A.1})$$

Table A.5 Summary of percent difference between evaporation rates (2014)

Date	Julian Day	% Diff. Evaporation	% Diff. Evaporation	% Diff. PE and ECV AME*
		Raw and Q (%)	Raw and Q & FP (%)	*Q & F (%)
2014-09-04	247	1.7	443.2	256.2
2014-09-05	248	0.3	15.9	218.2
2014-09-06	249	3.3	147.8	175.2
2014-09-07	250	0.0	200.0	201.0
2014-09-08	251	3.2	200.0	177.4
2014-09-09	252	0.0	200.0	149.9
2014-09-10	253	3.1	123.2	176.8
2014-09-11	254	0.0	104.1	361.8
2014-09-12	255	1.5	188.5	215.8
2014-09-13	256	1.3	153.8	162.3
2014-09-14	257	11.5	17.8	229.3
2014-09-15	258	0.0	43.5	204.9
2014-09-16	259	0.0	169.8	234.1
2014-09-17	260	0.0	1.4	251.2
2014-09-18	261	1.7	160.0	187.7
2014-09-19	262	0.0	1567.8	330.3
2014-09-20	263	0.0	194.7	280.5
2014-09-21	264	0.0	50.6	316.9
2014-09-22	265	0.0	2246.9	303.0
2014-09-23	266	10.5	200.0	197.6
2014-09-24	267	17.8	235.2	338.7
2014-09-25	268	87.1	333.4	184.6
2014-09-26	269	9.5	200.0	115.5
AVERAGE		6.5	302.9	224.4

In 2015, the percent difference between the Suncor measured evaporation and EddyPro evaporation data trimmed using quality data and footprint analysis was also calculated.

Table A.6 Summary of percent difference between evaporation rates (2015)

Date	Julian Day	% Diff. Evaporation	% Diff. Evaporation	% Diff. PE and ECV AME*	% Diff. Suncor E and ECV AME*
		Raw and Q	Raw and Q & FP	*Q & F	*Q & F
		(%)	(%)	(%)	(%)
2015-05-07	127	2.4	176.8	336.9	199.5
2015-05-08	128	4.6	150.0	350.2	196.0
2015-05-09	129	4.2	90.6	324.7	191.4
2015-05-10	130	57.6	8.3	405.1	195.8
2015-05-11	131	11.5	6.5	436.9	186.6
2015-05-12	132	6.9	32.2	500.2	184.5
2015-05-13	133	8.4	48.1	578.9	198.0
2015-05-14	134	53.4	156.8	577.0	200.7
2015-05-15	135	86.1	148.3	573.4	201.1
2015-05-16	136	16.2	207.3	404.5	200.3
2015-05-17	137	2.2	224.6	444.9	200.8
2015-05-18	138	4.2	215.3	489.7	199.6
2015-05-19	139	70.8	51.0	500.3	196.6
2015-05-20	140	11.1	26.3	524.7	194.8
2015-05-21	141	91.4	240.1	574.1	199.2
2015-05-22	142	17.7	523.5	628.6	201.0
2015-05-23	143	154.0	130.8	559.6	197.0
2015-05-24	144	35.2	12.8	532.6	196.9
2015-05-25	145	29.0	23.1	547.5	191.5
2015-05-26	146	38.1	214.2	505.2	200.2
2015-05-27	147	1.4	89.7	534.4	201.5
2015-05-28	148	55.3	192.8	443.9	199.8
2015-05-29	149	29.6	81.6	378.2	199.3
AVERAGE		34.6	135.0	489.7	196.9

Table A.7 Quality of latent heat flux data (2014)

Date	Julian Day	High Quality	Intermediate Quality	Low Quality
2014-09-04	247	24	22	1
2014-09-05	248	19	27	2
2014-09-06	249	20	26	2
2014-09-07	250	28	20	0
2014-09-08	251	19	28	1
2014-09-09	252	21	27	0
2014-09-10	253	24	23	1
2014-09-11	254	37	11	0
2014-09-12	255	23	24	1
2014-09-13	256	11	32	5
2014-09-14	257	22	25	1
2014-09-15	258	16	32	0
2014-09-16	259	26	22	0
2014-09-17	260	27	21	0
2014-09-18	261	22	25	1
2014-09-19	262	26	22	0
2014-09-20	263	27	21	0
2014-09-21	264	28	19	1
2014-09-22	265	27	21	0
2014-09-23	266	16	29	3
2014-09-24	267	28	19	1
2014-09-25	268	18	29	1
2014-09-26	269	23	24	1
TOTAL		547	581	23
% DATA		48%	50%	2%

Table A.8 Quality of latent heat flux data (2015)

Date	Julian Day	High Quality	Intermediate Quality	Low Quality
2015-05-07	127	1	13	0
2015-05-08	128	3	44	1
2015-05-09	129	9	39	0
2015-05-10	130	16	32	0
2015-05-11	131	20	28	0
2015-05-12	132	13	35	0
2015-05-13	133	33	15	0
2015-05-14	134	31	17	0
2015-05-15	135	29	19	0
2015-05-16	136	17	31	0
2015-05-17	137	16	32	0
2015-05-18	138	16	32	0
2015-05-19	139	23	25	0
2015-05-20	140	13	35	0
2015-05-21	141	16	32	0
2015-05-22	142	23	25	0
2015-05-23	143	21	27	0
2015-05-24	144	15	33	0
2015-05-25	145	9	34	3
2015-05-26	146	23	25	0
2015-05-27	147	17	31	0
2015-05-28	148	20	28	0
2015-05-29	149	6	14	0
TOTAL		390	646	4
% DATA		37.5	62.1	0.4

Appendix B Site Data provided by Suncor

Suncor provided both the atmospheric data of the site and the tailing pouring data for the test cell:

Table B.1 Atmospheric data collect by Suncor weather station (2014)

Date	Julian Day	Temperature	Relative Humidity	Rainfall	Temperature	Relative Humidity
		(°C)	(%)	(mm day ⁻¹)	(% diff)	(% diff)
2014-09-04	247	11.2	86.6	0.25	2.21	21.94
2014-09-05	248	8.0	85.3	0.25	1.96	27.70
2014-09-06	249	7.3	95.6	0.25	0.65	27.69
2014-09-07	250	4.7	88.6	0.25	3.35	34.08
2014-09-08	251	2.7	75.6	0.25	1.08	41.83
2014-09-09	252	3.2	71.9	0.25	0.84	43.05
2014-09-10	253	4.2	66.6	0.25	1.78	41.97
2014-09-11	254	7.0	60.0	0.00	9.76	34.77
2014-09-12	255	8.7	68.1	1.27	1.64	33.36
2014-09-13	256	6.6	80.6	0.25	3.20	29.91
2014-09-14	257	11.0	62.0	0.00	8.62	25.55
2014-09-15	258	13.0	66.2	0.00	4.81	23.19
2014-09-16	259	9.6	81.8	0.00	0.53	26.91
2014-09-17	260	7.9	85.4	0.00	1.75	26.86
2014-09-18	261	13.0	78.4	0.00	4.72	20.63
2014-09-19	262	14.9	70.8	4.32	2.85	19.19
2014-09-20	263	13.9	64.5	3.04	3.42	20.62
2014-09-21	264	17.9	58.3	0.00	5.26	17.22
2014-09-22	265	20.3	52.3	0.00	6.15	11.29
2014-09-23	266	17.3	58.2	0.00	2.34	19.38
2014-09-24	267	14.7	66.2	0.25	3.18	23.12
2014-09-25	268	11.2	82.1	0.51	0.46	24.42
2014-09-26	269	5.1	96.9	32	7.36	29.81
AVERAGE		10.0	74.6	1.82	3.34	27.40
MINIMUM		2.7	52.3	0.00	0.46	11.29
MAXIMUM		20.3	96.9	32.0	9.76	43.05

Table B.2 Atmospheric data collect by Suncor weather station (2015)

Date	Julian Day	Temperature	Relative Humidity	Temperature	Relative Humidity
				(% diff)	(% diff)
2015-05-07	127	4.1	62.5	60.09	79.04
2015-05-08	128	6.6	51.2	5.38	22.32
2015-05-09	129	7.2	68.9	6.76	16.50
2015-05-10	130	10.8	39.2	7.03	14.63
2015-05-11	131	14.2	31.2	5.47	6.70
2015-05-12	132	14.5	33.5	4.66	7.92
2015-05-13	133	15.9	29.4	5.91	1.79
2015-05-14	134	16.2	30.0	6.24	2.85
2015-05-15	135	16.2	37.0	4.80	3.36
2015-05-16	136	3.8	56.6	0.07	25.97
2015-05-17	137	7.4	39.1	8.54	20.00
2015-05-18	138	13.6	27.6	8.68	3.69
2015-05-19	139	18.0	21.4	7.43	8.43
2015-05-20	140	20.0	21.9	6.87	7.55
2015-05-21	141	20.9	22.9	5.69	2.63
2015-05-22	142	20.9	27.4	5.16	1.99
2015-05-23	143	19.0	36.9	4.06	6.95
2015-05-24	144	20.6	30.3	6.23	0.46
2015-05-25	145	19.5	45.4	5.41	2.01
2015-05-26	146	13.2	53.1	2.41	10.85
2015-05-27	147	12.2	50.6	2.22	13.67
2015-05-28	148	6.1	55.1	2.30	23.24
2015-05-29	149	9.3	39.0	96.48	7.19
AVERAGE	137.5	13.7	39.6	7.79	12.84
MINIMUM	127	3.8	21.4	0.07	0.46
MAXIMUM	148	20.9	68.9	60.09	79.04

In 2015, there was only recorded rainfall event occurred in June:

Table B.3 Rainfall data collected by Suncor weather station (2015)

Date	Julian Day	Rainfal
		(mm day ⁻¹)
2015-06-05	156	5.08
2015-06-08	159	5.07
2015-06-11	162	0.25
TOTAL		10.4

Table B.4 Test cell tailing pouring data

Date	Julian Day	Height of Lift	Solids Content
		[cm]	[wt% solids]
17-Sep-14	260	14.14	35.2%
08-May-15	128	12	39
15-June-15	166	14	51

Appendix C Footprint Analysis

C.I MatLab Script

Note that `calc_footprint_FFP` and `calc_footprint_FFP_percentage_rotate` are functions created by Kljun et. al (2015b); all other functions are built into MATLAB R2015b (version 8.6.0.267246).

`%reading data from EddyPro output`

`g = 1;`

`while g < 5`

`if g == 1`

`filename1 = 'Suncor2014.xls';`

`dt1 = '2014';`

`else if g == 2`

`filename1 = 'Suncor2015(01).xls';`

`dt1 = '201501';`

`else if g == 3`

`filename1 = 'Suncor2015(02).xls';`

`dt1 = '201502';`

`else`

`filename1 = 'Suncor2015(03).xls';`

`dt1 = '201503';`

`end`

`end`

`end`

`if g == 1`

`zm = 4; %the equipment height above the tailings surface in 2014`

`%B1 cell corner location 2014`

`xB1 = [-167, 102, 102, -167,-167];`

`yB1 = [-18,-18,-96,-96,-18];`

`%entire B cell corner location 2014`

`xB = [-167, 102, 102, -167,-167];`

`yB = [-18,-18,-550,-550,-18];`

`else`

`zm = 1.5; %the equipment height above the tailings surface in 2015`

`%B1 cell corner location 2015`

```

xB1 = [-205, 64, 64, -205,-205];
yB1 = [34,34,-44,-44,34];
%entire B cell corner location 2015
xB = [-205, 64, 64, -205,-205];
yB = [34,34,-498,-498,34];
end

```

% reads in the values from the xls file

```

numdata = xlsread(filename1);
rowcol = size(numdata);
rownum = rowcol(1,1);
colnum = rowcol(1,2);
zO = 0.00006; %roughness length [m] between 0.002 cm and 0.01 cm (Brutsaert,1982)
h = 1700; %boundary layer height [m] (Portelli, 1977)

```

%selecting variable from the flux output

```

doy = numdata(:,1); %numbering the period (date the measurements was done)
ustar = numdata(:,3); %friction velocity [ms-1]
L = numdata(:,4); %Obukhov length [m]
wind_dir = numdata(:,5); %main wind direction (degrees from north)
vvar = numdata(:,6); %variance of lateral velocity

```

```

b = rownum; %row number of the last valid measurement
c = b + 1;

```

```

b = 1;
e = 0;

```

while b < c

```

try
    [x_ci_max(b,1),x_ci,f_ci,x_2d,y_2d,f_2d] =
    calc_footprint_FFP(zm,zO,h,L(b,1),sqrt(vvar(b,1)),ustar(b,1));
catch
    x_ci_max(b,1) = -9999;
    x_ci = -9999;
    f_ci = -9999;
    x_2d = -9999;
    y_2d = -9999;
    f_2d = -9999;
end

```

%A = area of footprint

%Ab = area inside the area of interest (B1 cell)

%RB1 = percentage of the A that is inside area of interest (B1 cell) Ab/A

```

if x_ci ~= -9999

```

```

try
FFP =
calc_footprint_FFP_percentage_rotated(x_2d,y_2d,f_2d,[30:20:70,80,90],wind_dir(b,1));
xy30 = [FFP(1).x.', FFP(1).y.'];
xy50 = [FFP(2).x.', FFP(2).y.'];
xy70 = [FFP(3).x.', FFP(3).y.'];
xy80 = [FFP(4).x.', FFP(4).y.'];
xy90 = [FFP(5).x.', FFP(5).y.'];

A30(b,1) = polyarea(xy30(:,1),xy30(:,2));
[xb, yb] = polybool('intersection', xy30(:,1), xy30(:,2), xB1, yB1);
Ab30(b,1) = polyarea(xb,yb);
RB1_30(b,1) = Ab30(b,1)/A30(b,1);

A50(b,1) = polyarea(xy50(:,1),xy50(:,2));
[xb, yb] = polybool('intersection', xy50(:,1), xy50(:,2), xB1, yB1);
Ab50(b,1) = polyarea(xb,yb);
RB1_50(b,1) = Ab50(b,1)/A50(b,1);

A70(b,1) = polyarea(xy70(:,1),xy70(:,2));
[xb, yb] = polybool('intersection', xy70(:,1), xy70(:,2), xB1, yB1);
Ab70(b,1) = polyarea(xb,yb);
RB1_70(b,1) = Ab70(b,1)/A70(b,1);

A80(b,1) = polyarea(xy80(:,1),xy80(:,2));
[xb, yb] = polybool('intersection', xy80(:,1), xy80(:,2), xB1, yB1);
Ab80(b,1) = polyarea(xb,yb);
RB1_80(b,1) = Ab80(b,1)/A80(b,1);

A90(b,1) = polyarea(xy90(:,1),xy90(:,2));
[xb, yb] = polybool('intersection', xy90(:,1), xy90(:,2), xB1, yB1);
Ab90(b,1) = polyarea(xb,yb);
RB1_90(b,1) = Ab90(b,1)/A90(b,1);

catch
A30(b,1) = -999;
Ab30(b,1) = -999;
RB1_30(b,1) = -999;

A50(b,1) = -999;
Ab50(b,1) = -999;
RB1_50(b,1) = -999;

A70(b,1) = -999;
Ab70(b,1) = -999;
RB1_70(b,1) = -999;

```

```

    A80(b,1) = -999;
    Ab80(b,1) = -999;
    RB1_80(b,1) = -999;

    A90(b,1) = -999;
    Ab90(b,1) = -999;
    RB1_90(b,1) = -999;
end
else
    A30(b,1) = -9999;
    Ab30(b,1) = -9999;
    RB1_30(b,1) = -9999;

    A50(b,1) = -9999;
    Ab50(b,1) = -9999;
    RB1_50(b,1) = -9999;

    A70(b,1) = -9999;
    Ab70(b,1) = -9999;
    RB1_70(b,1) = -9999;

    A80(b,1) = -9999;
    Ab80(b,1) = -9999;
    RB1_80(b,1) = -9999;

    A90(b,1) = -9999;
    Ab90(b,1) = -9999;
    RB1_90(b,1) = -9999;
end

% noting the general direction of the measurement
if x_ci_max(b,1) ~= -9999 || A30 ~= -999
    if wind_dir(b,1) <= 135 && wind_dir(b,1) > 45
        s(b,1) = 'E';
    else if wind_dir(b,1) <= 225 && wind_dir(b,1) > 135
        s(b,1) = 'S';
    else if wind_dir(b,1) <= 315 && wind_dir(b,1) > 225
        s(b,1) = 'W';
    else
        s(b,1) = 'N';
    end
end
end
end
end

```

% noting the quadrant of the direction, and finding the x,y coordinates of x_ci_max

```

if wind_dir(b,1) <= 90
    q(b,1) = 0;
else if wind_dir(b,1) <= 180 && wind_dir(b,1) > 90
    q(b,1) = 1;
else if wind_dir(b,1) <= 270 && wind_dir(b,1) > 180
    q(b,1) = 2;
else
    q(b,1) = 3;
end
end
end

if q(b,1) == 0 || q(b,1) == 2
    x_x_ci_max(b,1) = x_ci_max(b,1)*sind(wind_dir(b,1)-90*q(b,1));
    y_x_ci_max(b,1) = x_ci_max(b,1)*cosd(wind_dir(b,1)-90*q(b,1));
else
    x_x_ci_max(b,1) = x_ci_max(b,1)*cosd(wind_dir(b,1)-90*q(b,1));
    y_x_ci_max(b,1) = x_ci_max(b,1)*sind(wind_dir(b,1)-90*q(b,1));
end

if q(b,1) == 2 || q(b,1) == 3
    x_x_ci_max(b,1) = - x_x_ci_max(b,1);
end

if q(b,1) == 1 || q(b,1) == 2
    y_x_ci_max(b,1) = - y_x_ci_max(b,1);
end

```

%determining which contour line x_ci_max is within

```

try
    inxy30(b,1) = inpolygon(x_x_ci_max(b,1), y_x_ci_max(b,1), xy30(:,1), xy30(:,2));
catch
    inxy30(b,1) = -999;
end

try
    inxy50(b,1) = inpolygon(x_x_ci_max(b,1), y_x_ci_max(b,1), xy50(:,1), xy50(:,2));
catch
    inxy50(b,1) = -999;
end

try
    inxy70(b,1) = inpolygon(x_x_ci_max(b,1), y_x_ci_max(b,1), xy70(:,1), xy70(:,2));
catch
    inxy70(b,1) = -999;
end

```

```

try
    inxy80(b,1) = inpolygon(x_x_ci_max(b,1), y_x_ci_max(b,1), xy80(:,1),xy80(:,2));
catch
    inxy80(b,1) = -999;
end

try
    inxy90(b,1) = inpolygon(x_x_ci_max(b,1), y_x_ci_max(b,1), xy90(:,1),xy90(:,2));
catch
    inxy90(b,1) = -999;
end

else
    s(b,1) = -9999;
    q(b,1) = -9999;
    x_x_ci_max(b,1) = -9999;
    y_x_ci_max(b,1) = -9999;
    inxy30(b,1) = -9999;
    inxy50(b,1) = -9999;
    inxy70(b,1) = -9999;
    inxy80(b,1) = -9999;
    inxy90(b,1) = -9999;
end

filename2 = ['FootprintResults','(',dt1,')(',num2str(b),').mat'];

if RB1_90(b,1)~=0 && RB1_90(b,1)~-999 && RB1_90(b,1)~-9999
    e = e + 1;
    save(filename2,'FFP');
end

clearvars FFP xy30 xy50 xy70 xy90
amount_complete = (b/(c-1))*100
b = b + 1;
end

filename3 = ['Relevance','(',dt1,').xlsx'];
T = table(x_ci_max,x_x_ci_max,y_x_ci_max,s,q,inxy30,inxy50,inxy70,inxy80,inxy90,
A30,A50,A70,A80,A90,Ab30,Ab50,Ab70,Ab80,Ab90,RB1_30,RB1_50,RB1_70,RB1_80,R
B1_90);
writetable (T, filename3,'Sheet',1,'Range','A1');
clearvars -except g
g = g + 1;
end

```

C.II Results of Footprint Analysis

Table C.1 Number of occurrences where footprint resulted in specified relevance (2014)

Relevance	30%	50%	70%	80%	90%	Overall
0%	531	494	473	464	441	441
10%	29	28	103	430	681	100
20%	26	17	320	138	33	61
30%	23	34	183	92	0	46
40%	27	51	24	25	0	62
50%	21	68	13	5	0	288
60%	22	117	15	0	0	159
70%	28	84	18	0	0	0
80%	42	101	6	0	0	0
90%	66	117	0	0	0	0
100%	342	44	0	0	0	0
Total	1157	1155	1155	1154	1155	1157

Table C.2 Percentage of occurrences where footprint resulted in specified relevance (2014)

Relevance	30%	50%	70%	80%	90%	Overall
0%	45.9%	42.8%	41.0%	40.2%	38.2%	38.1%
10%	2.5%	2.4%	8.9%	37.3%	59.0%	8.6%
20%	2.2%	1.5%	27.7%	12.0%	2.9%	5.3%
30%	2.0%	2.9%	15.8%	8.0%	0.0%	4.0%
40%	2.3%	4.4%	2.1%	2.2%	0.0%	5.4%
50%	1.8%	5.9%	1.1%	0.4%	0.0%	24.9%
60%	1.9%	10.1%	1.3%	0.0%	0.0%	13.7%
70%	2.4%	7.3%	1.6%	0.0%	0.0%	0.0%
80%	3.6%	8.7%	0.5%	0.0%	0.0%	0.0%
90%	5.7%	10.1%	0.0%	0.0%	0.0%	0.0%
100%	29.6%	3.8%	0.0%	0.0%	0.0%	0.0%
AVERAGE	41.8%	34.3%	11.9%	6.8%	2.3%	22.7%
STD. DEV.	44.3%	34.5%	14.2%	8.7%	3.1%	22.6%

Table C.3 Number of occurrences where footprint resulted in specified relevance (2015)

Relevance	30%	50%	70%	80%	90%	Overall
0%	1	1	1	1	1	1
10%	0	1	1	241	928	0
20%	0	0	141	433	40	1
30%	1	0	108	253	16	0
40%	0	1	210	28	13	1
50%	0	0	90	9	16	166
60%	0	0	62	7	8	309
70%	0	137	74	4	8	399
80%	0	55	161	4	10	101
90%	0	33	67	8	0	62
100%	1038	812	125	52	0	0
TOTAL	1040	1040	1040	1040	1040	1040

Table C.4 Percentage of occurrences where footprint resulted in specified relevance (2015)

Relevance	30%	50%	70%	80%	90%	Overall
0%	0.1%	0.1%	0.1%	0.1%	0.1%	0.1%
10%	0.0%	0.1%	0.1%	23.2%	89.2%	0.0%
20%	0.0%	0.0%	13.6%	41.6%	3.8%	0.1%
30%	0.1%	0.0%	10.4%	24.3%	1.5%	0.0%
40%	0.0%	0.1%	20.2%	2.7%	1.3%	0.1%
50%	0.0%	0.0%	8.7%	0.9%	1.5%	16.0%
60%	0.0%	0.0%	6.0%	0.7%	0.8%	29.7%
70%	0.0%	13.2%	7.1%	0.4%	0.8%	38.4%
80%	0.0%	5.3%	15.5%	0.4%	1.0%	9.7%
90%	0.0%	3.2%	6.4%	0.8%	0.0%	6.0%
100%	99.8%	78.1%	12.0%	5.0%	0.0%	0.0%
AVERAGE	99.9%	93.3%	55.1%	23.8%	9.0%	62.9%
STD. DEV.	3.3%	12.5%	28.1%	24.0%	13.6%	10.5%

Appendix D Sources

The following tables are reproduced from the Hydrology in Practice (as cited Shaw, 2005). Attached is the Canada's mineral production (preliminary estimates) of 2016 (Natural Resources Canada, 2016), and summary of Alberta Oil Sands plants statistics (Alberta Regulatory Energy, 2016).

Table D.1 Weight factor (Δ/γ) and temperature

Temperature	Temperature	Weighting Factor
$^{\circ}\text{F}$	$^{\circ}\text{C}$	Δ/γ
30	-1.11	0.66
30.5	-0.83	0.66
31	-0.56	0.67
31.5	-0.28	0.68
	0	0.69
	0.5	0.71
	1	0.73
	1.5	0.76
	2	0.78
	2.5	0.8
	3	0.83
	3.5	0.85
	4	0.88
	4.5	0.91
	5	0.94
	5.5	0.97
	6	1
	6.5	1.03
	7	1.06
	7.5	1.09
	8	1.13
	8.5	1.16
	9	1.19
	9.5	1.23

Temperature	Temperature	Weighting
°F	°C	Factor
		Δ/γ
	10	1.26
	10.5	1.3
	11	1.34
	11.5	1.38
	12	1.42
	12.5	1.47
	13	1.51
	13.5	1.56
	14	1.6
	14.5	1.65
	15	1.69
	15.5	1.74
	16	1.79
	16.5	1.84
	17	1.89
	17.5	1.94
	18	1.99
	18.5	2.04
	19	2.11
	19.5	2.17
	20	2.23
68.5	20.28	2.27
69	20.56	2.32

Table D.2 0.75 Ra expressed in equivalent evaporation (mm day⁻¹)

Month	50°	56°	56.9°	58°	60°
April	12.7	11.7	11.6	11.5	11.1
May	15.3	14.9	14.8	14.7	14.6
June	16.4	16.2	16.2	16.2	16.1
July	16.0	15.6	15.6	15.5	15.4
August	13.6	12.9	12.7	12.6	12.3
September	10.3	9.1	8.9	8.7	8.3
October	6.9	5.5	5.3	5.0	4.5

Table D.3 Values of theoretical black body radiation (mm of water)

Temperature	Black Body Radiation
(°C)	(mm of water)
-1	11
0	11.2
1	11.4
2	11.5
3	11.7
4	11.9
5	12
6	12.2
7	12.3
8	12.5
9	12.7
10	12.9
11	13.1
12	13.3
13	13.5
14	13.7
15	13.9
16	14
17	14.2
18	14.4
19	14.6
20	14.8
21	15

Table D.4 Preliminary estimates of the mineral production of Canada (Natural Resource Canada, 2016)

Resource	Mass Unit	Canada
Bismuth	t	2
Cadmium	t	55
Cobalt	t	4,245
Copper	t	702,310
Gold	kg	155,879
Iron ore	kt	47,083
Lead	t	10,858
Molybdenum	t	2,708
Nickel	t	227,364
Niobium	t	6,099
Platinum group	kg	31,093
Selenium	t	176
Silver	t	379
Tellurium	t	18
Uranium (U)	t	12,421
Zinc	t	294,288
Cement	kt	12,243
Coal	kt	60,501
Gemstones	t	224
Gypsum	kt	1,662
Lime	kt	1,797
Nepheline syenite	kt	475
Peat	kt	1,120
Potash (K₂O)	kt	10,154
Quartz (silica)	kt	1,959
Salt	kt	9,620
Sand and gravel	kt	315,588
Soapstone, talc, pyrophyllite	kt	202
Stone	kt	152,059
Sulphur, in smelter gas	kt	664
Sulphur, elemental	kt	4,653
TOTAL	t	615,948,109

Table D.5 Summary of Alberta Oil Sands plant statistics (Alberta Energy Regulator, 2016)

Company	Resource/Product	Total 2016 Production
Canadian Natural Resource Limited	Mined Oil Sands (tonnes)	88,855,216.00
	Grade of Mined Oil Sand (%)	10.89
	Crude Bitumen Production (m ³)	8,513,109.10
Imperial Oil Resources Ventures Limited	Mined Oil Sands (tonnes)	104,164,458.60
	Grade of Mined Oil Sand (%)	11.4
	Crude Bitumen Production (m ³)	10,783,943.10
Shell Canada Energy (Albian Sands Energy Inc.)	Mined Oil Sands (tonnes)	78,247,530.00
	Grade of Mined Oil Sand (%)	11.61
	Crude Bitumen Production (m ³)	8,274,571.60
Shell Canada Energy (Shell Jackpine Mine)	Mined Oil Sands (tonnes)	61,252,655.00
	Grade of Mined Oil Sand (%)	11.75
	Crude Bitumen Production (m ³)	6,605,628.10
Suncor Energy Inc.	Mined Oil Sands (tonnes)	128,303,818.00
	Grade of Mined Oil Sand (%)	11.52
	Crude Bitumen Production (m ³)	13,869,028.00
Syncrude Canada Ltd. (Mildred Lake)	Mined Oil Sands (tonnes)	91,912,003.40
	Grade of Mined Oil Sand (%)	10.34
	Crude Bitumen Production (m ³)	8,055,284.70
Syncrude Canada Ltd. (Aurora)	Mined Oil Sands (tonnes)	99,203,845.70
	Grade of Mined Oil Sand (%)	11.52
	Crude Bitumen Production (m ³)	10,625,690.30
TOTAL	Mined Oil Sands (tonnes)	651,939,526.70
	Crude Bitumen Production (m³)	66,727,254.90
AVERAGE	Grade of Mined Oil Sand (%)	11.28